# MAGNETOM Flash

## BioMatrix and *syngo* MR XA11 special issue

Not for distribution in the US

MAGNETOM Sola 1.5T
MAGNETOM Vida 3T



Cover images MAGNETOM Vida

siemens.com/magnetom-world

SIEMENS Healthineers

Professor Konstantin Nikolaou

**Konstantin Nikolaou** is Chairman of the Department of Diagnostic and Interventional Radiology in the Department of Radiology at the Eberhard-Karl-University in Tübingen, Germany. Professor Nikolaou received his MD from the Ludwig-Maximilians-University of Munich, Germany, in the year 2000, where he also became an Assistant Professor at the Department of Clinical Radiology, University Hospitals Munich, after finalizing his PhD-thesis on the topic of modern cardiovascular computed tomography techniques in 2007.

After working as a section chief of CT/PET-CT and MRI at the same department, he became Vice Chair of the Department of Clinical Radiology at the Ludwig-Maximilian-University in Munich in April 2007.

# Precision Medicine and Adaptive Technologies in Medical Imaging

## Dear colleagues, dear readers,

I feel honored and excited to be invited to write an editorial for MAGNETOM Flash on the topic of 'precision medicine' – a term that might seem overused these days. Whilst this term is not new – medicine always wants to deliver the right treatment to the right patient at the right time – our under-standing of correlations between genome, habits, and diseases is evolving rapidly and exponentially.
It feels like there is a need to re-imagine and re-organize health services.

All fields of medicine are adapting to an increasing and increasingly complex demand of phenotyping and genotyping our patients, identifying precise cohorts, and optimizing health care. To us as radiologists, it may seem obvious, that radiology should certainly play a key role in phenotyping these sub-populations by means of dedicated imaging strategies [1]. This should be complementary, and not compete with other ways of phenotyping, including, for example, advanced laboratory tests, histo-pathology, and immuno-pathology. To integrate our radiological imaging data and reports in a phenotyping system that categorizes patients into well-defined prognostic and therapeutic categories, we will have to learn and adapt to a rising demand of 'imaging biomarkers', 'reproducible parameters' and 'standardized' as well as 'structured' reporting.

I am sure our readers are optimistic as I am that we will be able to successfully master these challenges. However, at the same time, we are facing new opportunities and threats, in terms of increasing economic pressure and increasing workload, 'value-based' healthcare, introducing artificial intelligence in clinical routine, and commoditization of imaging procedures and radiological reports [2, 3].
We need clear and concerted strategies to handle these challenges and these include,

A) Accepting and taking on a stronger role of radiologists, as clinical partners and information specialists,

B) Setting new standards in quality and workflows, and

C) Finding answers to an increasing demand of personalization and parametrization in our daily routine.

In this volume of MAGNETOM Flash, exciting views and reports on advancements in MR technologies, enabling us to improve quality, workflows, flexibility, and standardization, clearly reflect these trends and endeavors – in a way that I find very convincing.

### 1. A new role for radiologists?

Radiologists will have to adapt. And we will have to adapt quickly, to both an increasing economic pressure and to the 'fourth industrial revolution', i.e., a rapidly improving process automatization on the basis of big data and artificial intelligence (AI) [4, 5]. The first challenge will be to adapt and re-invent our ever more complex imaging procedures and skills in the era of 'value-based healthcare'. Since 'value' is defined as health or patient outcomes, or

He also is president of the European Society of Molecular and Functional Imaging in Radiology (ESMOFIR) and treasurer for the European Society of Cardiac Imaging (ESCR), Member of the Research Committee of the European Society of Radiology (ESR) and Honorary Member of the Greek Society of Radiology.

Professor Nikolaou joined the Eberhard-Karl-University Tübingen in April 2014 as Chairman of the Department of Diagnostic and Interventional Radiology. His main fields of interest are multimodality and multi-parametric imaging modalities in oncology as well as non-invasive imaging of cardiovascular diseases.

Tübingen, Germany

costs, we should therefore be measured on the results and quality of our care and not on the volumes of service delivered. However, if we agree to enter this circle of optimizing our workflows and outcome-centered care, will we be degraded to delivering standardized services and reports within a (short) given time, i.e., will medical imaging become a commodity? The strength of radiology is not only in the delivery of (automated) results from using sophisticated technologies, but even more by providing an optimized diagnostic process and data integration, provided by dedicated, highly skilled, specialized and communicating colleagues in our field, i.e., radiologists and technicians.

Radiology's value chain has to be high-quality, patient-centered, and results-oriented at the same time. This will enable us to develop from volume-based imaging to value-based imaging, demonstrating the added value of imaging in each phase of patient care and transforming imaging results into measurable metrics (e.g., quantitative imaging results, or cost effectiveness). The primary objective is to maintain and improve our visibility and demonstrating our capabilities as radiologists, imaging experts and highly trained specialists to our clinical partners and patients in daily practice, in our conferences, tumor boards, telephone calls, patient interactions, and interven-tional procedures. Optimizing our workflows and constant quality-control of our daily work (scheduling, protocols, procedures, reporting, distribution, and communication) is the foundation, basis, and pre-requisite for this, and should be self-evident, but how our report affects therapeutic decisions will directly influence patient outcome and costs of healthcare.

Will this process include an increasing automatization of our reports, at least in parts? Maybe yes. Is this detrimental or dangerous for our field? No, not, if we lead the way and use these new tools to our and our patients' advantage. Even the best trained colleague will not be able to stay perfectly up-to-date with all medical advancements. At the same time, age distribution in our western societies is changing drastically and imaging volumes are steadily increasing and will continue to do so. Thus, should we not embrace help from technology, rather than to fear it?

There are a number of ways how we could profit from AI. Besides the problem of data, image and information overflow, we will need AI for rare diseases, complex syndromes, or for decision-support systems, to face the growing complexity of our multi-disciplinary, multi-modal, and multi-scale clinical work, combining information from imaging, -omics, lab test, clinical history, and physical exams. The risk is not in the automatization, even of routine reports on frequent imaging procedures such as chest X-rays, mammograms, or CT angiographies to exclude pulmonary embolism. The crucial question will be: Who is in the driver's seat, for technical implementation of these new AI techniques, and for the final decisions. We will have to take action and participate in these developments rather than ignore them, and – if we do it right – we will be able to improve our services and quality. In this process radiologists will transform to information specialists, implementing innovative forms of data handling and data presentation, and focusing on image-guided personalization of our own interventional measures and procedures.

**2. New quality standards of radiological services**

Multimodal, molecular, and functional imaging is becoming increasingly important in the context of personalized medicine. Our non-invasive diagnostic and imaging procedures are increasingly used to support and complement the data of advanced molecular diagnostics. Complementary qualitative and quantitative imaging parameters play a major role in the assessment of our patients' individual prognosis, the prediction of treatment success and in the monitoring of the therapy effectiveness and outcome. With '-omics' technologies reaching maturity, these will be more and more implemented in clinical practice. Prospective and, where necessary, randomized clinical studies will be needed to validate novel imaging biomarkers, imaging phenotypes, and imaging signatures.

**"With recent advances in MR technology, we will optimize workflow and scanning efficiency, while providing consistent, high-quality personalized examination results at the same time, entering a new era in precision medicine."[1]**

**Professor Konstantin Nikolaou**

High quality collections of biological samples procured in a standardized manner from age- and disease-stratified collections coupled to omics- and imaging-based phenotype information are required for the purpose of identification and validation of new, ideally quantitative, imaging biomarkers. By implementing these reproducible, quantitative, and standardized imaging biomarkers, multimodal image information can be integrated with patient-specific data for the development of individualized and predictive disease models.

To reach this goal, examination protocols and image acquisition must be standardized and homogenized as far as possible, in order to achieve a comparability and transferability of results from the various imaging modalities and between different sites. In addition, strategies for a systematic structuring of our reports and findings will have to be implemented, in order to replace the traditional, descriptive reporting of findings. Structured reporting will lead to the possibility of systematic data extraction from our reports, making them more accessible to statistical correlative analyses and bioinformatics. The term 'structured analysis and reporting' thus describes the establishment of objective, quantitative, extractable, and reproducible standards, e.g., in the context of tumor-specific diagnostic criteria and follow-up. This results in complete and comprehensive reports and considerably increases the objectivity and comparability between different investigators and sites and at the same time creates the possibility to link these image data with those from molecular diagnostics and to scientifically evaluate them or integrate them in complex disease models. The implementation of standardized vocabularies and reporting rules, supported by radiological lexicons and glossaries, established and disseminated by national and international radiological societies, will further harmonize the use or radiological terms and expressions and will enable optimized indexing of our reports.

### 3. Adaptive imaging technologies in the era of precision medicine

So how, we may ask, do recent MR developments anticipate these challenges and react to the growing demands described above? Due to high levels of exam complexity, patient properties, and user variability, MRI is still considered to be one of the most complex medical imaging modalities. Innovative MR scanner technology should therefore be able to automatically or semi-automatically address anatomical and physiological differences among individual patients, thus, a wider range of routine scanning procedures as well as complex protocols will be applicable to a larger extent of patients, even those formerly not eligible for MRI examinations, delivering more robust and more consistent results. Also, in times of economic pressure, MR scanning will have to be more cost-effective, by greater robustness and acquisition speed, reducing re-scans and increasing productivity.

To provide our patients with individualized and personalized diagnostic strategies and tailored therapies, we need robust, standardized, and reproducible acquisition techniques that are constantly delivering high and comparable quality. Only then we can compare results and link them with additional information, such as data from laboratory medicine or genetic analyses. Recent technologies will allow us to access new and growing clinical fields – for instance, enabling scans in patients with cardiac arrhythmias, excess weight, or other health problems that prevent them from actively supporting the scan.

An impressive array of various innovative MR technologies will be discussed in this present edition of MAGNETOM Flash. For example, dedicated acceleration techniques implementing Compressed Sensing (GRASP-VIBE) enable dynamic, free-breathing liver examinations in one comprehensive scan by the push of button and for every patient, making breath-holds and complex timing of several dynamic contrast phases unnecessary. Optimized shimming technologies based on new hardware and transmit technologies, such as

CoilShim, one of the BioMatrix Tuners, homogenize the static magnetic field and significantly improve fat saturation and signal exploitation, e.g., in diffusion-weighted imaging (DWI) of body regions difficult to image, such as the neck. Slice-specific shimming (SliceAdjust) is introduced with MAGNETOM Vida[1] as an effective method to reduce susceptibility effects in whole-body DWI at 3T. Automatization of whole-body MR examinations, e.g. the Whole-Body Dot Engine, will significantly reduce overall imaging time, increase patient comfort and will potentially change our use of MRI, e.g., for an increased implementation of whole-body tumor staging. In cardiac imaging, implementation of highly accelerated real-time sequences will preserve diagnostic image quality even in challenging scenarios, such as in arrhythmic patients. Finally, complete free-breathing cardiac examinations will become possible.

The challenges in our field are increasing and may be greater than ever; our clinical and scientific working environment is getting more complex and more demanding. Only if we understand the challenges and take our chances, we will stay in the driver's seat, developing radiology to play an even more central role in clinical care. With recent advances in MR technology, we will optimize workflow and scanning efficiency, while providing consistent, high-quality personalized examination results at the same time, entering a new era in precision medicine.

**Konstantin Nikolaou**

**References**

1 Herold CJ, Lewin JS, Wibmer AG, Thrall JH, Krestin GP, Dixon AK, Schoenberg SO, Geckle RJ, Muellner A, Hricak H. Imaging in the Age of Precision Medicine: Summary of the Proceedings of the 10th Biannual Symposium of the International Society for Strategic Studies in Radiology. Radiology 2016;279(1):226-238.
2 Beam AL, Kohane IS. Translating Artificial Intelligence Into Clinical Care. JAMA 2016;316(22):2368-2369.
3 Jha S, Topol EJ. Adapting to Artificial Intelligence: Radiologists and Pathologists as Information Specialists. JAMA 2016;316(22):2353-2354.
4 Forsting M. Hot Topics: Will Machine Learning Change Medicine? J Nucl Med 2017.
5 Kohli M, Prevedello LM, Filice RW, Geis JR. Implementing Machine Learning in Radiology Practice and Research. AJR Am J Roentgenol 2017:1-7.

[1] The statements by Siemens' customers presented here are based on results that were achieved in the customer's unique setting. Since there is no 'typical' hospital and many variables exist (e.g., hospital size, case mix, level of IT adoption), there can be no guarantee that other customers will achieve the same results.

## Editorial Board

We appreciate your comments.
Please contact us at magnetomworld.med@siemens.com

**Antje Hellwich**
*Editor-in-chief*

**Reto Merges**
*Head of Scientific Markting*

**Sunil Kumar S.L., Ph.D.**
*Senior Manager Applications, Canada*

**Wellesley Were**
*MR Business Development Manager Australia and New Zealand*

**Gary R. McNeal, MS (BME)**
*Advanced Application Specialist, Cardiovascular MR Imaging Hoffman Estates, IL, USA*

## Review Board

**Lisa Chuah, Ph.D.**
*Global Segment Manager Neurology, Pediatrics, and Orthopedics*

**Daniel Fischer**
*Head of Outbound Marketing MR Applications*

**Berthold Kiefer, Ph.D.**
*Head of Oncological Applications*

**Heiko Meyer, Ph.D.**
*Head of Neuro Applications*

**Efren Ojeda**
*MR Marketing Application Center*

**Gregor Thörmer, Ph.D.**
*Global Segment Manager Men's and Women's Health*

# Content

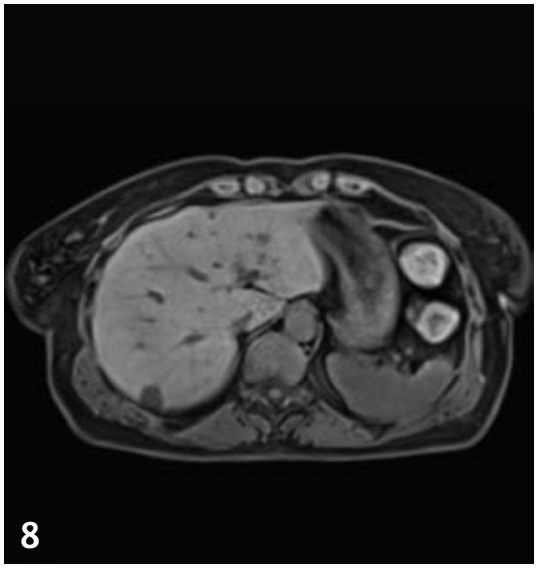


Free-breathing liver dynamics with Compressed Sensing GRASP-VIBE

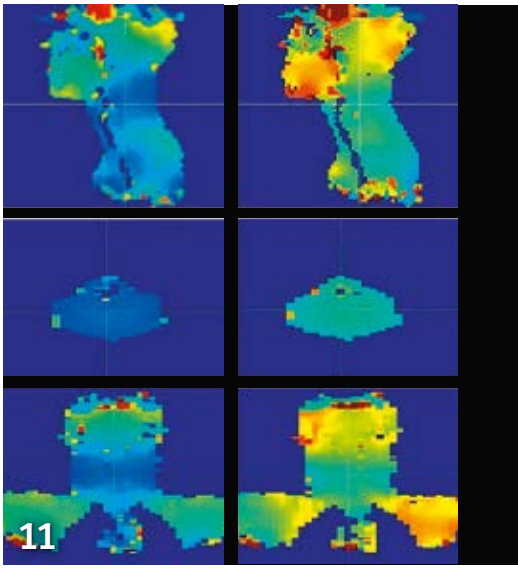


$B_0$ field map with and without BioMatrix Tuners: CoilShim


## Learn from the experience of other MAGNETOM users

The MAGNETOM World is the community of Siemens Healthcare MR users worldwide, providing you with relevant clinical information. Here you will find application tips and protocols to optimize your daily work. Lectures and presentations from experts in the field will allow you to be exposed to new ideas and alternative clinical approaches.

Put the advantages of the MAGNETOM World to work for you!

**siemens.com/magnetom-world**

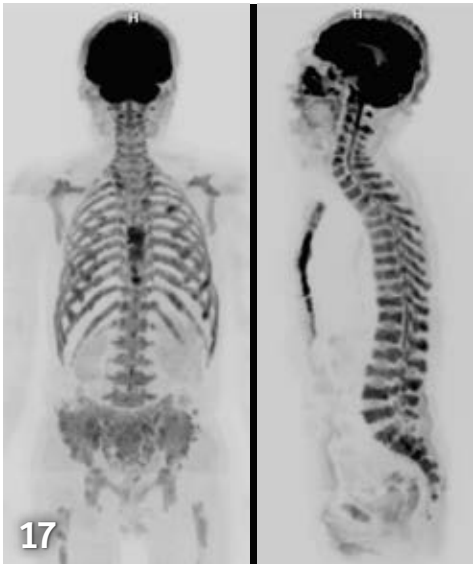


**Slice specific shimming for whole-body diffusion-weighted imaging**

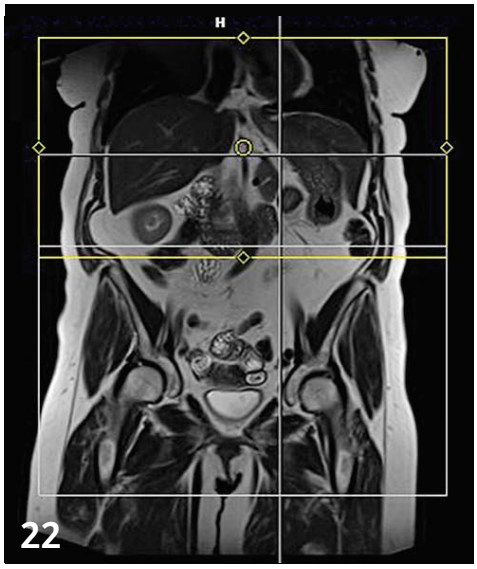


**Automated chest, abdomen, and pelvis examinations with Whole-Body Dot Engine**

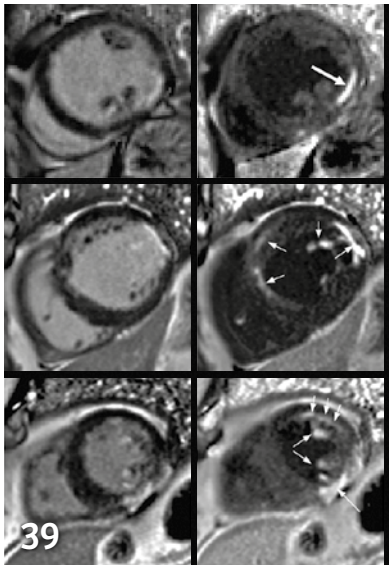


**Complete free-breathing cardiac MRI examinations with PSIR HeartFreeze**

# MAGNETOM Vida
# Embrace human nature at 3T. With BioMatrix

BioMatrix represents a paradigm shift in MRI imaging. MAGNETOM Vida is the first BioMatrix system and the latest 3T Open Bore system.

BioMatrix is a revolutionary new technology, evolving from Tim (Total imaging matrix), and it consists of three unique technologies – BioMatrix Sensors, BioMatrix Tuners, and BioMatrix Interfaces. As part of the BioMatrix Tuners, CoilShim has integrated shimming elements in the Head/Neck Coil to improve $B_0$ homogeneity, thus enabling excellent results in the c-spine in all patients (Fig. 2). New, ultra-flexible 18-channel surface coils help to consistently deliver excellence in daily clinical routine: faster setup with dedicated positioning devices, shorter exam times with Pat factors up to 3 and higher spatial resolution due to substantially higher SNR than conventional flex coils (Figs. 4, 5). Trendsetting applications for highly accelerated imaging such as Simultaneous Multi-Slice (SMS) and Compressed Sensing strongly benefit from high coil element density in the field-of-view (FOV). By introducing a new Spine 72 coil (12 rows of 6 elements) which can be seamlessly combined with Body 30 coils and the Head/Neck 64 coil it is, for example, possible to perform whole-spine examinations accelerated by a factor of 4 (Fig. 3). Equipped with a new magnet with 55 x 55 x 50 cm FOV, full coverage abdominal scans or long bone exams in one station with excellent fat saturation are feasible (Figs. 6, 7D).

Besides excellent routine clinical capabilities, MAGNETOM Vida also allows to expand the patient population eligible for MR imaging: For the first time, free-breathing liver dynamics will become clinical reality with Compressed Sensing GRASP-VIBE and children[1], multi-morbid patients, patients with hearing impairment and others can be examined without restrictions (Figs. 7C, E). At the same time, complete free-breathing

cardiac examinations are introduced with Compressed Sensing Cardiac Cine for functional assessment (Fig. 8) and PSIR HeartFreeze for late gadolinium enhancement.

With the strongest commercially available gradients in a 70 cm bore system, facilitating up to 25% higher SNR in diffusion-weighted imaging (DWI), MAGNETOM Vida is perfectly balancing the needs of neuro imaging research and high-end body imaging. The particular combination of gradient power, the new Whole-Body Dot Engine and SliceAdjust, a new technique for distortion-free whole-body DWI (Fig. 9), allows to deliver decisive information for personalized treatment decisions, e.g. in patients with multiple myeloma.

[1] MR scanning has not been established as safe for imaging fetuses and infants less than two years of age. The responsible physician must evaluate the benefits of the MR examination compared to those of other imaging procedures.

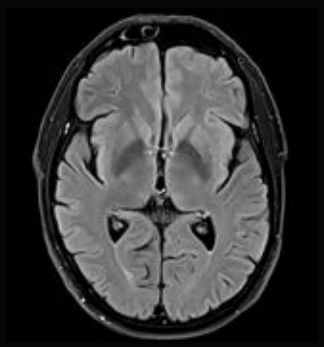

**1A**
**T2w Quiet TSE DarkFluid tra**
Head/Neck 20 with 18° tilt, TA 1:39 min x 2, TI 2500 ms, TR 9000 ms, TE 84 ms, FOV 199 x 220, matrix 203 x 320, SL 5 mm

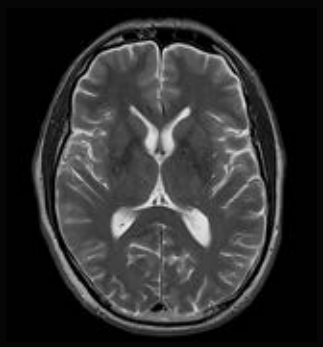

**1B**
**T2w Quiet TSE tra**
Head/Neck 20 with 18° tilt, TA 0:45 min, TR 6400 ms, TE 96 ms, PAT factor 3, FOV 220 x 220, matrix 640 x 640 interpolated, SL 5 mm

**1C**
**T2w TSE cor**
Head/Neck 64, TA 3:49 min, TR 6200 ms, TE 89 ms, FOV 220 x 220, matrix 288 x 384, SL 4 mm

**1D**
**Multi-directional diffusion-weighted EPI**
64 directions, Head/Neck 64, TA 15:45 min, TR 4500 ms, TE 76 ms, FOV 220 x 220, matrix 109 x 128

**2A**
**T2w TSE sag with CoilShim**
Head/Neck 20, TA 1:34 min x 2,
TR 3500 ms, TE 92 ms,
FOV 220 x 220, matrix 256 x 320,
SL 3 mm

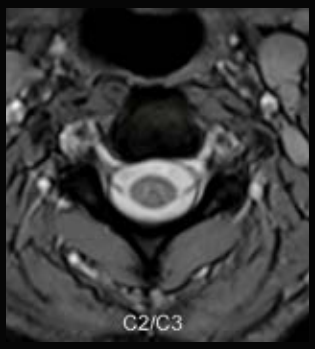


**2B**
**T2w MEDIC tra**
C-spine, TA 1:41 min x 2,
TR 373 ms, TE 12 ms,
FOV 180 x 180, matrix 436 x 512
interpolated, SL 3 mm

**4A**
**T1w TSE cor**
Ultra Flex coil small,
TA 1:57 min, TR 809 ms,
TE 13 ms, FOV 120 x 120,
matrix 358 x 512, SL 2.5 mm

**4B**
**PDw TSE sag**
Ultra Flex coil small, TA 2:20 min,
TR 3420 ms, TE 36 ms,
PAT factor 2, FOV 120 x 120,
matrix 448 x 448, SL 2.5 mm

**3A**
**T2w TSE sag**


**3B**
**Spine Dot Engine AutoLabeling**

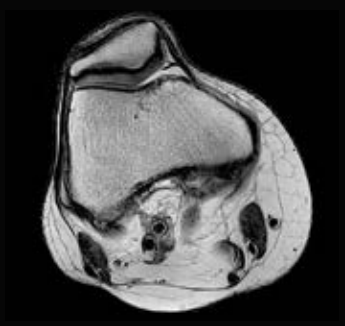

**5A**
**T2w TSE tra**
Ultra Flex coil large,
TA 2:06 min, TR 4690 ms,
TE 76 ms, FOV 140 x 140,
matrix 384 x 512, SL 3 mm

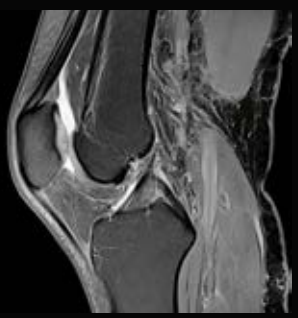

**5B**
**PDw TSE fatsat sag**
Ultra Flex coil large,
TA 3:45 min, TR 3260 ms,
TE 33 ms, FOV 140 x 140,
matrix 307 x 384, SL 3 mm

**6A**
**PDw TSE Dixon cor**
Body 18, Spine coil 72,
TA 2:01 min x 2,
TR 2700 ms, TE 37 ms,
FOV 309 x 550,
matrix 351 x 832, SL 3 mm

**6B**
**PDw TSE STIR cor**
Body 18, Spine coil 72,
TA 3:14 min, TI 220 ms,
TR 3670 ms, TE 31 ms,
FOV 309 x 550,
matrix 297 x 704, SL 3 mm

**6C**
**T1w TSE cor**
Body 18, Spine coil 72,
TA 2:02 min x 2,
TR 793 ms, TE 11 ms,
FOV 241 x 550,
matrix 274 x 896, SL 3 mm

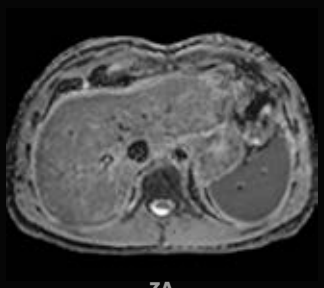

**7A**
**ADC map EPI diffusion with respiratory sensor**
Body 18, Spine 72, TA 41 sec,
TR 2000 ms, TE 44 ms,
FOV 306 x 280, matrix 108 x 134,
SL 5 mm

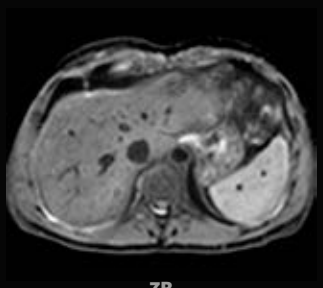

**7B**
**Trace-weighted EPI diffusion with respiratory sensor**
Body 18, Spine 72, TA 41 sec,
TR 2000 ms, TE 44 ms,
FOV 306 x 280, matrix 108 x 134,
SL 5 mm

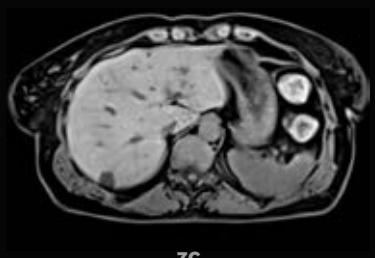

**7C**
**T1w GRASP-VIBE fat sat tra**
Body 18, Spine 72, TA 8 sec,
TR 3.5 ms, TE 1.3 ms,
FOV 355 x 355, matrix 256 x 256

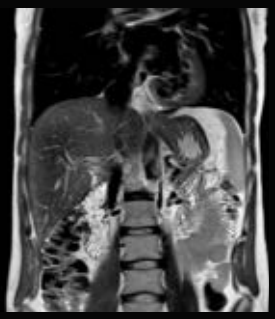

**7D**
**T2w HASTE cor triggered**
Body 18, Spine 72, TA 39 sec,
TR 2000 ms, TE 85 ms,
FOV 400 x 400, matrix 307p x 384

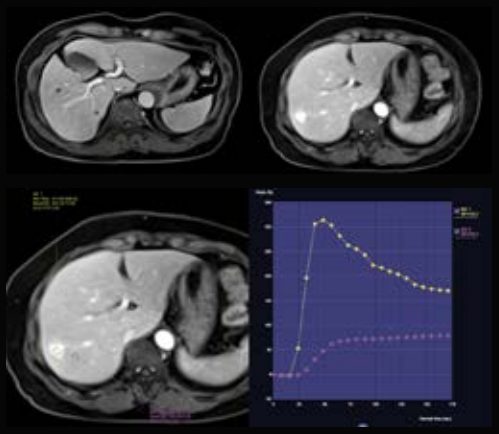

**7E**
**T1w GRASP-VIBE fat sat tra**
Series 22, TA 8.1 sec,
TR 3.5 ms, TE 1.5 ms,
FOV 450, matrix 256 x 256,
SL 3 interpolated

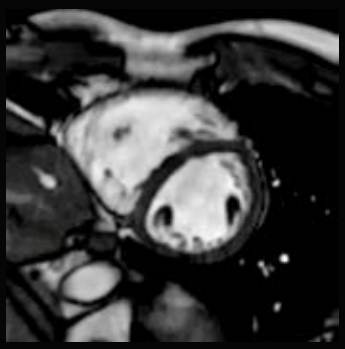

**8**
**Compressed Sensing Cardiac Cine TrueFISP 5 shot sax 5 slices**
Body 18, Spine 32, TA 0.5 sec,
TR 12 ms, TE 1.3 ms, FOV 360 x 294,
matrix 189 x 240, SL 8 mm

**9A**
**Whole-body DWI b-value 800 MIP cor**

**9B**
**Whole-body T2w TIRM cor**

**9C**
**Whole-body VIBE Dixon water cor**

# BioMatrix Tuners: CoilShim

**Miriam R. Keil, Ph.D.; Jörg Rothard; Carmel Hayes, Ph.D.**

Siemens Healthineers, Erlangen, Germany

A cervical spine or neck MRI can provide valuable diagnostic information for a wide range of different conditions. In particular, MRI's soft tissue contrast helps to detect and monitor a variety of pathologies, misalignments or injuries. It can be useful in evaluating symptoms such as pain, foreign body sensations, numbness, tingling or weakness in the arms, shoulder or neck area and can assist in detecting certain chronic diseases of the nervous system. It is also used in tumor diagnosis and in the assessment of bleeding, swelling, infections, or inflammatory conditions in the vertebrae or surrounding tissues.

In many patients, MR image quality in the neck or cervical spine region might be degraded by $B_0$ field distortions. These typically arise from tissue interfaces with different susceptibilities in this region, for example in the vicinity of the lung, between vertebrae, fluid-filled cavities, as well as from the body contour itself in the shoulders and neck area (Fig. 1). The low field homogeneity poses a challenge to MR imaging in this region and is often the source of image quality issues. Examples include insufficient fat saturation, spatial variations in the signal strength along the vertebrae, as well as regions showing complete signal loss.

With MAGNETOM Vida a new technology platform, BioMatrix, is introduced, which combines the ability to adapt to the individual patient's biovariability and the established Tim integrated matrix coil technology. This, in particular, allows to substantially improve image quality in the neck area by utilizing CoilShim. CoilShim is one of the new BioMatrix technologies which allows for correction of patient-induced $B_0$ field inhomogeneities using dedicated shimming channels integrated into the Head/Neck coil.

Two new Head/Neck coils support CoilShim: the BioMatrix Head/Neck 20 TCS (Tiltable, CoilShim) and the BioMatrix 64 CS (CoilShim). A first step in the compensation of patient-induced $B_0$ field inhomogeneities is the identification of the origin of these variations. Experiments indicate that there are two major sources of $B_0$ field inhomogeneities in head and neck MRI. These are the patients' shoulders on the one hand and the $B_0$ field distortion due to the neck on the other hand. The inhomogeneity pattern originates from the geometric shape of the human body in the head and neck area and the resulting difference in susceptibilities. Figure 1 shows a typical $B_0$ field inhomogeneity 'map' of the head and neck region. The map was generated from a principal component analysis performed on datasets from 19 volunteer scans. The analysis showed that only the first main component contains significant information. This suggests that the inhomogeneity pattern is likely to be the same for different body shapes and sizes and that only the magnitude of the inhomogeneity varies. To correct for $B_0$ field inhomogeneities in the shoulder and neck region, each of the two head and neck coils is equipped with two CoilShim channels (Fig. 2). The CoilShim channels are located in the posterior part of the Head/Neck coils,

1

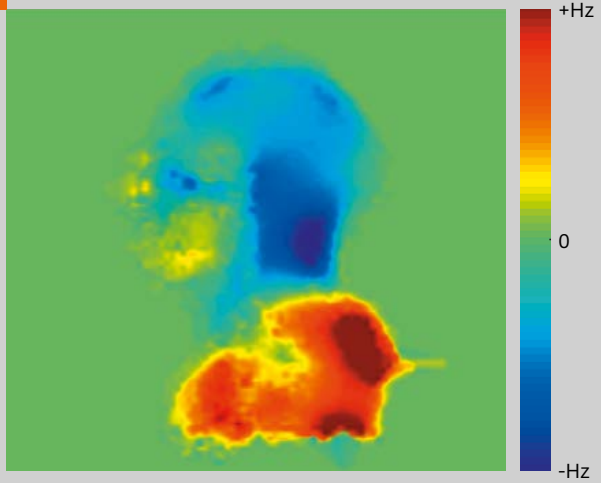


**Figure 1:** Typical $B_0$ field distortion pattern as seen in the sagittal orientation.

2

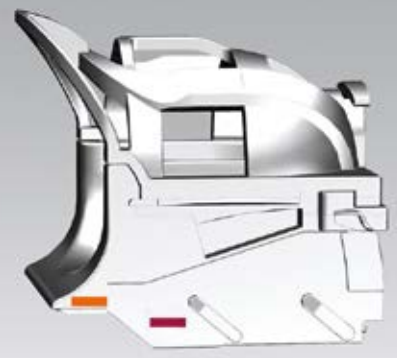


**Figure 2:** BioMatrix Head/Neck 20 TCS coil design and the location of the CoilShim elements in the BioMatrix Head/Neck 20 TCS coil.

allowing the CoilShim technology to be used even when the anterior part of the Head/Neck coils are detached. The magnitude of the $B_0$ field generated by each CoilShim channel can be adjusted independently with very fine resolution. This allows for best possible $B_0$ homogenization for each individual patient.

In order to ensure both adequate image quality and patient safety with the new Head/Neck coils with integrated CoilShim, special measures have been taken. These measures ensure decoupling of the CoilShim elements during the transmit phase and decoupling from the gradient system during the transmit and receive phase of the MR acquisition.

## Applications

The usage of CoilShim requires no dedicated patient preparation: the patient can be positioned within the Biomatrix Head/Neck coil[1] as with any other head coil. When using the 20-channel TCS coil, the tilt angle may be adapted to the patients' needs, thereby providing increased patient comfort. Tilting the coil does not interfere with the CoilShim functionality but CoilShim may improve image quality degradations resulting from tilting.

CoilShim can be used with all clinical head and neck sequences and protocols, provided that the BioMatrix Head/Neck coil is plugged and active. "CoilShim" is turned on in the user interface by switching the respective parameter, which can be found on the tabcard "System", sub tab "Adjustments" from "Off" to "Auto". The actual enabling of CoilShim technology itself is therefore controlled automatically, depending on the slice geometry and the protocol parameters.

## Results

The physical effect of the CoilShim feature on the $B_0$ field is illustrated in Figure 3, acquired in a healthy volunteer. The images compare $B_0$ field maps obtained using clinical state-of-the-art standard shimming with those which result from the usage of CoilShim technology.

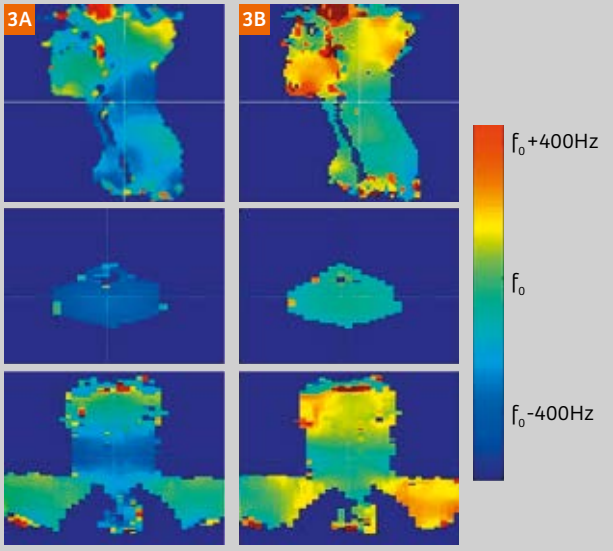


**Figure 3:** $B_0$ field map in the all three main orientations without **(3A)** and with CoilShim **(3B).** The frequency shift relative to $f_0$ is shown in Hz.

The images show relative resonance frequency shifts in three orthogonal slice orientations. Once again, the two dominant sources of field inhomogeneity in the shoulder and in the neck area can be observed. In this example the frequency shift in the shoulder region is about 400 Hz and the frequency shift in the neck area is about -200 Hz. Given that the frequency shift between fat and water is 430 Hz at 3T, non-uniform fat saturation can be expected in such cases.

To further illustrate the impact of CoilShim on the quality of the shimmed region of interest, Figure 4 shows the frequency distribution of all voxels within the adjustment volume both with and without CoilShim. The spectrum of the frequencies within the adjustment volume is significantly narrowed on applying CoilShim.

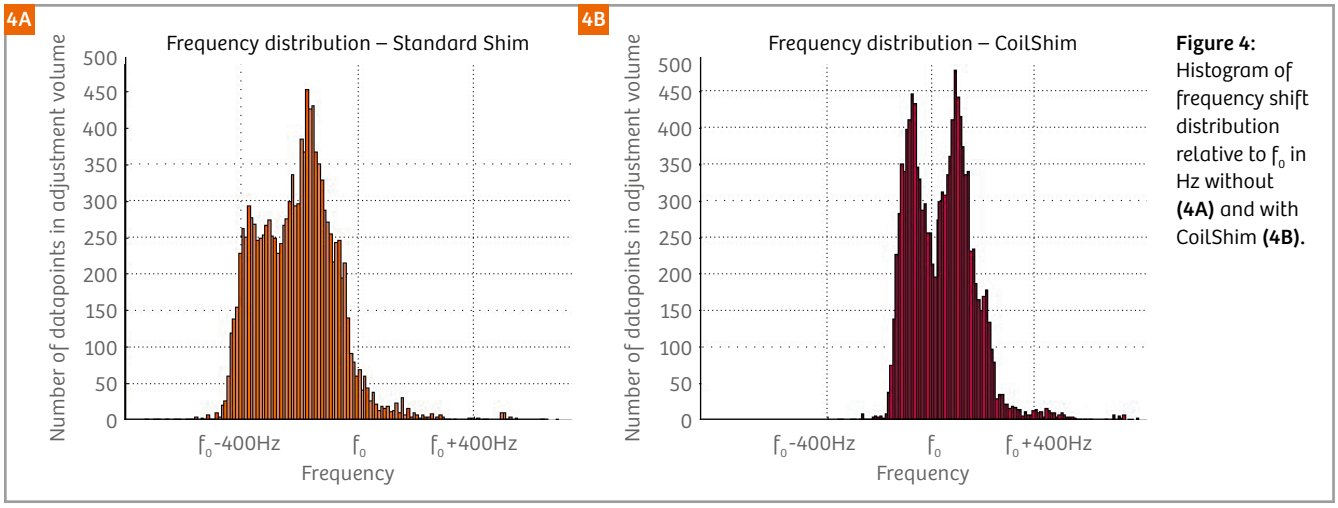


**Figure 4:** Histogram of frequency shift distribution relative to $f_0$ in Hz without **(4A)** and with CoilShim **(4B).**

The improved field homogeneity is beneficial for all MR imaging studies in the head and neck. Applications which require a highly homogenous field, for example fat saturated or SPAIR images, or EPI-based imaging, benefit in particular from local shimming. Figures 5 and 6 show typical image examples obtained in several volunteers of different physical constitution. Figure 5 shows T1-weighted, fat saturated TSE images of the c-spine, Figure 6 illustrates the benefits of CoilShim in T2-weighted TSE images obtained with SPAIR preparation pulses. An axial T2-weighted BLADE image with SPAIR preparation pulses is shown in Figure 7. All examples show that more homogeneous fat saturation

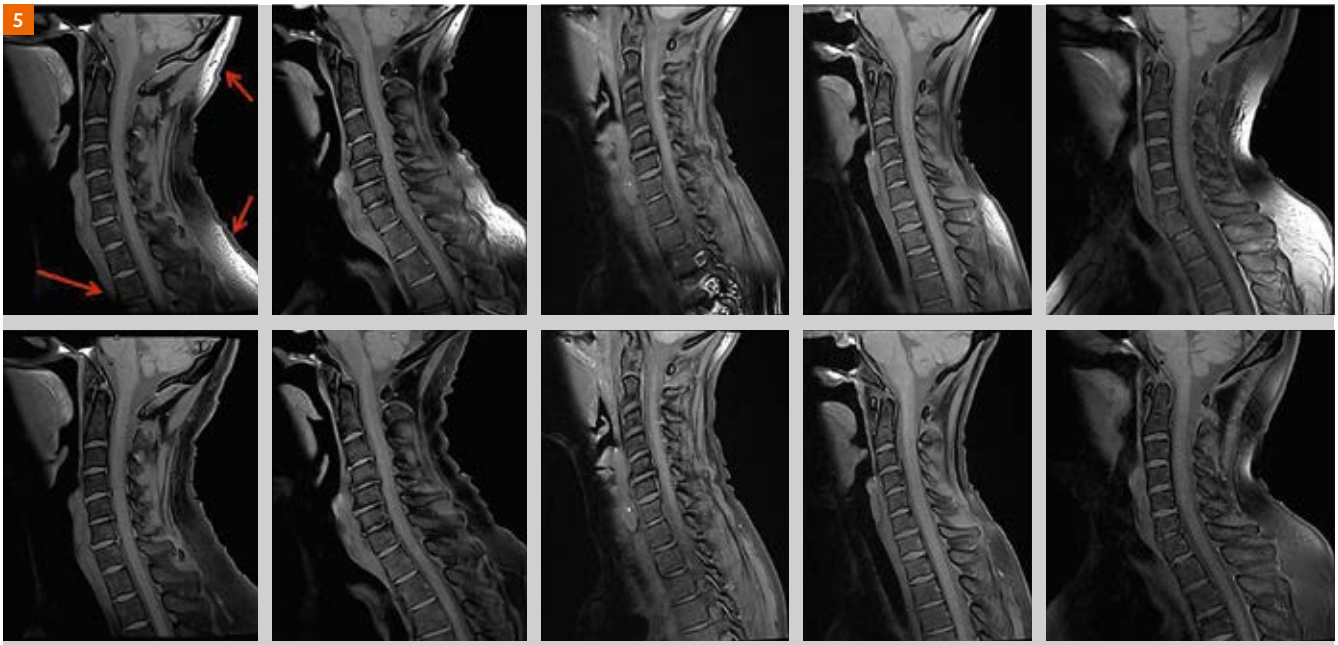


**Figure 5:** T1-weighted TSE images with fat saturation in five different volunteers. Using CoilShim (lower row) improved the fat saturation not only within the vertebrae but also in the posterior areas. The contrast between vertebrae and disk is also improved.

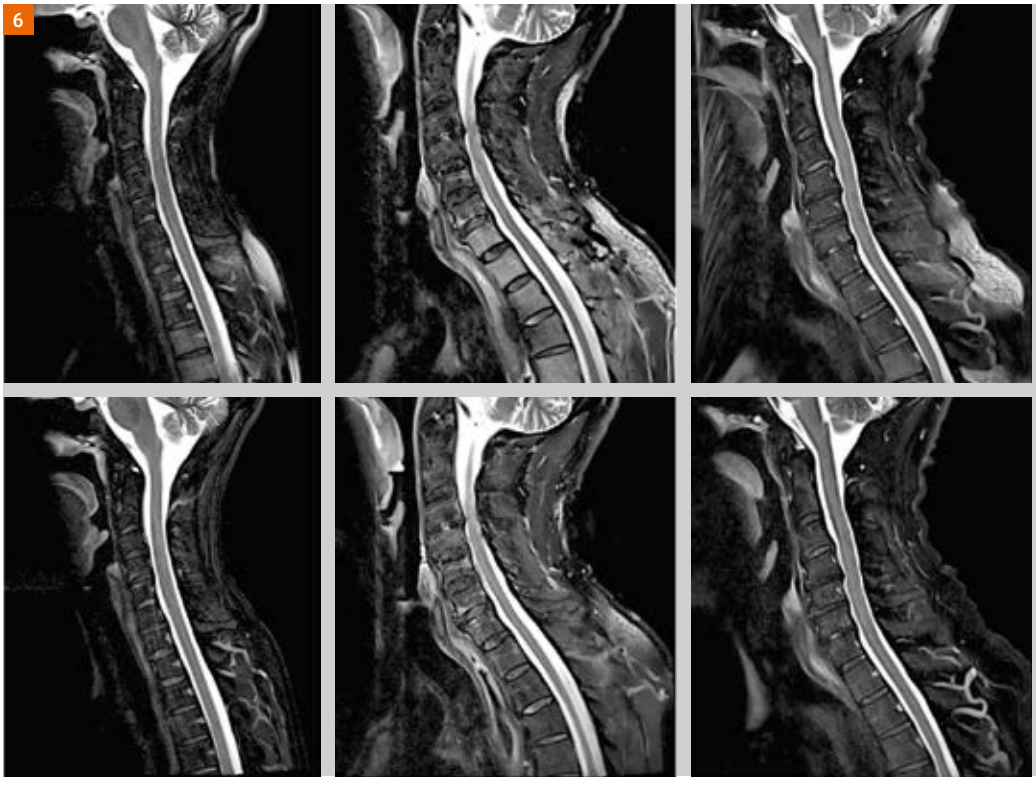


**Figure 6:** T2-weighted TSE images with SPAIR fat saturation in three different volunteers. Note the intensity gradient within the vertebrae without CoilShim (upper row). The image with active CoilShim on the right shows better homogeneity within the vertebrae and less contribution of unsaturated fatty tissue.

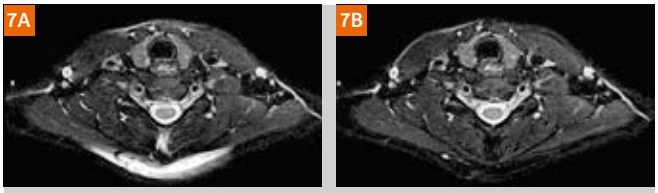


**Figure 7:** T2-weighted BLADE images with SPAIR fat saturation. The same imaging protocol was used with **(7A)** and without **(7B)** CoilShim. The fat saturation is more homogeneous when CoilShim is active.

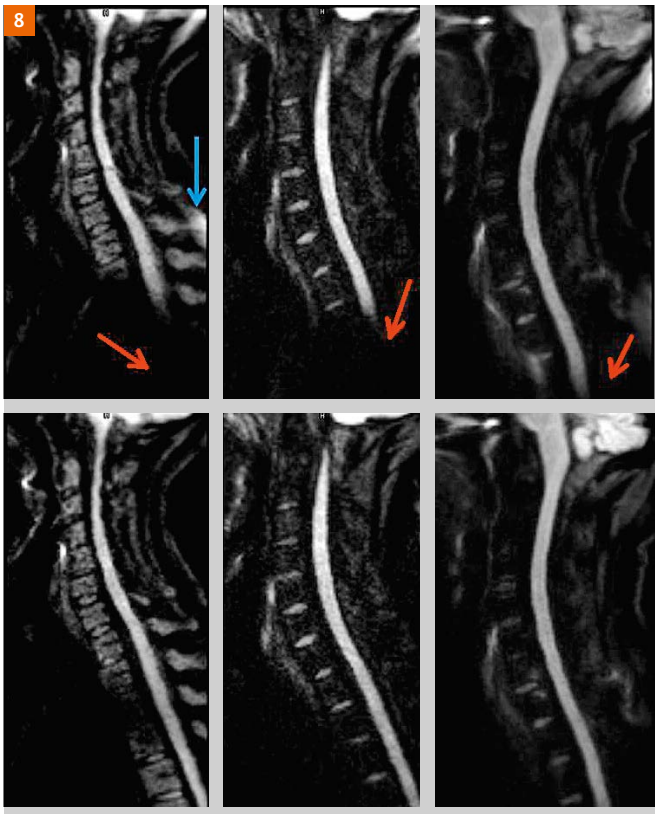


**Figure 8:** RESOLVE images of the c-spine with b=600 mm/s² in three volunteers. Note the lack of signal (red arrow) in the spinal canal when measured without CoilShim (upper row). Fat saturation is also more consistent (blue arrow).

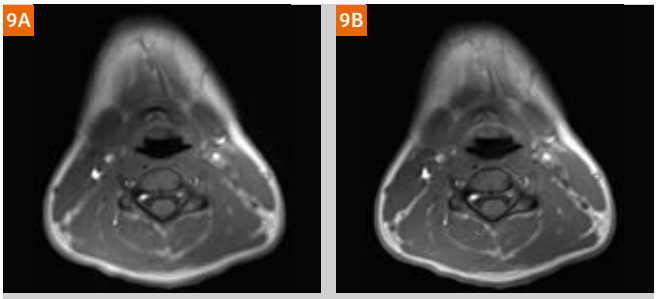


**Figure 9:** Radial sequences like the StarVIBE also benefit from higher field homogeneity. **(9A)** was measured without CoilShim, **(9B)** with active CoilShim. Note the increased image sharpness with CoilShim.

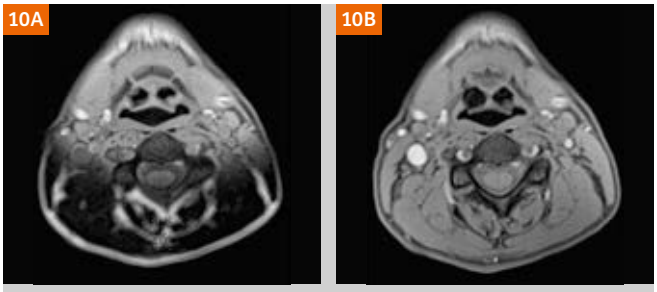


**Figure 10:** T1-weighted StarVibe images acquired in the neck. CoilShim **(10B),** can correct the field distortions which caused a shift in the frequency spectrum, inducing water saturation and corrupting image quality.

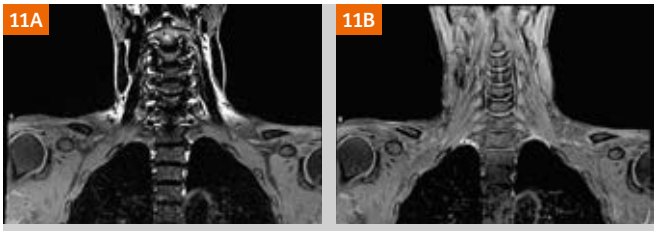


**Figure 11:** In rare cases, the field inhomogeneities at the border between neck and thorax are so severe, that the frequency is shifted. In these extreme examples, CoilShim **(11B)** also helps to mitigate the effects.

can be achieved with CoilShim. This in turn facilitates better lesion differentiation, in particular in the lower vertebrae.

Figure 8 shows RESOLVE diffusion-weighted images with a b-value of 600 mm/s² with and without CoilShim. Until now the display of the entire spinal canal was challenging, with CoilShim it becomes feasible to follow the spinal canal over the whole field-of-view.

Imaging methods which employ radial trajectories, for example the StarVIBE sequence, or methods such as TrueFISP, which demand a high field uniformity, also benefit from CoilShim technology and produce sharper or more homogeneous images. Figure 9 compares StarVIBE images obtained with and without CoilShim. Less homogeneous $B_0$ fields broaden the frequency spectra, leading to a shift in the readout direction. Since radial sequences sample *k*-space not in one, but in various directions, any off-resonance dephasing shift effect is propagated into a different direction, leading to blurred images. Larger variations in $B_0$ homogeneity can cause frequency shifts, which in turn lead to a degradation in image contrast, as shown in Figure 10 for a StarVIBE, and in Figure 11 for a TSE acquisition. Such issues can be avoided when using CoilShim.

12

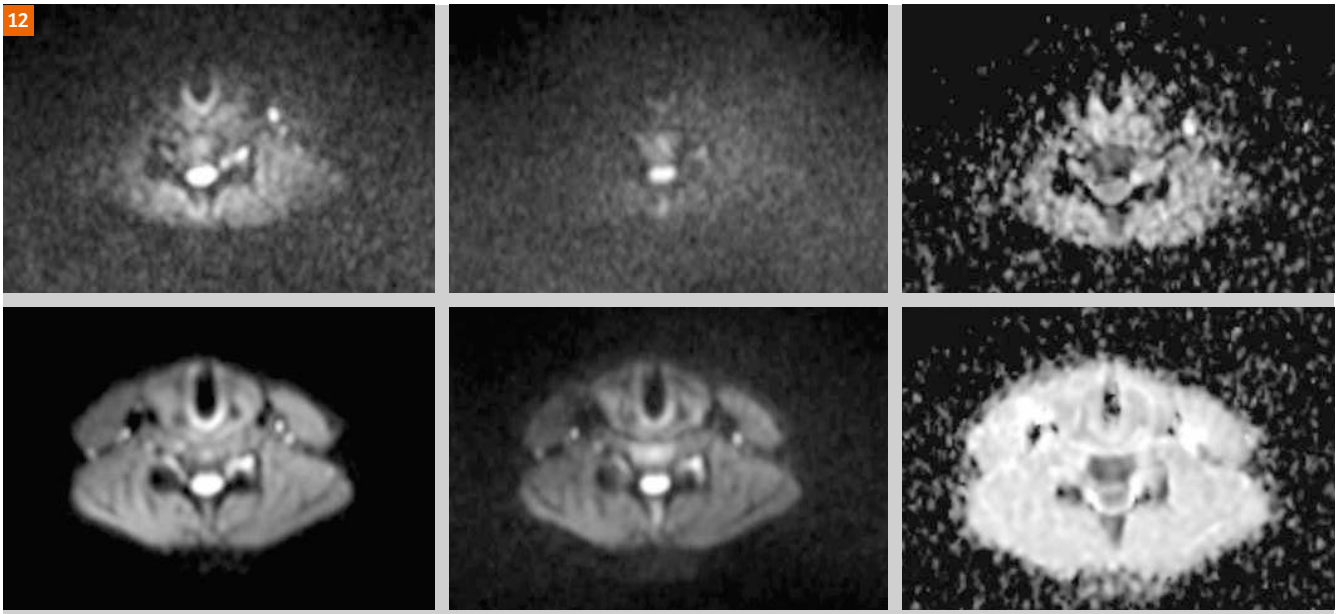

**Figure 12:** Combining CoilShim with SliceAdjust leads to significant image quality improvements in diffusion-weighted imaging. Less distortions and better spatial fidelity, significantly higher SNR for all b-values provides a new level of diagnostic reliability. The same slice is compared without CoilShim and SliceAdjust (upper row) and with active CoilShim and SliceAdjust (lower row). From left to right: b=50 s/mm², b=800 s/mm², ADC.

In combination with SliceAdjust, CoilShim technology allows for robust diffusion-weighted imaging (DWI) in the neck area. In the past, DWI imaging of the c-spine or neck soft tissue was challenged by distortions, low signal intensity and artefacts. On enabling the BioMatrix Tuners, the image quality can be improved significantly. Figure 12 illustrates the advantages of CoilShim and SliceAdjust when activated in a DWI image of the neck.

## Practical tips

CoilShim is designed to optimize, in particular, the field homogeneity in the cervical spine. Therefore, it works best when imaging the cervical spine, especially in sagittal slice orientations. However, the whole neck area benefits when using CoilShim, although there are some physical limitations. First of all, as the CoilShim elements are located for safety reasons in the lower part of the Head/Neck coil, the scope of the feature is regionally restricted. For this reason, a drop in $B_0$ field homogeneity in the vicinity of the anterior part of the neck or the chin area may be observed. This effect may be manifested, as shown in Figure 13 for example, by inhomogeneous fat saturation in the chin area due to the regional limitations of the CoilShim field. The same applies to the shoulders, since the CoilShim elements cannot cover the entire shoulder region. This is shown in Figure 14. Another occasionally-observed effect is a frequency change in the t-spine next to the lung, seen usually in coronal images. As CoilShim optimizes the c-spine and cannot reach the vertebrae of the t-spine, the $B_0$ field

13

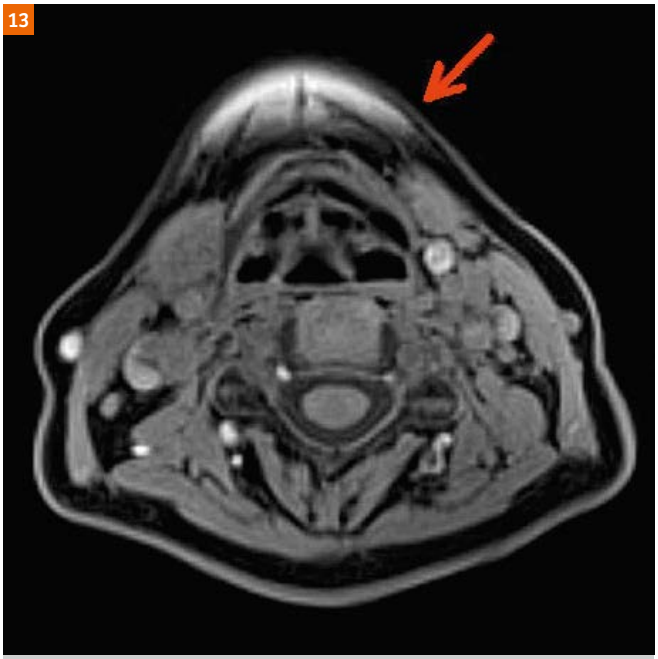

**Figure 13:** Anterior regions like the chin cannot be reached by CoilShim, which is located in the posterior neck coil region. Typically, in such cases, small regions with insufficient fat saturation are observed.

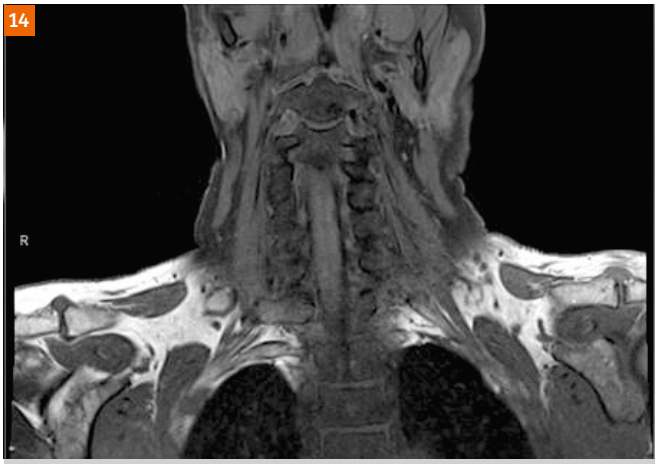


**Figure 14:** The local effectiveness of the CoilShim elements can lead to less efficient fat saturation in the lateral shoulder area.

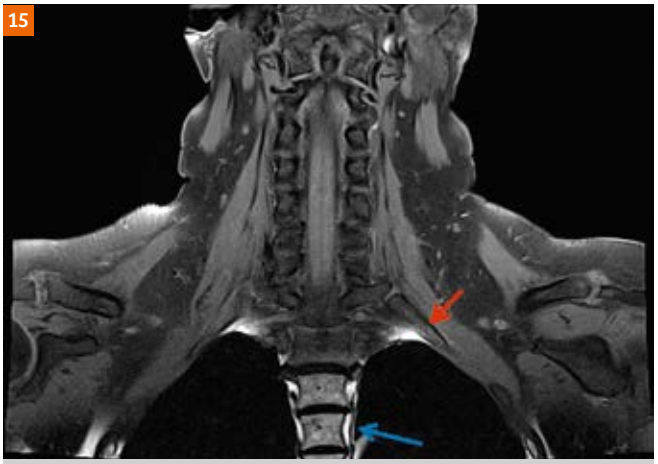


**Figure 15:** Typical lung-tip artefact (red arrow) and water saturation (blue arrow) in the t-spine. Note the homogeneous fat saturation in the neck/shoulder area.

is dominated by the lung, which might lead to lower field homogeneity with degradations in image quality in the t-spine as shown in Figure 15. The same image also shows the so called lung-tip artefact, which originates from local field distortions, leading to a less efficient fat saturation in a small area around the lung apex.

## Summary

CoilShim addresses field disturbances within the head and neck region by local, patient-adapted shim currents. This helps to homogenize the static magnetic field in this region. Thereby the image quality can be improved. Typical benefits include more homogeneous fat saturation, less blurring in radial sequences and more signal with diffusion weighted imaging. Since CoilShim is based on new hardware and transmit pathways, it is currently only available with the BioMatrix Head/Neck coils. Nonetheless, this new technology might also be useful to improve $B_0$ homogeneity in other body regions in the future.

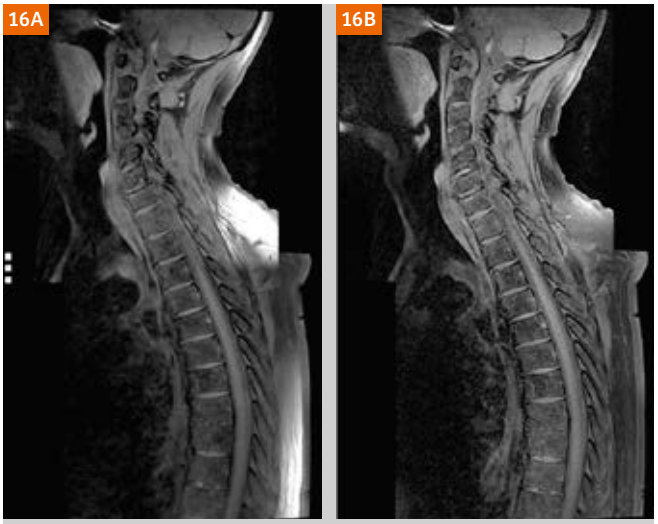


**Figure 16:** Composing for whole-spine representations also benefits from CoilShim **(16B).**

**Contact**

Miriam Keil

Siemens Healthcare GmbH

HC DI MR R&D SYS APPL
Post Box 91050
91050 Erlangen
Germany
Phone: +49 (9131) 84-4671
miriam.keil@siemens-healthineers.com

Miriam R. Keil

Jörg Rothard

Carmel Hayes

# Slice Specific Shimming Improves the Image Quality of Whole-Body Diffusion-Weighted Examinations at 3T

**Zhang Haibo[1]; Xue Huadan[2]; Alto Stemmer[3]; Liu Hui[4]; Stephan Kannengiesser[3]; Berthold Kiefer[3]; Jin Zhengyu[2]**

[1] Department of Radiology, China-Japan Friendship Hospital, Beijing, China
[2] Department of Radiology, Peking Union Medical College Hospital, Peking Union Medical College and Chinese Academy of Medical Sciences, Beijing, China
[3] MR Application-Predevelopment, Siemens Healthcare, Erlangen, Germany
[4] MR Collaboration, Siemens Healthcare, Shanghai, China

## Current whole-body diffusion-weighted imaging

Whole-body diffusion-weighted imaging (WBDWI) is considered a powerful clinical tool in the detection, characterization, and treatment-response monitoring of tumors [1, 2]. It has been increasingly used in the evaluation of multiple myeloma, lymphoma, and skeletal metastases [3–8]. Being a measure of the microscopic water motion, WBDWI provides a quantitative way of evaluating the tissue cellularity using the apparent diffusion coefficient (ADC). For example, whole-body magnetic resonance imaging including WBDWI is sensitive to multiple myeloma, especially in the case of diffuse bone marrow infiltration [9]. The combination of WBDWI with Fluorodeoxyglucose Positron Emission Tomography (FDG-PET) may provide a multi-parametric assessment of tumors due to complementary imaging principles, where diffusion-weighted imaging (DWI) evaluates the tumor cellularity and the FDG-PET assesses the tumor metabolism [10].

At present it is challenging to meet the clinical demands for image quality with WBDWI at 3 Tesla. The signal-to-noise ratio (SNR) is increased at 3T, but it is still a challenge to perform WBDWI due to the drawback of single-shot echo planar imaging (EPI) acquisition and the stronger susceptibility effects, which lead to stronger geometric distortions and poor fat-suppression performance in specific body regions such as the neck. The distortions $\Delta d$ in EPI are proportional to the physical field-of-view (FOV) in the phase-encoding direction ($FOV_{PE}$), the echo spacing $\Delta t_{PE}$, and the local off-resonance $\Delta B_0$ ($\Delta d \sim FOV_{PE} \times \Delta t_{PE} \times \Delta B_0$). Recent technical developments in DWI acquisition such as

1

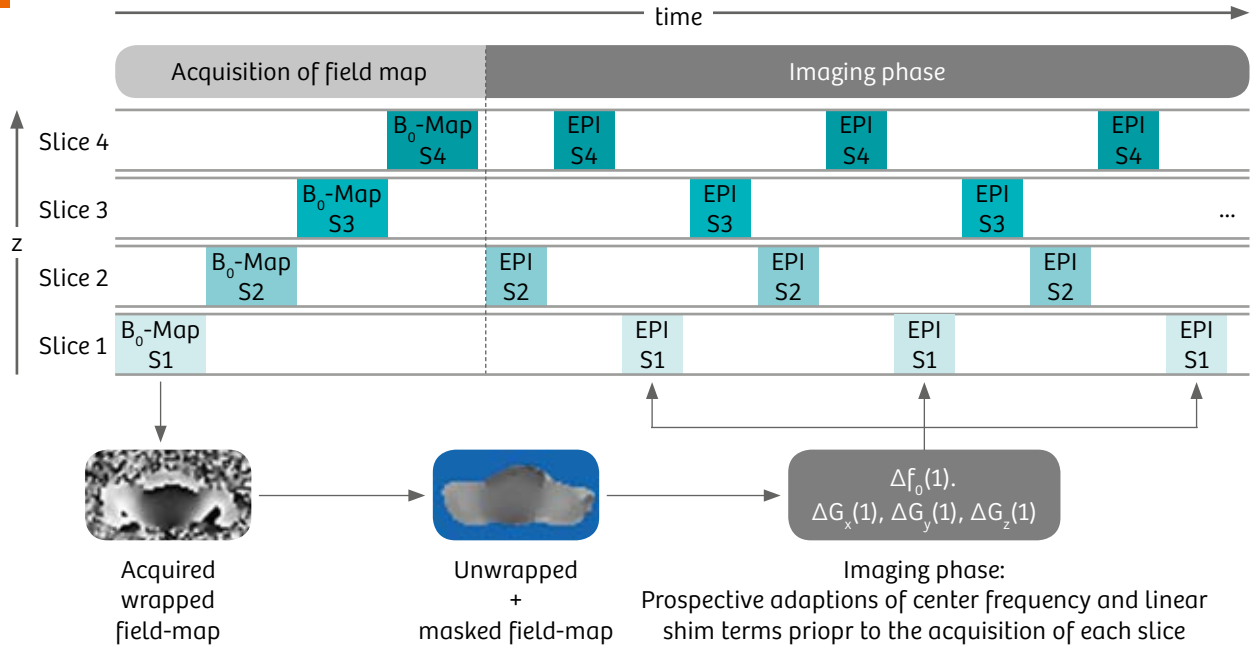


**Figure 1:** Schematics of the prototype of a slice specific adjustment sequence.

readout segmented EPI [11, 12], other multi-shot [13] and zoomed techniques [14, 15] have shown improvements with less geometric distortion and higher image quality from the perspective of reducing $\Delta t_{PE}$ or $FOV_{PE}$. However, the above techniques are not clinically feasible for whole-body imaging because of longer acquisition time, FOV restrictions, or sensitivity to motion.

## Slice specific adjustment

Several past studies have shown the feasibility of reduced susceptibility artifact by dynamically updating optimized shim settings for each individual slice in a multi-slice acquisition [16]. Another study using slice-dependent adjustment has also shown improved image quality in 3T breast DWI [17]. However, its advantage to WBDWI is still unknown. The approach described here is to use slice specific adjustments[1] for WBDWI, where a 2D multi-echo gradient echo (GRE) sequence preceding the WBDWI EPI scan is used to acquire a $B_0$-map for each imaging slice. From the $B_0$-map an optimal center frequency and linear shim terms are determined for each imaging slice. Center frequency and gradient offsets are then updated before the acquisition of each EPI imaging slice in real time. In a recent study, its performance was evaluated, comparing slice specific adjustment to a conventional pre-scan based shimming technique (3D Shim) [18].

For the 3D Shim protocol, one set of shim terms up to 2$^{nd}$ order is used for the entire slice stack of each patient table position, and the acquisition of the field map is included in the automatic scanner adjustment, which takes approximately 33 seconds per station (35 slices per station). Additionally, a single center frequency is determined in a separate frequency adjustment. Center frequency and shim currents are set once prior to the EPI scan.

For the slice specific adjustment protocol, the patient-specific 3D Shim procedure in the automatic scanner adjustment is disabled. The acquisition of the field map is integrated into the single-shot DWI EPI sequence. This prototype sequence first acquires 2D multi-gradient-echo images for each imaging slice with its FOV and orientation adapted from the respective imaging slice. The echo-time difference of the first and last echo is chosen such that fat and water are in-phase. Then a phase difference image is calculated from these two echoes. The remaining processing of the field map data is done in 3D and comprised phase unwrapping, background masking and a calibration to avoid global 2π offsets after unwrapping. For the dynamic shimming, a 2D plane is fitted to each field map slice to determine the center frequency and gradient offsets (1$^{st}$ order shim terms). Center frequency and gradient offsets are then updated before the acquisition of each EPI imaging slice in real time (Fig. 1). The time for the acquisition of the field map is approximately 540 ms per slice, or 19 s for a 35 slices station. Processing time of the field map is negligible.

## Clinical evaluation

The evaluation of the slice specific adjustment technique for WBDWI in comparison to the conventional 3D Shim was performed at Peking Union Medical College Hospital. The slice specific adjustment and the 3D Shim WBDWI acquisitions with the exact same scan parameters were performed sequentially, and the impact of different shimming techniques on the image quality and detectability of conspicuous lesions were quantitatively analyzed and evaluated. Body-region-dependent signal-to-noise ratio (SNR), body-region-dependent shimming parameters, image quality, and the number of suspicious lesions were compared in 2 volunteers and 29 patients with suspected plasma-disorder. The results were as follows:

**1. SNR**
Two volunteers' position-dependent SNR ratio of slice specific adjustment over 3D Shim showed a significant SNR improvement with slice specific adjustment in the neck region, and a comparable SNR in other body regions. For the neck region, none of the 29 patients showed obvious signal loss with slice specific adjustment, while 25 patients showed partial to complete signal loss with 3D Shim scanning (Fig. 2).

**2. Position-dependent slice specific adjustment parameters**
The position-dependent slice specific adjustment parameters, center frequency shift, and linear frequency shift in phase-encoding direction, deviated significantly from the corresponding values of the 3D Shim settings only in the neck region, while they were comparable in the other body regions.

**3. Image quality**
Spatial displacement of DWI images was quantified by comparison with reformatted T2 SPACE images. This displacement was evaluated from cervical to coccyx vertebrae, excluding the neck region with signal loss (Figs. 2, 3). The mean absolute spatial displacement of the spine was 3.89 mm for slice specific adjustment and 7.21 mm for 3D Shim, respectively. The slice specific adjustment technique showed a significantly better illustration of the body shape than 3D Shim WBDWI.

**4. Lesion detection assessment**
Visual inspection of slice specific adjustment and 3D Shim DWI images side by side showed that the same lesions could be observed with both techniques in the thorax, abdomen and pelvis regions, while 24 of 72 lesions visible in slice specific adjustment DWI images of the neck region were not visible in 3D Shim DWI images; all lesions observed in 3D Shim DWI were also visible in slice specific adjustment DWI images.

## Discussion

Signal loss is very common in the neck region of conventional 3D Shim WBDWI because there the $B_0$ varies rapidly along the head-foot direction caused by the sudden change of the body shape. Especially when a body station covers

the neck and part of the shoulder region, the 3D Shim adjustment may be insufficient since one single setting of resonance frequency and shim terms is not able to homogenize the $B_0$ field in the whole volume. In this study, the neck region showed a larger variation of center frequency shift and linear frequency shift in the phase-encoding direction than other body regions, and at the same time the lowest image quality of 3D Shim images, which supports this hypothesis. By applying a slice-based individual center frequency and gradient offset setting, the slice specific adjustment technique produced improved SNR and reliable image quality in the neck region and therefore outperforms 3D Shim. In other body regions such as thorax, abdomen and pelvis, there were no significant differences between slice specific adjustment and 3D Shim WBDWI for lesions and muscle.

WBDWI provides a global assessment of whole-body tumor burden by visually assessing the signal intensity distribution on maximum intensity projections (MIPs) from high-b-value images. But practically the whole-body images are acquired with multiple patient table positions, and are then composed to show the whole-body view (Fig. 3). Therefore, the signal homogeneity across different body parts is quite important, and lesions spanning images from adjacent patient table positions might be missed or misidentified as a result of large signal differences between these images. The image quality evaluation showed that the slice specific adjustment technique produced a smoother signal transition between adjacent patient table positions than the 3D Shim technique.

It is possible to further reduce the remaining distortions significantly with a recent extension of the slice specific adjustment prototype sequence as described in [19]. The modification combines the prospective slice-specific center-frequency adjustment and 1st order shimming with retrospective distortion correction based on the field-map method [20]. The field-map method uses a measured field-map to undo the distortion on a pixel-wise scale during post-processing. In the combined method, the field-map needed for the distortion correction is not re-measured after center frequency adjustment and shimming but calculated from the field-map measured at the beginning and the known frequency and shim settings. It therefore does not prolong the acquisition time. It is a matter of further evaluation to enroll new patients to test the slice specific adjustment method together with retrospective distortion correction.

Short TI Inversion Recovery (STIR) fat suppression, which was used here, leads to lower SNR compared with chemical-shift-based fat suppression methods since water signal which is also inverted by the inversion pulse is not fully recovered at excitation time. Chemical shift based fat suppression techniques, however, are very sensitive to $B_0$ inhomogeneity [21, 22], so that the image quality can be degraded by fat ghosting or water suppression. As slice specific adjustment helps to significantly reduce the $B_0$ inhomogeneity, chemical shift based fat suppression techniques might provide an efficient fat suppression from head to toe. Chemical shift based fat suppression techniques

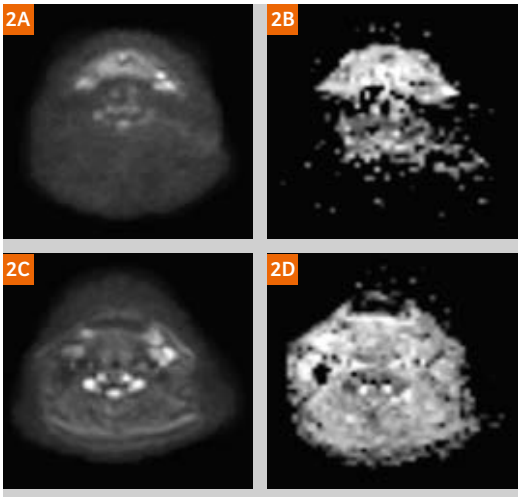


**Figure 2:** Transversal view of the selected single slice of the neck of the same patient: **(2A)** 3D Shim DWI (b = 800 s/mm²), **(2B)** ADC map of 3D Shim DWI (b = 800 s/mm²), **(2C)** slice specific adjustment DWI (b = 800 s/mm²) and **(2D)** ADC map of slice specific adjustment DWI (b = 800 s/mm²). **2A, B** showed massive signal loss in the neck region of 3D Shim DWI, however slice specific adjustment technique improved the image quality of the neck region obviously.

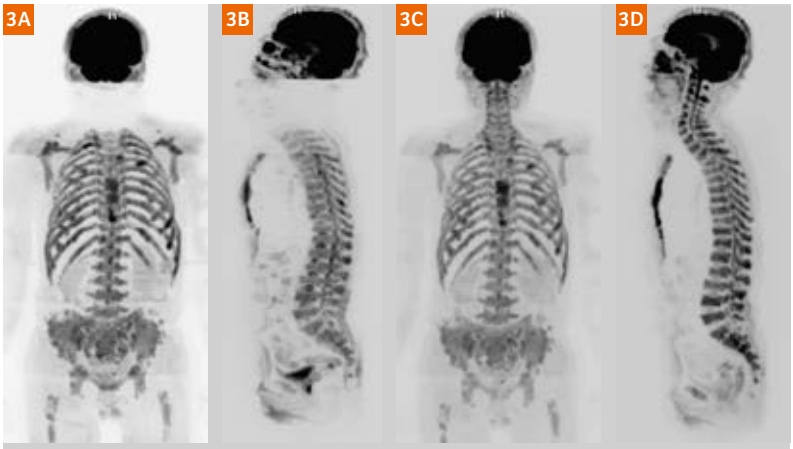


**Figure 3:** Maximum intensity projections (MIPs) with inverted grayscale from high-b-value WBDWI images. **(3A, B)** 3D Shim WBDWI images. The image quality of WBDWI was remarkably improved on 3T MRI. However, in the neck region a strong image quality deterioration can be observed. **(3C, D)** Slice specific adjustment WBDWI images. Compared with 3D Shim WBDWI, slice specific adjustment WBDWI showed artifact-free images.

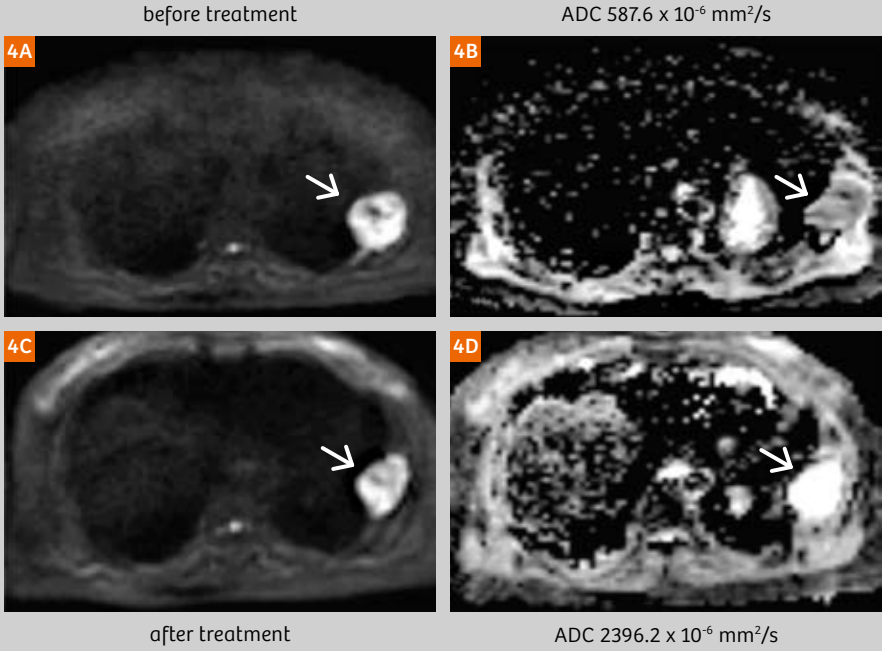


**Figure 4:** 57-year-old female patient with multiple myeloma on the left chest wall (arrows). **(4A, B)** show a lesion with high signal on DWI (b = 800 s/mm²) image and low ADC value (587.6 × $10^{-6}$ mm²/s) before treatment. **(4C, D)** show that the lesion still existed five months later after treatment, but ADC value was much higher than before. The change in ADC corresponds with the clinical results.

like Spectral Adiabatic Inversion Recovery (SPAIR) are not compatible with slice specific adjustment as they exploit non-selective RF-pulses. Instead, slice selective water excitation could be used with slice specific adjustment. The inherently higher SNR of water excitation may allow reducing the number of averages and hence the total acquisition time, and it merits evaluation in a clinical setting.

## Conclusion

The slice specific adjustment technique is an effective method to reduce the negative impact of susceptibility effects on whole-body diffusion-weighted imaging at 3T, as supported by the apparent improvement in image quality, as well as improved SNR in the neck region. Compared with the 3D Shim technique, slice specific adjustment showed improved performance in detecting suspicious lesions in the neck region. The slice specific adjustment technique has entered the clinical arena, improving WBDWI. Slice specific adjustment and its future refinements may further improve the accuracy of lesion assessment and monitoring treatment response (Fig. 4).

### References

1 Padhani AR, Liu G, Koh DM, et al. Diffusion-weighted magnetic resonance imaging as a cancer biomarker: consensus and recommendations. Neoplasia 2009;11(2):102–125.
2 Padhani AR, Koh DM, Collins DJ. Whole-body diffusion-weighted MR imaging in cancer: current status and research directions. Radiology 2011;261(3):700–718.
3 Attariwala R, Picker W. Whole body MRI: improved lesion detection and characterization with diffusion weighted techniques. J MagnReson Imaging 2013;38(2):253–268.
4 Petralia G, Padhani A, Summers P, et al. Whole-body diffusion-weighted imaging: is it all we need for detecting metastases in melanoma patients? EurRadiol. 2013;23(12):3466–3476.
5 Brioli A, Morgan GJ, Durie B, Zamagni E. The utility of newer imaging techniques as predictors of clinical outcomes in multiple myeloma. Expert RevHematol 2014;7(1):13–16.
6 Mayerhoefer ME, Karanikas G, Kletter K, et al. Evaluation of diffusion-weighted MRI for pretherapeutic assessment and staging of lymphoma: results of a prospective study in 140 patients. Clin Cancer Res 2014;20(11):2984–2993.
7 Littooij AS, Kwee TC, Barber I, et al. Whole-body MRI for initial staging of paediatric lymphoma: prospective comparison to an FDG-PET/CT-based reference standard. EurRadiol 2014;24(5):1153–1165.
8 Klenk C, Gawande R, Uslu L, et al. Ionising radiation-free whole-body MRI versus (18)F-fluorodeoxyglucose PET/CT scans for children and young adults with cancer: a prospective, non-randomised, single-centre study. Lancet Oncol 2014;15(3):275–285.
9 Zamagni E, Nanni C, Patriarca F, et al. A prospective comparison of 18F-fluorodeoxyglucose positron emission tomography-computed tomography, magnetic resonance imaging and whole-body planar radiographs in the assessment of bone disease in newly diagnosed multiple myeloma. Haematologica.2007; 92(1):50-55.
10 Schmidt H, Brendle C, Schraml C, et al. Correlation of simultaneously acquired diffusion-weighted imaging and 2-deoxy-[18F] fluoro-2-D-glucose positron emission tomography of pulmonary lesions in a dedicated whole-body magnetic resonance/positron emission tomography system. Invest Radiol. 2013;48(5):247-55.
11 Bogner W, Pinker-Domenig K, Bickel H, et al. Readout-segmented echo-planar imaging improves the diagnostic performance of diffusion-weighted MR breast examinations at 3.0 T. Radiology 2012;263(1):64–76.
12 Porter DA, Heidemann RM. High resolution diffusion-weighted imaging using readout-segmented echo-planar imaging, parallel imaging and a two-dimensional navigator-based reacquisition. Magn Reson Med. 2009;62(2):468–475.
13 Chen NK, Guidon A, Chang HC, et al. A robust multi-shot scan strategy for high-resolution diffusion weighted MRI enabled by multiplexed sensitivity-encoding (MUSE). Neuroimage 2013;72:41–7.

**14** Riffel P, Michaely HJ, Morelli JN, et al. Zoomed EPI-DWI of the head and neck with two-dimensional, spatially-selective radiofrequency excitation pulses, EurRadiol 2014; 24(10):2507–12.
**15** Thierfelder KM, Scherr MK, Notohamiprodjo M, et al. Diffusion-weighted MRI of the prostate: advantages of Zoomed EPI with parallel-transmit-accelerated 2D-selective excitation imaging. EurRadiol 2014; 24(12):3233–41.
**16** Morrell G, Spielman D. Dynamic shimming for multi-slice magnetic resonance imaging. MagnResonMed 1997;38(3):477–83.
**17** Lee SK, Tan ET, Govenkar A, et al. Dynamic slice-dependent shim and center frequency update in 3 T breast diffusion weighted imaging. MagnReson Med 2014;71(5):1813–1818.
**18** Zhang H, Xue H, Stemmer A, et al. Integrated Shimming Improves Lesion Detection in Whole-Body Diffusion-Weighted Examinations of Patients With Plasma Disorder at 3 T. Investigative Radiology, 2015 [Epub ahead of print]
**19** Stemmer A and Kiefer B. Combination of integrated slice-specific dynamic shimming and pixel-wise unwarping of residual EPI distortions. Proc. Intl. Soc. Mag. Reson. Med. 2015; 23:3729.
**20** Jezzard P and Balaban RS. Correction for geometric distortion in echo planar images from $B_0$ field variations. Magnetic Resonance in Medicine 1995; 34:65–73.
**21** Takahara T, Imai Y, Yamashita T, et al. Diffusion weighted whole body imaging with background body signal suppression (DWIBS): technical improvement using free breathing, STIR and high resolution 3D display. Radiat Med. 2004;22:275–282.
**22** Thomas C. Kwee, Taro Takahara, Reiji Ochiai, et al. Diffusion-weighted whole-body imaging with background body signal suppression (DWIBS): features and potential applications in oncology". EurRadiol. 2008; 18:1937–1952
**23** Messiou C, Giles S, Collins D J, et al. Assessing response of myeloma bone disease with diffusion-weighted MRI [J]. The British journal of radiology, 2012, 85(1020): e1198–203.
**24** Giles S L, Messiou C, Collins D J, et al. Whole-body diffusion-weighted MR imaging for assessment of treatment response in myeloma [J]. Radiology, 2014, 271(3): 785–94.

## Contact

Professor Xue Huadan, M.D.

Department of Radiology

Peking Union Medical College Hospital,
Peking Union Medical College and
Chinese Academy of Medical Sciences

Shuaifuyuan 1#, Wangfujing Street,
Dongcheng District
Beijing, China, 100730
bjdanna95@hotmail.com

Zhang Haibo, M.D.

Department of Radiology

Chinese-Japan Friendship Hospital

Yinghuayuan East Street #2
Chaoyang District
Beijing, China, 100029
zhb_hello@163.com

# Whole-Body Dot Engine: First Clinical Experience with Automated Chest, Abdomen and Pelvis Examinations

**Cäcilia S. Reiner[1]; Bernd Kuehn[2]; Daniel Nanz[1]; Tim Finkenstädt[1]; Berthold Kiefer[2]; Gustav Andreisek[1]**

[1] Institute of Diagnostic and Interventional Radiology, University Hospital Zurich, University of Zurich, Switzerland
[2] Oncology Application Predevelopment, Siemens Healthcare GmbH, Erlangen, Germany

## Introduction

Time and cost efficiency are among the major challenges in clinical magnetic resonance imaging (MRI), mainly driven by the funding cuts in most health care systems [1]. At the same time, there is an increasing overall demand for a higher quality of MRI exams with regard to comparability, i.e. important for primary and/or follow-up studies in oncologic patients. To address these challenges, several vendors and researchers are developing automated scanner workflows for clinical MRI systems. The hypothesis is that these workflows allow a standardized and time-efficient use and provide a robust image quality at only little user interaction. The Whole-Body Dot Engine was developed to meet these needs for multi-station MRI exams of chest, abdomen, pelvis, and even the whole body. Potential indications of multi-station body MRI exams are oncologic staging or follow-up, rheumatic disease and evaluation of myopathies.

## MRI technique

The Whole-Body Dot Engine automatically detects landmarks like lung apex, lung recesses, diaphragm, liver apex, iliac bone on a fast low-resolution whole-body scout, which is acquired during moving table. Based on this scout the

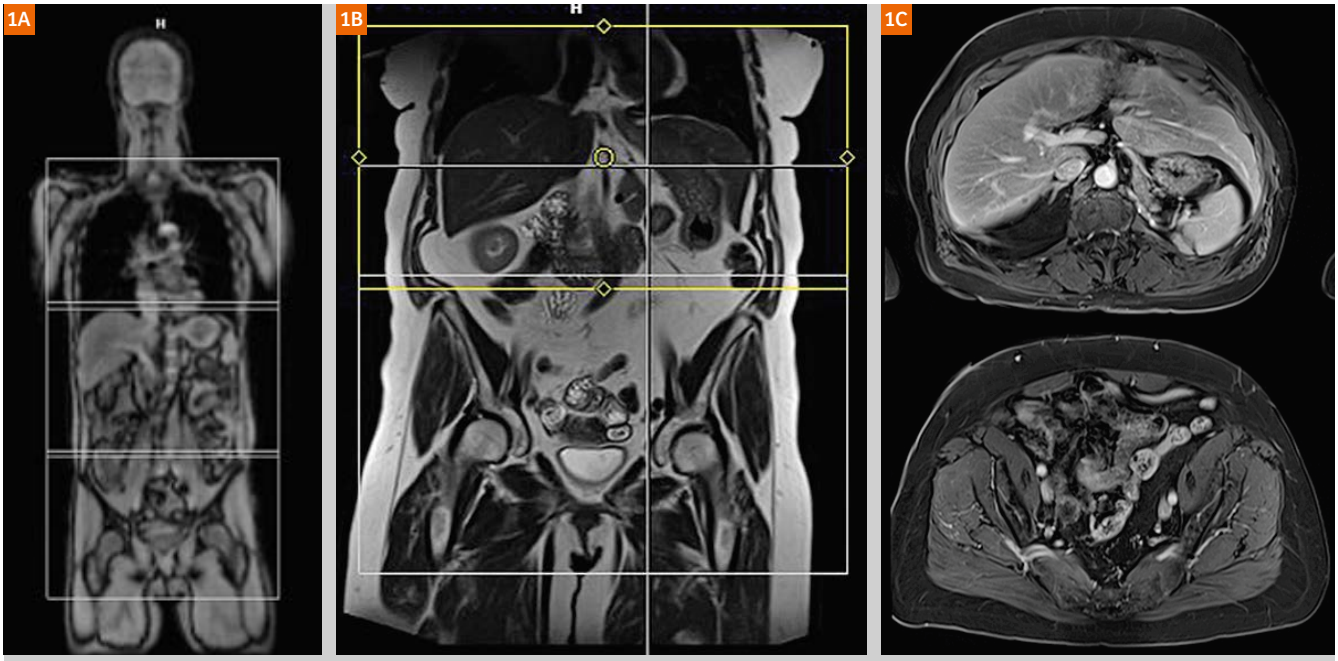


**Figure 1: (1A)** Fast low resolution whole-body scout with automatically segmented abdomen and pelvis for multi-station scanning. **(1B)** Coronal T2 single-shot turbo-spin-echo images with automatically segmented abdomen and pelvis split into two blocks for the transverse T1-weighted sequence **(1C)** with an acquisition time of 15 s for each lying within the preset 20-second breath-hold capacity. The cranio-caudal coverage per block is set to 400 mm with a fixed overlap of 2 cm between blocks and is adjusted to patient size and breath-hold capacity.

| | **T2w HASTE** | **T2w HASTE** | **iShim[1] EPI DWI** | **T1w VIBE Dixon** without and with contrast | **T1w VIBE Dixon** with contrast |
|---|---|---|---|---|---|
| Scan plane | coronal | transverse | transverse | transverse | coronal |
| Repetition time / Echo time (ms) | 1230/92 | 1000/60 | 6100/56 | 4.27/1.28 | 3.93/1.23 |
| Flip angle (°) | 160 | 160 | 90 | 12 | 12 |
| Slice thickness (mm) | 6 | 5 | 6 | 3 | 1,5 |
| Spacing (mm) | 1 | 1 | 1 | 0 | 0 |
| Acquisition matrix | 256 x 256 | 256 x 109 | 128 x 84 | 320 x 180 | 192 x 162 |
| Acceleration, factor | GRAPPA, 3 | GRAPPA, 3 | GRAPPA, 2 | CAIPIRINHA, 2 | CAIPIRINHA, 6 |
| Number of excitations | 1 | 1 | 6 and 15 | 1 | 1 |
| b-values (s/mm²) | na | na | 50, 800 | na | na |

**Table 1:** MRI protocol.


**Figure 2:** 73-year-old female patient with follow-up MRI of abdomen and pelvis after resection of a retroperitoneal liposarcoma. T1-weighted post-contrast 3D spoiled gradient-echo 2-point Dixon sequences in coronal **(2A)** and transverse **(2B)** plane show an enhancing mass cranial to the left kidney (white arrows), which shows a slightly restricted diffusion on the diffusion-weighted image **(2C**, b-value 800 s/mm²) and was highly suspicious of tumor recurrence. In addition a liver lesion was seen with peripheral nodular enhancement on the T1-weighted post-contrast 3D spoiled gradient-echo 2-point Dixon sequence **(2D)** and hyperintense on the T2-weighted single-shot turbo-spin-echo images **(2E)**, which was diagnosed as hemangioma (white arrowheads).

body regions selected for scanning, namely chest, abdomen and/or pelvis are automatically segmented (Fig. 1). With the information of the segmentation the sequence parameters (field-of-view [FOV] and number of slices) are automatically adjusted in order to ensure proper coverage of the body regions of interest. Additionally, the Whole-Body Dot Engine uses an anticipated patient's breath-hold capacity to automatically adjust the imaging protocols in body regions where breath-hold is required to generate optimal image quality. The user can configure which parameters shall be adjusted for each protocol individually. In our protocol, base resolution was used for this purpose in 3D sequences, and number of concatenations was used in 2D sequences. We set the breath-hold capacity to 20 seconds. The protocol included a coronal and transverse T2-weighted single-shot turbo-spin-echo sequence (HASTE) acquired in breath-hold technique, transverse single-shot diffusion-weighted echo-planar imaging with slice-specific shim optimization (EPI-DWI, iShim [2]) in free-breathing, and a transverse T1-weighted pre- and post-contrast 3D spoiled gradient-echo 2-point Dixon (VIBE) sequence acquired in breath-hold technique pre- and post-contrast (delay: chest 35 s, abdomen 70 s, pelvis 90 s after injection of 0.1 mmol/kg bodyweight gadoterate meglumine, Dotarem, Guerbet) (Table). Imaging after contrast-injection was timed by using automated bolus detection. The cranio-caudal coverage per block was adjusted to 400 mm.

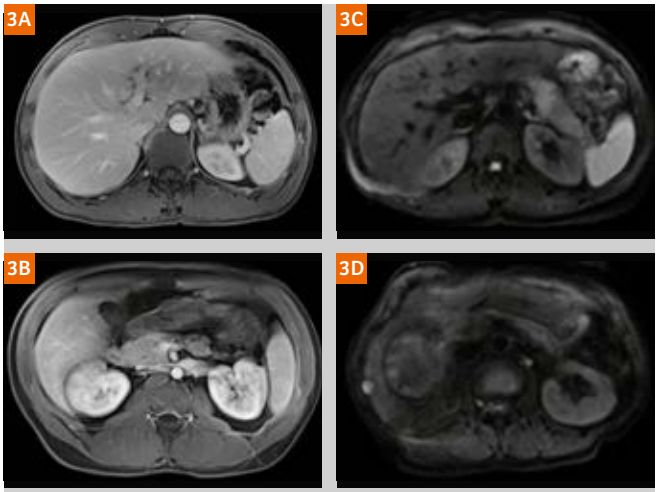


**Figure 3:** T1-weighted post-contrast 3D spoiled gradient-echo 2-point Dixon sequences with excellent image quality **(3A)** and with mild respiratory motion artifacts **(3B)**. Single-shot diffusion-weighted echo-planar imaging sequence with slice-specific shim optimization with excellent image quality **(3C)** and with mild motion artifacts **(3D)**.

We chose a rather short scan protocol without dynamic acquisitions in a focus region (e.g. liver), because we wanted a fast and straightforward protocol for general oncologic imaging comparable to computed tomography. We used this scan protocol for oncologic follow-up imaging of abdomen and pelvis or chest, abdomen, and pelvis.

## Patients

20 patients (9 females, 11 males; mean age 52 years, range 21–79 years) were examined on a 3T MRI scanner (MAGNETOM Skyra, Siemens Healthcare) using the Whole-Body Dot Engine. Multi-station exams were performed on 11 patients for oncologic follow-up, in 2 for primary staging, and in 7 for tumor screening. The clinical diagnosis of these patients was: genitourinary malignancy (n=8), sarcoma (n=3), gastrointestinal malignancy (n=1), poly-posis syndromes (n=2), and chronic abdominal pain (n=6). In 18 patients abdomen and pelvis were scanned and in 2 patients chest, abdomen and pelvis. An image example is given in Figure 2. To validate whether our straightforward protocol results in an acceptable duration of this multi-station MRI, patients scored their satisfaction with exam duration on a visual analogue scale from 0 (not acceptable, too long) to 10 (ideal exam duration).

## Image quality

The scans were evaluated for overall image quality (IQ) (5 = excellent, 4 = good, 3 = moderate, 2 = poor, 1 = non-diagnostic) and artifacts (5 = no artifacts, 4 = mild artifacts, 3 = moderate artifacts, 2 = severe artifacts, 1 = non-diagnostic) on a 5-point scale by a board-certified abdominal radiologist with 8 years of experience. The image acquisition time was noted, as well as whether the coverage of the targeted body region was complete.

In all but one patient (19 of 20, 95%), the selected body regions were covered completely by the automated algorithm. An exception was the DWI, which showed markedly reduced signal in the sub-diaphragmatic part of the right liver in four patients (4 of 20, 20%), which impaired diagnostic ability of DWI in these liver parts.

The mean score for overall IQ was 4.7 ± 0.47 standard deviation (SD) and for artifacts overall was 4.4 ± 0.5 SD. Mild to moderate respiratory motion artifacts were seen in three patients (3 of 20, 15%) on T1-weighted post-contrast images with a mean IQ score of 4.8 ± 0.52 (Fig. 3). Mild motion artifacts were observed in four patients (5 of 20, 25%) on DWI with a mean IQ score of 4.75 ± 0.44. The mean examination time was 27.4 ± 6.5 min for chest, abdomen and pelvis and 21.0 ± 6.9 min for abdomen and pelvis. The mean score of patient satisfaction regarding exam duration was 6.45 ± 2.19 (median, 6) and did not correlate with scan duration.

## Conclusion

MR scanning with the automated Whole-Body Dot Engine results in good to excellent image quality within a reasonable total examination time with only small patient-dependent variations. An almost 'single-button protocol' for standardized fast, reproducible, and automated workflow of chest, abdomen, and pelvis could open up new possibilities in the diagnostic process. However, further comparison studies with traditional manual scan modes need to be performed to support our preliminary experience.

**Contact**

Cäcilia Reiner, M.D.

Institute of Diagnostic and Interventional Radiology
University Hospital Zurich

Raemistrasse 100
8091 Zurich, Switzerland
caecilia.reiner@usz.ch

**References**

1 Andreisek G. Point-of-Care MR Imaging and how we can learn from other imaging modalities. Thoughts on a potential new strategy. MAGNETOM Flash (63) 3/2015:4-7. www.siemens.com/magnetom-world

2 Stemmer A, Kiefer B. Combination of integrated slice-specific dynamic shimming and pixel-wise unwarping of residual EPI distortions. Proc Intl Soc Mag Reson Med. 2015;23:3729.

# MAGNETOM Sola*
# Embrace human nature at 1.5T. With BioMatrix

MAGNETOM Sola is our latest 1.5T Open-Bore 70 cm system and the first 1.5T system with BioMatrix technology. With this system, the scope of BioMatrix will be expanded: e.g., with new potential to address cardiac and head motion with BioMatrix Sensors*. New sequence-support for anatomy-adaptive shimming with SliceAdjust will be available as part of the BioMatrix Tuners. AI-powered BioMatrix Interfaces will now cover more regions for automatic iso-center positioning. The result: higher diagnostic confidence, fewer rescans, predictable patient scheduling, and consistent, high-quality imaging.

MAGNETOM Sola embraces efficiency. GO technologies provide fast patient preparation, standardized acquisitions, ready-to-read results, and even initial post-processing options, all integrated within one workflow. Artificial intelligence-based technology supports the automation of routine tasks, for robust and consistent workflows, even in a high-volume environment. New speed technologies such as Simultaneous Multi-Slice – now new for TSE acquisitions* – can significantly accelerate entire MSK exams by up to 46%.

MAGNETOM Sola expands the patient population eligible for MRI with free-breathing Compressed Sensing applications. Free-breathing cardiac exams with Compressed Sensing Cardiac Cine and push-button, free-breathing liver dynamics with Compressed Sensing GRASP-VIBE now become clinical reality at 1.5T.

Free-breathing exams not only help to improve the patient experience, they also offer a solution when patients cannot hold their breath or follow breath-hold exams. With dynamic liver exams, Compressed Sensing GRASP-VIBE furthermore simplifies the exam process: one continuous acquisition is started, where previously technologists had to perfectly synchronize breath-holds and contrast agent administration.

Whole-body examinations are significantly simplified. Whole-body MRI provides key information for earlier treatment decisions, but has so far been avaided due to its length and complexity. This now changes with the new Whole-Body Dot Engine.

**Respiratory triggering with BioMatrix Respiratory Sensors – No navigator setup, no breathing belt**

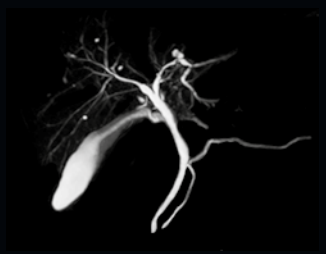

**3D T2 SPACE, MIP cor with Respiratory Sensor**

Body 12*, Spine 24*, TR 5689 ms, TE 701 ms, SL 1 mm, Matrix 648 x 704, FOV 320 x 320
1aaaa1430

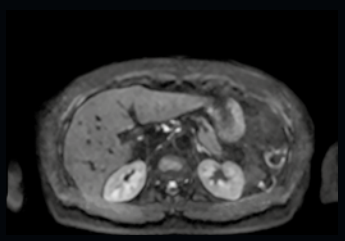

**SMS accelerated DWI b800 with Respiratory Sensor**

Body 12, Spine 24, TR 2700 ms, TE 71 ms, TA 3 min, SL 6 / 1.2 mm, SMS 2, Matrix 216 x 268, FOV 306 x 380
1aaaa1437

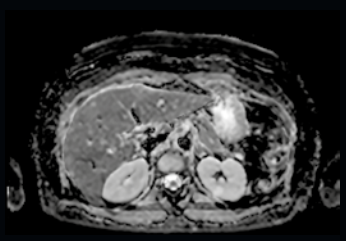

**DWI ADC**

**NATIVE TrueFISP with Respiratory Sensor**

Body 12, Spine 24, TR 1398 ms, TE 1.7 ms, SL 1.1 mm, Matrix 180 x 256, FOV 319 x 88
1aaaa1430

* The product is still under development and is not commercially available yet. Its future availability cannot be ensured.

**T2 TSE FS sag with CoilShim**

Head/Neck 20*, Spine 24,
TR 3200 ms, TE 81 ms,
TA 2:56 min, SL 3 mm,
Matrix 112 x 320, FOV 110 x 220
1aaaa1427

**RESOLVE sag b600 with CoilShim**

Head/Neck 20, Spine 24,
TR 3130 ms, TE 54 ms,
TA 3:12 min, SL 3 mm,
GRAPPA 2, Matrix 74 x 164,
FOV 110 x 220

## Consistent results in the entire imaging volume with BioMatrix Tuners: CoilShim and SliceAdjust

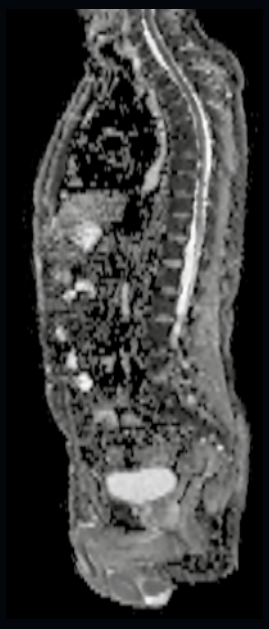

**ADC map with SliceAdjust**

Body 18, Spine 24,
TI 180 ms, TR 4980 ms,
TE 63 ms, TA 2:26 min, SL 5 mm,
GRAPPA 2, Matrix 176 x 268,
FOV 330 x 502
1aaaa1522

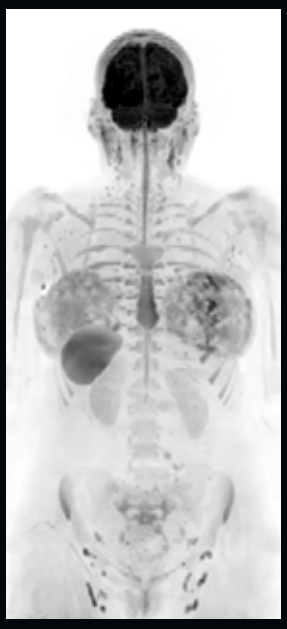

**Inverted b800 DWI MIP**

Head/Neck 20, Body 18,
Spine 24, TI 180 ms,
TR 5200 ms, TE 63 ms,
TA 2:07 min, SL 5 mm,
Matrix 160 x 268,
FOV 304 x 500
1aaaa1579

## BioMatrix Beat Sensor* – designed for cardiac triggering* without the need for ECG

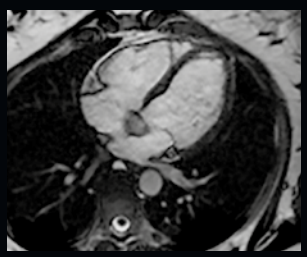

**Segmented cine 4-chamber view with Beat Sensor***

Body 12, Spine 24,
TR 38.6 ms, TE 1.3 ms,
TA 3:94 min, SL 6 mm,
GRAPPA 3, Matrix 169 x 176,
FOV 300 x 300
1aaaa14333

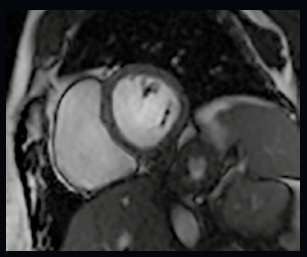

**Segmented cine short axis with Beat Sensor***

Body 12, Spine 24,
TR 37.6 ms, TE 1.3 ms,
TA 3:33 x 3 min, SL 8 mm,
GRAPPA 3, Matrix 141 x 176,
FOV 300 x 300

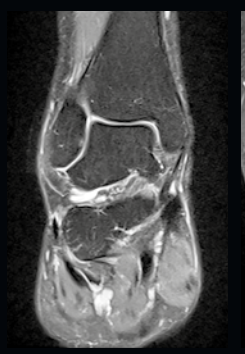

**PD fs cor with SMS 2**

Ultra Flex coil 18,
TR 2600 ms, TE 31 ms,
TA 1:25 min, SL 3 mm,
GRAPPA 2, SMS 2,
Matrix 246 x 352,
FOV 140 x 140
1aaaa1441

**PD TSE fs sag with SMS 2***

Ultra Flex coil 18,
TR 2110 ms, TE 35 ms,
TA 1:18 min, SL 3 mm,
GRAPPA 2, SMS 2,
Matrix 224 x 320,
FOV 140 x 140
1aaaa1442

* The product is still under development and is not commercially available yet. Its future availability cannot be ensured.

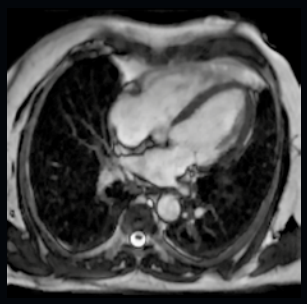

**CS Cardiac Cine Realtime***
**4-chamber view**

Body 18, Spine 32, TT 65,
TR 42.2 ms, TE 1.1 ms,
1 breath-hold, SL 8 mm,
FOV 315 x 36, Matrix 140 x 208
1aaaa1524

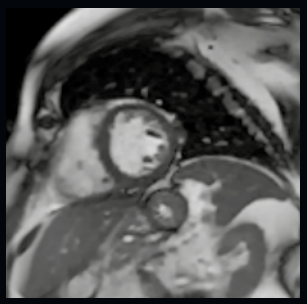

**CS Cardiac Cine Realtime**
**short axis view**

Body 18, Spine 32, TT 22,
TR 43.7 ms, TE 1.1 ms,
10 slices in 1 breath-hold,
SL 8 mm, FOV 365 x 400,
Matrix 146 x 208

## PSIR HeartFreeze

**PSIR with Motion Correction 4-chamber view**

Body 18, Spine, TT 772.5 ms, TI 425 ms, TR 876.8 ms, TE 1.2 ms,
TA 14.8 s, SL 8 mm, Matrix 124 x 256, FOV 303 x 380
1aaaa1433

## Compressed Sensing GRASP-VIBE

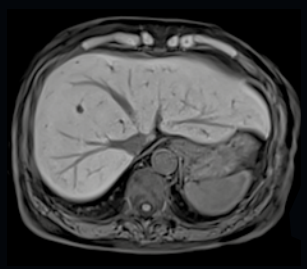

**4D T1 CS GRASP-VIBE fs tra**

Body 18, Spine, TR 3.7 ms,
TE 2.0 ms, TA 19.1 s, SL 2.5 mm,
Matrix 256 x 256, FOV 380 x 380
1aaaa1431

## High-resolution breast MRI

**T1 FLASH 3D Dixon tra**

TR 10 ms, TE 4.8 ms, TA 1:13 min,
SL 1.5 mm, GRAPPA 4,
Matrix 396 x 352, FOV 330 x 220
1aaaa1578

## Whole-Body Dot Engine

**Easy, push-button workflow**
**with Whole-Body Dot Engine**
1aaaa1472

# Compressed Sensing: a Paradigm Shift in MRI

**Christoph Forman[1]; Jens Wetzl[2]; Dominik Nickel[1]; Robert Grimm[1]; Carmel Hayes[1]; Michaela Schmidt[1]**

[1] Siemens Healthineers, Magnetic Resonance, Erlangen, Germany
[2] Pattern Recognition Lab, Friedrich-Alexander-University Erlangen-Nuremberg, Erlangen, Germany

## Introduction

Reducing the complexity and length of examinations has been a major direction of research in magnetic resonance imaging (MRI) in recent years. With the introduction of the Dot engines, the complexity of MR examinations could be reduced through automatization and guidance, providing standardized and time-efficient workflows. Considerable effort has also been spent on developing methods to speed up data acquisition without degrading image quality. Accelerated imaging is a key factor to enable the visualization of rapid physiological or contrast changes in dynamic imaging. Moreover, short scans reduce the risk of artifacts due to any kind of motion during the scan.

A significant speed-up of data acquisition allows both respiratory and cardiac motion to be frozen while maintaining an adequate temporal and spatial resolution. This in turn results in a high-quality and robust examination even for uncooperative patients, since data acquisition may be performed in free breathing. Furthermore, reduced scan time and a decreased number of breath-holds improve patient comfort. Last but not least, accelerated imaging means shorter examinations that can be invested in additional scans, higher resolution, or to improve the overall patient throughput. In this context, parallel imaging and compressed sensing techniques have been proposed to significantly speed up the acquisition time while maintaining diagnostic image quality.

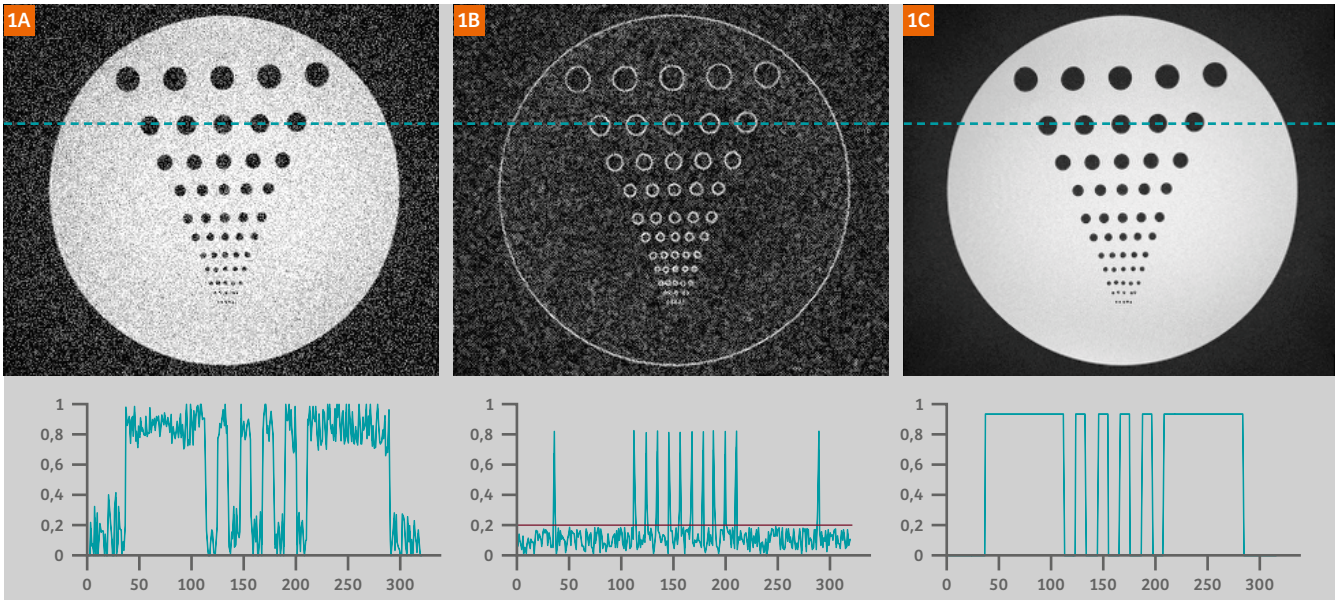


**Figure 1:** Additional noise reduces the homogeneity in the image of the resolution phantom **(1A),** which can also be observed in the line plot along the dashed line. After transformation into a sparse representation using finite differences **(1B),** the homogeneity can be restored by denoising, i.e., setting all pixels below a threshold level (red line) to 0. After the image is transformed back to its original domain, the phantom is piecewise constant **(1C).**

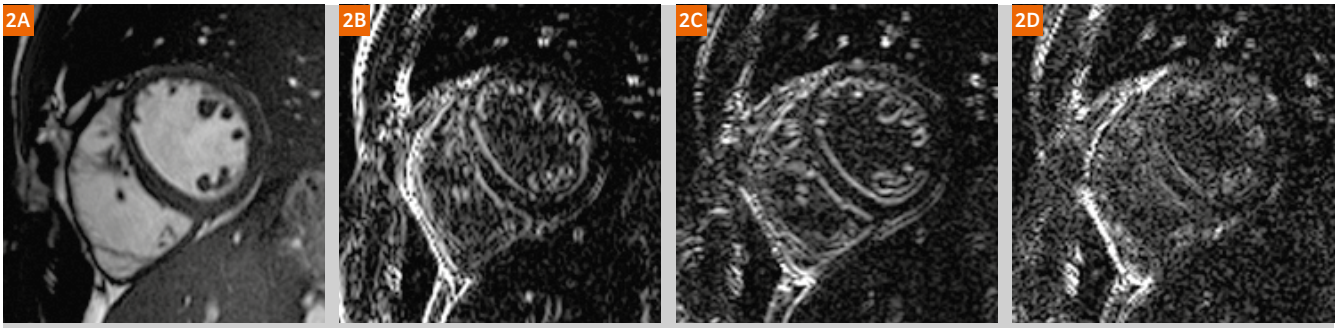


**Figure 2:** The short-axis view of the heart **(2A)** is transformed by the wavelet transform to achieve a sparse representation. In addition to the low-resolution representation of the original image, the wavelet transform results in three edge images **(2B–2D):** While **(2B)** and **(2C)** contain the edges in horizontal and vertical direction, respectively, Figure 2D shows the diagonal edge components of the image. In the wavelet domain, the content of the image is sufficiently described by only few coefficients, i.e. the bright pixels.

## Parallel imaging

Parallel imaging [1, 2] is well established in current clinical practice to speed up data acquisition in a large number of applications. With this technique, scan acceleration is usually achieved by uniformly sub-sampling *k*-space, for example, by skipping every other line. The resulting aliasing can be unfolded by incorporating the spatial encoding capabilities of multi-coil receiver arrays. However, the scan time reduction is often restricted to moderate acceleration factors between 2 and 4. This limitation is due to the restricted encoding capabilities in terms of number and position of the receiver coils. Additionally, acquiring less data also leads to a reduced signal-to-noise ratio (SNR).

## Compressed sensing

In recent years, compressed sensing[1] has gained large scientific attention. Originally, it was proposed as a general concept to accurately reconstruct a signal from a small number of random measurements [3, 4]. A few years later, compressed sensing was introduced to MRI [5] and successfully combined with parallel imaging [6, 7]. Exploiting the compressibility of medical images, this method promises to markedly exceed the acceleration rates that are feasible with parallel imaging. Although compressed sensing has denoising properties, it also has to deal with SNR loss from scan acceleration. Hence, possible acceleration factors scale with the native SNR of the scan. Up to now, the potential of compressed sensing has been shown in a large number of applications from 2D to 5D imaging [8–16].

The successful utilization of compressed sensing is a team play of data acquisition and image reconstruction. In the paper introducing compressed sensing to MRI, three criteria were identified as being essential to ensure successful image recovery from sub-sampled data [5]:

- First, the object that is acquired should have a *sparse representation* after conversion with a mathematical transformation.
- Second, *k*-space should be sub-sampled such that the aliasing results in *incoherent*, i.e. noise-like, artifacts in the image.
- Finally, image reconstruction requires a *nonlinear, iterative optimization* that simultaneously enforces a sparse representation of the resulting image. Thereby, it removes the noise-like artifacts, while it preserves its consistency to the acquired data.

These three essential requirements are discussed in detail below.

## Transform sparsity

An image is considered as sparse when its informational content is represented by only a few pixels, while the contribution of the remaining majority of pixels is close to zero. In medical imaging, an angiogram provides a good example for such a sparse representation. However, in MRI, not all images are inherently sparse. But these images can also have a sparse representation utilizing a sparsifying transform. This transform provides an invertible mapping from an image to a sparse representation. Finite differences, i.e. images that contain only edge information, provide a simple technique to achieve a sparse representation, if the image is piecewise constant as shown in Figure 1. Discrete cosine transform and discrete wavelet transform are frequently used in the context of image compression, for example, in JPEG image compression. Utilizing such methods, images may be transformed into a sparse representation (see Fig. 2). In this domain, the content of the image is sufficiently described by only few coefficients, i.e. the bright pixels. The percentage of these pixels relative to the total number of pixels defines the sparsity of the image. For image compression, pixels in this sparse representation that are below a certain threshold can be set to zero, which facilitates a compression of the signal. Once the compressed signal is converted back to its initial domain, the visual difference between the resulting image and its original version is negligible. In particular, the discrete wavelet transform has been shown to be a suitable

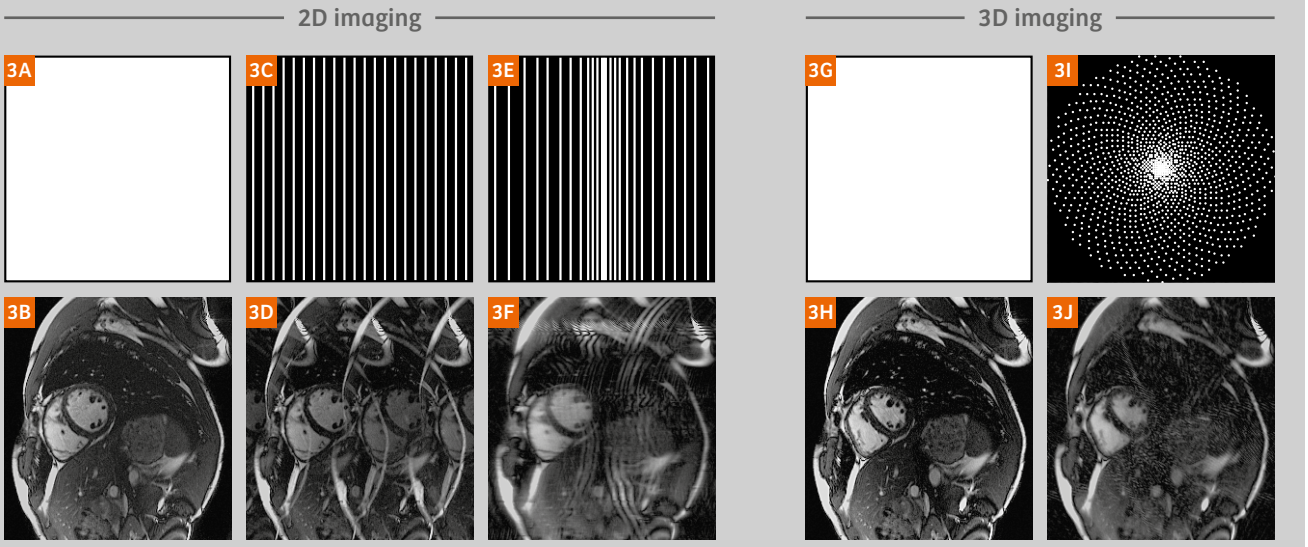


**Figure 3:** Examples of different sampling schemes, where *k*-space locations that are acquired are highlighted in white and the ones that are skipped are black (upper row) with corresponding image results and aliasing artifacts after Fourier transform (lower row). In 2D imaging, sub-sampling is limited to one phase-encoding direction whereas for 3D sub-sampling can be applied in two phase-encode directions. In case of CINE imaging, additional incoherence can be achieved in the temporal domain. **(3A, 3B)** Fully sampled *k*-space with artifact free result image; **(3C, 3D)** Regular subsampled *k*-space like PAT resulting in superposition of multiple ghosts; **(3E, 3F)** Irregular subsampled *k*-space as used in CS leading to incoherent aliasing artifacts similar to noise; **(3G, 3H)** Fully sampled *k*-space with artifact free result image; **(3I, 3J)** Irregular subsampled *k*-space as used in CS with noise-like artifacts.

sparsifying transform for many natural images, including MRI images, and is commonly used in compressed sensing applications. In the case of dynamic imaging, including CINE imaging, this transform can also be applied in the temporal dimension. The redundancy of information along this temporal dimension can be exploited, and often the sparsity is even higher compared to the spatial dimensions.

## Incoherent sampling

Unlike the regular sub-sampling patterns used for parallel imaging, the data acquisition process for compressed ensing requires that *k*-space sub-sampling is irregular (see Fig. 3C for regular and 3E, 3I for irregular sampling). In conventional Cartesian parallel imaging, regular sub-sampling of *k*-space is advantageous in that the phase-encoding gradient is increasing linearly during the measurement, which is beneficial for physical and MRI hardware limitation reasons. However, violating the Nyquist sampling theorem in this manner results in a superposition of shifted replicas of the original signal as illustrated in Figure 3D. The number of replicas equals the chosen sub-sampling rate. This aliasing can then be unfolded utilizing the spatial encoding capabilities of the multi-coil receiver array and parallel imaging. In contrast, irregular, incoherent sub-sampling of *k*-space, as required for compressed sensing, would result in a noise-like appearance of sub-sampling artifacts (see Figs. 3F, 3J). Theoretically, completely random sub-sampling is optimal to ensure this noise-like behavior. However, purely random sampling is impractical in the case of MRI. On the one hand, large and random steps in *k*-space may require large-amplitude gradient steps and should be avoided due to hardware limitations and physical reasons. On the other hand, the sampling trajectory must be repeatable to allow the same acquisition to be reproduced with consistent image quality. Therefore, sub-sampling patterns featuring deterministic properties that mimic random sampling within the given constraints are frequently used for compressed sensing data acquisition. In 2D Cartesian imaging with pure spatial coverage, the sub-sampling is limited to one dimension, as only the phase-encoding direction is sub-sampled in MRI. But in case of 2D dynamic imaging, the sampling pattern can be varied from one time frame to the next in order to maintain sufficient incoherence for compressed sensing. In 3D Cartesian imaging, sub-sampling can be applied in two phase-encoding directions. Alternatively, non-Cartesian sampling trajectories can be used, e.g., radial or spiral imaging, that already facilitate an incoherent sampling of *k*-space for 2D imaging.

## Nonlinear image reconstruction

If the two above-mentioned requirements are sufficiently met, the image can be recovered from the sub-sampled data by nonlinear, iterative reconstruction. In this reconstruction, a data fidelity term ensures consistency of the estimated image to the acquired data and a transform sparsity term enforces a sparse representation of the image in the transform domain by solving the following equation:

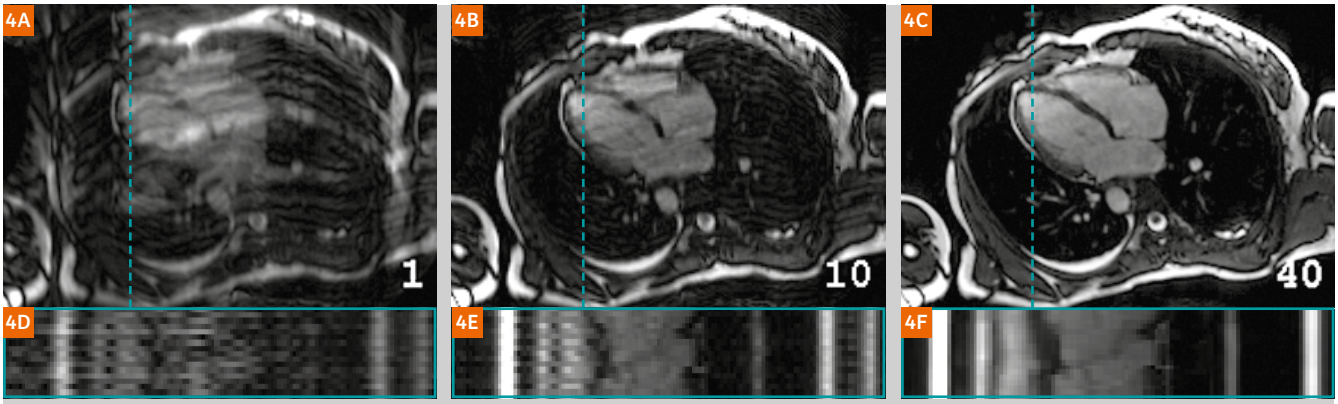


**Figure 4:** This Figure shows the progress of the optimization procedure to preserve data fidelity and reduce noise-like artifacts exemplarily in a Cardiac 2D CINE dataset **(4A–4C).** While the top image shows one image of the time series, a temporal profile along the dashed line is plotted below. The incoherent sub-sampling in the spatio-temporal domain results in incoherent artifacts that dominate the image after the first iteration **(4A).** Enforcing a sparse representation of the image and exploiting temporal redundancy, these artifacts are reduced with an increasing number of iterations **(4B).** The compressed sensing reconstruction is terminated after 40 iterations and results in an aliasing-free image **(4C).**

$$\min_x \underbrace{\|Ax - y\|_2^2}_{\text{data fidelity}} + \lambda \underbrace{\|\Phi(x)\|_1}_{\text{transform sparsity}}$$

The data fidelity term minimizes the least-squares difference ($\|\cdot\|_2^2$) between the estimated image, x, and the acquired *k*-space data, y. The system matrix, A, describes the data acquisition process, i.e., the transform from spatio-temporal to frequency domain, which is required for the comparison of the image and acquired data. Incorporating parallel imaging, it consists of the coil sensitivity maps of the individual receiver coil elements, the Fourier transform, and the applied sub-sampling pattern during data acquisition. In the transform sparsity term, the image is transformed into a sparse representation by $\Phi(\cdot)$, for example, using the discrete wavelet transform. In this term, the sum of the absolute values of the pixels in the transform domain, denoted by the $\ell_1$ norm ($\|\cdot\|_1$), is minimized. Hence, the optimization procedure minimizing this equation seeks to find a solution that fulfills both criteria, data consistency and transform sparsity. This optimization procedure is more computationally intensive than conventional reconstruction, e.g., parallel imaging. The balance between data fidelity and sparsity is adjusted with the regularization parameter λ, which is usually found empirically. While small values of λ lead to an image that is closer to the acquired data, increasing this value tends to produce an image that is in favor of the sparse solution. When λ is too low, the image will be noisy, and when λ is too high a strongly filtered image appearance may be the consequence. The equation described above is iteratively minimized until a convergence criterion is met or a fixed number of iterations is reached. Figure 4 illustrates this optimization in the example of real-time CINE imaging of the heart.adverse surgical outcomes.

## Transition into clinical routine

Compressed sensing acquisition and reconstruction have been completely integrated into our clinical MRI scanners. Works-in-progress packages have been developed and tested by our clinical cooperation partners world-wide for various applications in the fields of cardiovascular [17–20], neurological [21], musculoskeletal [22–24] and oncological [25] imaging. The additional parameters needed to compose the compressed sensing protocols, for both acquisition and reconstruction, have been seamlessly integrated into our user interface (UI). A selection of possible continuous acceleration factors takes the place of discrete numbers that were familiar from parallel imaging. This facilitates a UI experience with a low level of complexity. The award-winning algorithm for compressed sensing reconstruction [9], ranking first at the ISMRM 2014 "sub-Nyquist" reconstruction challenge, has been fully integrated into the Siemens image reconstruction environment. Without the need for additional hardware, the images are directly calculated inline utilizing the full computational power of the reconstruction computer. Compressed sensing reconstruction is performed on a graphics processing unit, which provides a significant speed-up in processing time. For example, the image series of one cardiac real-time CINE slice is processed in 10 to 15 seconds.

Thanks to its high acceleration rate due to compressed sensing, real-time sequences allow for a temporal and spatial resolution comparable to that of conventional segmented acquisitions. For example, compressed sensing in cardiac imaging permits fast quantification of left-ventricular (LV) function in a single breath-hold [26]. As demonstrated in Figure 5, this sequence still provides diagnostic images for LV function quantification even in challenging scenarios, such as in the presence of arrhythmia, where conventional sequences usually fail.

This sequence may also be applied in free breathing, which is beneficial for patients who are not able to hold their breath sufficiently and, in general, allows for a simplified and more patient-friendly examination workflow.

A new experience of time-resolved 3D dynamic imaging is offered by Golden-angle RAdial Sparse Parallel MRI (GRASP) [27] that is incorporated into the Compressed Sensing GRASP-VIBE package. It extends the StarVIBE sequence by a time-incoherent golden-angle stack-of-star reordering, which can be exploited using a time-resolved compressed sensing reconstruction. As a consequence the advantages of two worlds are obtained: The motion robustness of the StarVIBE and the high temporal resolution of a time-resolved compressed sensing reconstruction TWIST-VIBE [28]. GRASP-VIBE even allows reconstructions with varying temporal resolution over the course of an acquisition, and support of auto-bolus detection. These features can be used, e.g. in liver imaging to set the desired temporal resolution for the pre-contrast, arterial, portal-venous and delayed phase individually. An example is shown in Figure 6.

## Conclusion

Compressed sensing facilitates rapid MR imaging by exploiting the fact that medical images have a sparse representation in a certain transfer domain. Representing a team play of data acquisition and image reconstruction, this allows for the reconstruction of artifact-free images following incoherent data acquisition. The acceleration enables a reduction in the acquisition time or an improvement in the spatial and/or temporal resolution. Real-time imaging featuring compressed sensing helps to reduce the need for breath-holding or ECG triggering. The integration of protocols based on compressed sensing in clinical workflows allows a significant reduction in the examination time for each patient. Our generalized integration of compressed sensing in the scanner environment will allow for the straightforward introduction of further applications that are likely to come in the near future.

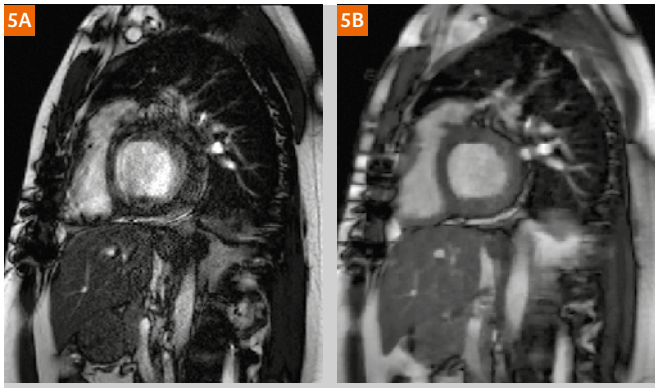


**Figure 5:** In cardiac imaging, the high acceleration rate due to compressed sensing enables real-time CINE imaging with a temporal and spatial resolution in a comparable range as conventional segmented acquisitions. While conventional imaging might fail in challenging scenarios, like in case of arrhythmia **(5A),** the compressed sensing real-time sequence preserves a diagnostic image quality that still enables the quantification of LV function **(5B).** *Images courtesy of Dr. François Pontana, Lille University Hospital, Lille, France.*

### References

1 M. A. Griswold, P. M. Jakob, R. M. Heidemann, M. Nittka, V. Jellus, J. Wang, B. Kiefer, and A. Haase. "Generalized Autocalibrating Partially Parallel Acquisitions (GRAPPA)". Magnetic Resonance in Medicine, Vol. 47, No. 6, pp. 1202–1210, June 2002.

2 K. Pruessmann, M. Weiger, M. B. Scheidegger, and P. Boesiger. "SENSE: Sensitivity Encoding for Fast MRI". Magnetic Resonance in Medicine, Vol. 42, No. 5, pp. 952–962, Nov. 1999.

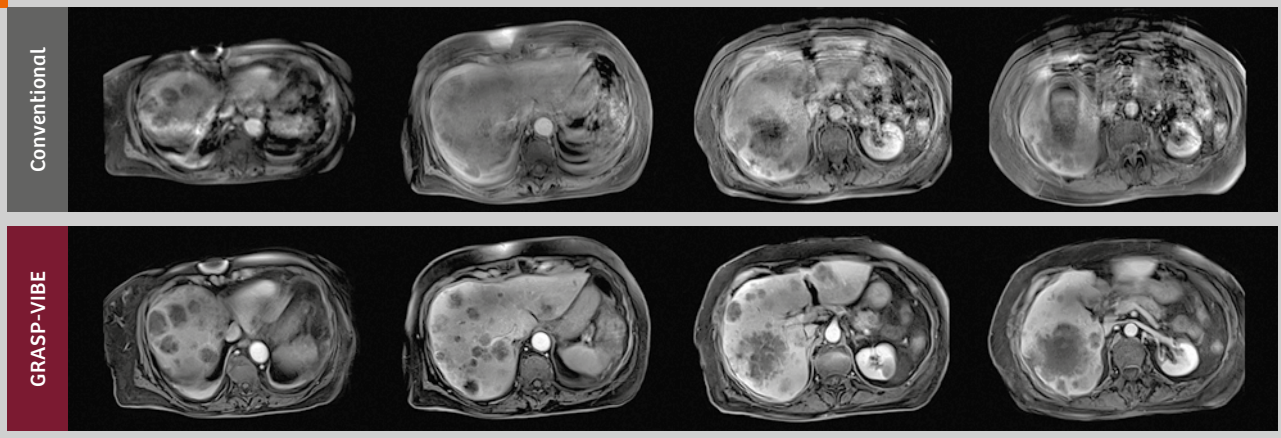


**Figure 6:** 82-year-old female patient with dementia, unable to hold her breath. With GRASP-VIBE failure rates may be reduced and non-diagnostic examinations may be avoided in abdominal MRI with free-breathing liver dynamics.
*Images courtesy of Universitätsspital Basel, Switzerland.*

**3** D. Donoho. “Compressed Sensing”. IEEE Transactions on Information Theory, Vol. 52, No. 4, pp. 1289–1306, Apr. 2006.
**4** E. Candes and J. Romberg. “Sparsity and incoherence in compressive sampling”. Inverse problems, Vol. 23, No. 3, pp. 969–985, Apr. 2007.
**5** M. Lustig, D. Donoho, and J. M. Pauly. “Sparse MRI: The Application of Compressed Sensing for Rapid MR Imaging”. Magnetic Resonance in Medicine, Vol. 58, No. 6, pp. 1182–1195, Dec. 2007.
**6** D. Liang, B. Liu, J. Wang, and L. Ying. “Accelerating SENSE Using Compressed Sensing”. Magnetic Resonance in Medicine, Vol. 62, No. 6, pp. 1574–1584, Dec. 2009.
**7** Block, K. T., Uecker, M. and Frahm, J., “Undersampled radial MRI with multiple coils. Iterative image reconstruction using a total variation constraint”, Magnetic Resonance in Medicine, Vol. 57, No. 6, pp. 1086-1098, May 2007.
**8** G. Adluru, L. Chen, S. Kim, N. Burgon, E. G. Kholmovski, N. F. Marrouche, and E. V. R. DiBella. “Three-dimensional late gadolinium enhancement imaging of the left atrium with a hybrid radial acquisition and compressed sensing”. Journal of Magnetic Resonance Imaging, Vol. 34, No. 6, pp. 1465-1471, Dec. 2011.
**9** J. Liu, J. Rapin, T.-C. Chang, A. Lefebvre, M. O. Zenge, E. Mueller, and M. S. Nadar. “Dynamic cardiac MRI reconstruction with weighted redundant Haar wavelets”. In: Proceedings of the 20th Annual Meeting of ISMRM, p. 4249, Melbourne, Australia, May 2012.
**10** F. Han, S. Rapacchi, S. Kahn, I. Ayad, I. Salusky, S. Gabriel, A. Plotnik, J. P. Finn, and P. Hu, “Four-dimensional, multiphase, steady-state imaging with contrast enhancement (MUSIC) in the heart: A feasibility study in children”. Magnetic Resonance in Medicine, Vol. 74, No. 4, pp. 1042-1049, Oct. 2015.
**11** S. T. Ting, R. Ahmad, N. Jin, J. Craft, J. Serafim da Silveira, H. Xue, and O. P. Simonetti. “Fast Implementation for Compressive Recovery of Highly Accelerated Cardiac Cine MRI Using the Balanced Sparse Model”. Magnetic Resonance in Medicine, doi: 10.1002/mrm.26224.
**12** D. Stäb, T. Wech, F. A. Breuer, A. M. Weng, C. O. Ritter, D. Hahn, and H. Köstler, “High resolution myocardial first-pass perfusion imaging with extended anatomic coverage”. Journal of Magnetic Resonance Imaging, Vol. 39, No. 6, pp. 1575–1587, Jun. 2014.
**13** X. Chen, M. Salerno, Y. Yang, and F. H. Epstein, “Motion-compensated compressed sensing for dynamic contrast-enhanced MRI using regional spatiotemporal sparsity and region tracking: Block low-rank sparsity with motion-guidance (BLOSM)”, Magnetic Resonance in Medicine, Vol. 72, No. 4, pp. 1028-1038, Oct 2014.
**14** H. Xue, S. Inati, S. Sørensen, P. Kellman, and M. S. Hansen, “Distributed MRI Reconstruction Using Gadgetron-Based Cloud Computing”, Magnetic Resonance in Medicine, Vol. 73, No. 3, pp. 1015-1025, March 2015.
**15** J. Wetzl, F. Lugauer, M. Schmidt, A. Maier, J. Hornegger, and C. Forman. “Free-Breathing, Self-Navigated Isotropic 3-D CINE Imaging of the Whole Heart Using Cartesian Sampling”, In: Proceedings of the 24th Annual Meeting of ISMRM, p. 411, Singapore, May 2016.
**16** L. Feng, L. Axel, H. Chandarana, K. T. Block, D. K. Sodickson, and R. Otazo. “XD-GRASP: Golden-angle radial MRI with reconstruction of extra motion-state dimensions using compressed sensing”. Magnetic Resonance in Medicine, Vol. 75, No. 2, pp. 775–788, Feb. 2016.
**17** C. Forman, D. Piccini, R. Grimm, J. Hutter, J. Hornegger, and M.O. Zenge. “Reduction of respiratory motion artifacts for free-breathing whole-heart coronary MRA by weighted iterative reconstruction”, Magnetic Resonance in Medicine, Vol. 73, No. 5, pp. 1885-1895, May 2015.
**18** A. F. Stalder, M. Schmidt, H. H. Quick, M. Schlamann, S. Maderwald, P. Schmitt, Q. Wang, M. S. Nadar, and M. O. Zenge. “Highly under-sampled contrast-enhanced MRA with iterative reconstruction: Integration in a clinical setting”, Magnetic Resonance in Medicine, Vol. 74, No. 6, pp. 1652-1660, Dec. 2015
**19** T. Yamamoto, K. Fujimoto, T. Okada, Y. Fushimi, A. Stalder, Y. Natsuaki, M. Schmidt, and K Togashi, “Time-of-Flight Magnetic Resonance Angiography With Sparse Undersampling and Iterative Reconstruction: Comparison With Conventional Parallel Imaging for Accelerated Imaging”, Investigative Radiology, Vol. 51, No. 6, pp. 372-378, Jun 2016.
**20** J. Wetzl, C. Forman, B. J. Wintersperger, L. D’Errico, M. Schmidt, B. Mailhe, A. Maier, and A. F. Stalder. “High-resolution dynamic CE-MRA of the thorax enabled by iterative TWIST reconstruction”, Magnetic Resonance in Medicine, doi: 10.1002/mrm.26146.
**21** E. Mussard, T. Hilbert, R. Meuli, J.-P. Thiran, and T. Kober. “Accelerated MP2RAGE Imaging Using Sparse Iterative Reconstruction”, In: Proceedings of the 24th Annual Meeting of ISMRM, p. 4216, Singapore, May 2016.
**22** R. Otazo, M. Nittka, M. Bruno, E. Raithel, C. Geppert, S. Gyftopoulos, M. Recht, and L. Rybak. “Sparse-SEMAC: Rapid and Improved SEMAC Metal Implant Imaging Using SPARSE-SENSE Acceleration”, Magnetic Resonance Imaging, July 2016, Early View, DOI: 10.1002/mrm.26342.
**23** J. Fritz, S. Ahlawat, S. Demehri, G.K. Thawait, E. Raithel, W.D. Gilson, M. Nittka. “Compressed Sensing SEMAC: 8-fold Accelerated High Resolution Metal Artifact Reduction MRI of Cobalt-Chromium Knee Arthroplasty Implants”, Investigative Radiology, October 2016, Vol. 51, Issue 10, pp 666–676.
**24** J. Fritz, E. Raithel, G. K. Thawait, W. Gilson, and D. F. Papp. “Six-Fold Acceleration of High-Spatial Resolution 3D SPACE MRI of the Knee Through Incoherent k-Space Under-sampling and Iterative Reconstruction – First Experience”. Investigative Radiology, Vol. 51, No. 6, pp. 400-409, Jun 2016.
**25** D. Nickel, X. Chen, B. Mailhe, Q. Wang, Y. Son, J. M. Lee, and B. Kiefer. “Motion-resolved 3D dynamic contrast enhanced liver MRI”, In: Proceedings of the 24th Annual Meeting of ISMRM, p. 4253, Singapore, May 2016.
**26** G. Vincenti, P. Monney, J. Chaptinel, T. Rutz, S. Coppo, M.O. Zenge, M. Schmidt, M.S. Nadar, D. Piccini, P. Chèvre, M. Stuber, and J. Schwitter, “Compressed Sensing Single–Breath-Hold CMR for Fast Quantification of LV Function, Volumes, and Mass” JACC: Cardiovascular Imaging, Vol. 7, No. 9, pp. 882–892, Sep. 2014.
**27** L. Feng, R. Grimm, T.K. Block, H. Chandarana, S. Kim, J. Xu, L. Axel, D.K. Sodickson, and R. Otazo, "Golden-angle radial sparse parallel MRI: combination of compressed sensing, parallel imaging, and golden-angle radial sampling for fast and flexible dynamic volumetric MRI", Magnetic Resonance in Medicine, Vol. 72, No. 3, pp. 707-17, September 2014.
**28** H. Chandarana, L. Feng, T.K. Block, A.B. Rosenkrantz, R.P. Lim, J.S. Babb, D.K. Sodickson, and R. Otazo, "Free-Breathing Contrast-Enhanced Multiphase MRI of the Liver Using a Combination of Compressed Sensing, Parallel Imaging, and Golden-Angle Radial Sampling", Investigative Radiology, Vol. 48, No. 1, pp. 10-16, January 2013.

## Contact

Christoph Forman

Siemens Healthcare GmbH
HC DI MR PI TIO CARD

Postbox 32 60
91050 Erlangen
Germany
christoph.forman@siemens.com

# GRASP: Tackling the Challenges of Abdominopelvic DCE-MRI

**Kai Tobias Block[1]; Li Feng[1]; Robert Grimm[2]; Hersh Chandarana[1]; Ricardo Otazo[1]; Christian Geppert[2]; Daniel K. Sodickson[1]**

[1] Department of Radiology, NYU Langone Medical Center, New York, NY, USA
[2] Siemens Healthcare, Erlangen, Germany

## Introduction

Dynamic contrast-enhanced (DCE) T1-weighted acquisition after injection of a gadolinium-based contrast agent is an integral part of most diagnostic abdominopelvic MRI examinations and essential for identifying and properly characterizing lesions and tumors, such as the hepatocellular carcinoma (HCC) or renal cancer [1]. Because tumors show a specific temporal contrast-enhancement pattern, it is necessary to obtain images of the whole region-of-interest at multiple short time points following the injection. While technically infeasible years ago, parallel-imaging acceleration techniques such as GRAPPA [2] have made it possible to achieve the required acquisition speed using standard clinical MRI systems, so that these scans can nowadays be performed at almost all imaging centers. However, in routine practice abdominopelvic DCE-MRI exams remain challenging and the failure rates are undesirably high.

One main challenge is that the data has to be collected precisely at defined time points relative to the arrival time of the contrast agent in the aorta (see Fig. 1). To this end, usually a small test bolus is injected prior to the actual diagnostic scan and monitored using a bolus-tracking sequence to determine the patient-specific circulation delay [3]. Once estimated, the delay is then incorporated into the timing calculation of the dynamic scans, which are scheduled relative to the injection time of the contrast dose. This procedure is, of course, prone to inaccuracies and mistakes – with the potential risk of missing the important arterial phase (AP) of contrast enhancement. As additional complication, the dynamic acquisitions have to be performed during a strict breath hold of the patient and, thus, need to be properly synchronized with breath-hold commands. While the latter can be automated using computer-controlled voice instructions [3], it cannot be guaranteed that the patient is actually following these breath-hold instructions. Continued respiration occurs due to various reasons, including inability to hold breath for the scan duration (usually ~15 sec per acquisition), hearing or language problems, and uncertainty when exactly to stop breathing after hearing the command. Especially elderly or severely sick patients often struggle to properly suspend respiration, resulting in compromised or even fully non-diagnostic image quality. A particular problem here is that once the injection has been done, the acquisitions cannot be repeated before the contrast agent has been extracted from the body, which takes several hours and requires rescheduling of the examination on a different day. Strongly compromised image quality is also obtained when examining

1

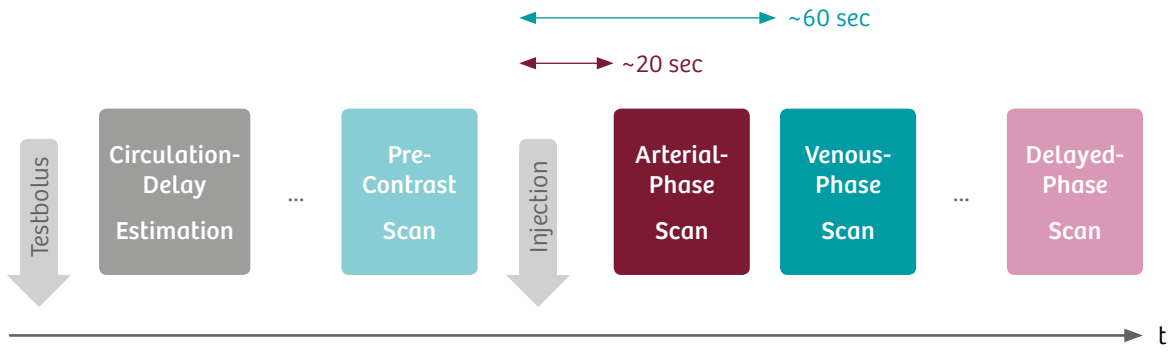


**Figure 1:** Conventional scheme for abdominopelvic DCE-MRI exams, starting with the injection of a test bolus to determine the circulation delay. Afterwards, a pre-contrast image is acquired as well as images in arterial, venous, and delayed phases of contrast enhancement. The acquisitions must be properly timed relative to the injection and accounting for the circulation delay, which makes the procedure prone to timing errors. Furthermore, the scans need to be performed during breath holding.

sedated or anesthetized patients, where suspending the respiration is not possible at all.

## DCE-MRI with continuous radial acquisition

The requirement to perform abdominal scans during breath-holding results from the high motion sensitivity of conventional MRI techniques, as motion translates into appearance of numerous overlapping object copies known as ghosting artifacts. This problem can be ameliorated by using non-Cartesian acquisition techniques such as radial *k*-space sampling, which inherently prevent the appearance of motion-induced ghosting artifacts. Radial scanning techniques, such as the Radial VIBE or StarVIBE sequence [4], have recently become available for routine imaging, and it has been demonstrated that these sequences can be used to image the abdomen during free-breathing [5]. However, the higher motion robustness of radial *k*-space trajectories comes at the price of lower scan efficiency. With typical scan durations of around 60 sec per image volume, sequences such as Radial VIBE are by itself too slow for dynamic abdominopelvic imaging as it would be impossible to separate the arterial and venous phases of enhancement.

To overcome this problem, our group has recently developed a technique called GRASP that enables using the Radial VIBE sequence for DCE-MRI applications and that resolves many of the aforementioned challenges [6]. The key idea of GRASP is that, instead of performing several individual acquisitions for the required time points, data is acquired continuously throughout the whole exam while the contrast agent is injected (see Fig. 2). Image sets for the needed time points are then calculated from the continuously acquired data using an iterative reconstruction procedure (as described in the next section).

This concept leads to a significant simplification of the overall clinical workflow. Because data is acquired all the time during the examination, it is not necessary anymore to determine the circulation delay using a test bolus. Also, the possibility of missing one of the important enhancement phases as a result of a timing or synchronization error is eliminated. Furthermore, because based on radial *k*-space acquisition, GRASP examinations can be performed during continued breathing [7], which removes the need for breath-hold commands, improves patient comfort, and makes the technique well-suited for patients where holding breath is impossible, such as pediatric[1] patients. Hence, with GRASP, the formerly complex and stressful abdominopelvic DCE-MRI exams now become a simple one-click procedure.

[1] MR scanning has not been established as safe for imaging fetuses and infants under two years of age. The responsible physician must evaluate the benefit of the MRI examination in comparison to other imaging procedures.

2

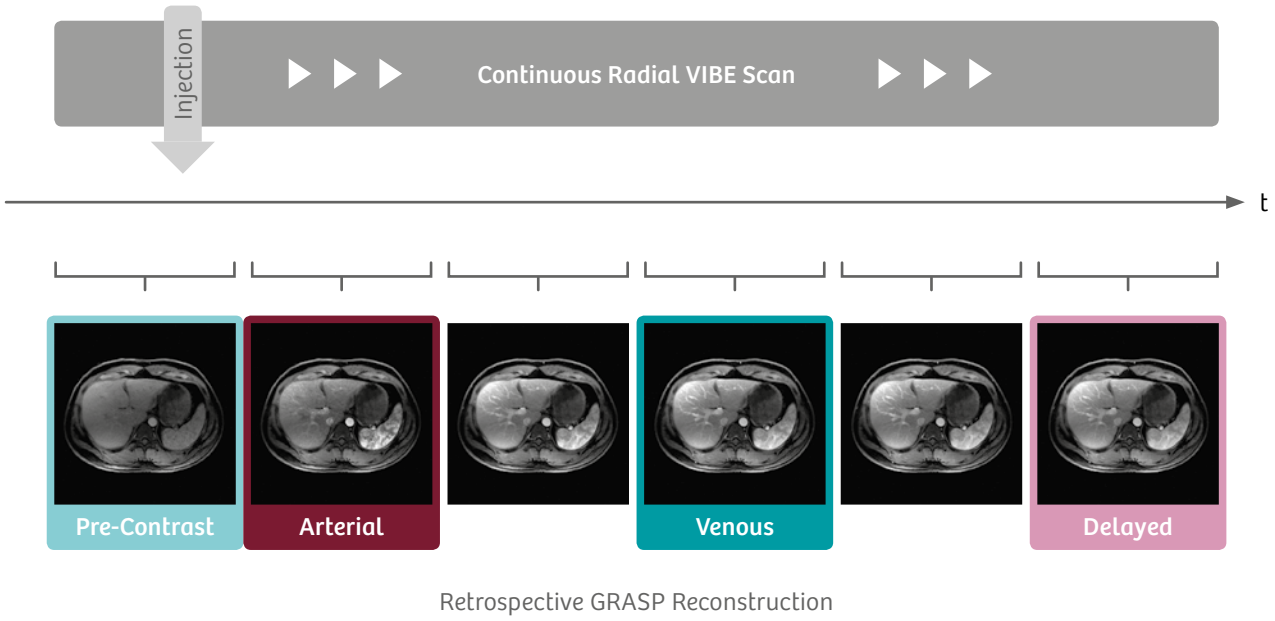


**Figure 2:** GRASP scheme for DCE-MRI, which uses a single continuous acquisition while the contrast agent is injected. Because radial sampling of *k*-space is used, the data can be acquired during free-breathing. Images are calculated from the continuous data using an iterative reconstruction that allows selecting the desired time points and temporal resolution retrospectively. This eliminates the possibility of timing errors and leads to significant simplification of the workflow.

## Technical background

On a technical level, GRASP combines several concepts for MRI scan acceleration that have been described previously as individual techniques. The data acquisition is based on the radial golden-angle ordering scheme, which was originally proposed by Winkelmann et al. [8]. When acquiring radial data with constant angular increment of 111.25 degrees (referred to as 'golden angle' because it corresponds to 180 degrees multiplied by the golden ratio), successively sampled radial spokes always add complementary *k*-space information to the previously acquired data, and any number of grouped spokes cover *k*-space approximately uniformly. This means that if data is acquired continuously over some time, any number of successively acquired spokes can be combined into an individual image (e.g., 144 spokes for low temporal resolution, or 21 spokes for high temporal resolution). Furthermore, the reconstruction window can be placed at any time point of the scan. In other words, it is possible to retrospectively decide which temporal resolution and which time points should be reconstructed.

When grouping only few spokes into each image to achieve high temporal resolution, as needed in DCE-MRI for separating the phases of enhancement, the data available for each time point is highly incomplete or, according to MR terminology, undersampled. For radial sequences, this means that the images are affected by severe 'streak' artifacts, which render the images diagnostically unusable. However, GRASP applies two known tricks to suppress this effect and to recover artifact-free images from the undersampled data: Compressed sensing [9] and parallel imaging [10]. The use of compressed sensing is motivated from the fact that the streak artifacts lead to strongly flickering patterns if viewed along time, whereas the true contrast enhancement occurs in a 'smooth' non-flickering fashion. In other words, flickering pixel intensities can be considered as artificial effects. Therefore, artifact-free images can be obtained by employing an iterative reconstruction procedure that, during each calculation step, matches the solution with the available undersampled data and, in addition, suppresses flickering pixels. Mathematically, this is achieved by calculating the total variation (TV) of each pixel along time and using this value as penalty measure during the iterations (because the true solution should have low total variation). By running the iterative procedure for a certain number of iterations, the streak artifacts disappear and the underlying true solution is recovered – even for severely undersampled data. As second mechanism, parallel imaging is integrated into the iterative scheme by using a CG-SENSE-type formalism [11], which contributes to the suppression of streaking artifacts by exploiting local coil sensitivities. Due to the synergistic combination of these two MR acceleration techniques, GRASP is able to compensate for the lower scan efficiency of radial sampling and achieves even higher temporal resolution than possible with most conventional DCE-MRI techniques. The key advantage, however, consists in the aforementioned workflow simplification.

## Clinical integration and evaluation

The downside of using such an iterative reconstruction approach is that the image calculation involves a very computationally demanding numerical process (because the solution has to be mapped between image space and radial *k*-space over and over again). This property is not specific to GRASP and applies to other compressed-sensing techniques likewise. However, a difference is that the amount of data acquired during continuous GRASP acquisitions is enormous (up to 10 GB per scan). Processing such a vast amount of data with the described algorithm is not feasible using the computer components of current clinical MRI scanners, as the MRI systems would be blocked from clinical scanning for an unacceptable long time. Hence, for validating the feasibility of the GRASP technique in actual clinical practice, it was necessary for us to derive a workflow-friendly solution that completely circumvents the normal reconstruction pipeline. Therefore, we developed an offline-processing framework [12] that automatically transfers the acquired GRASP data from our various clinical MRI scanners to a central reconstruction server. Incoming reconstruction tasks are queued according to urgency (clinical vs. research scan) and processed with a parallelized and performance-optimized C++ implementation of the GRASP algorithm. Upon completion, the reconstructed images are sent into the clinical PACS without any user interaction. Our radiologists can then read the GRASP exams side-by-side with other scans that were reconstructed directly on the MRI scanner. Using our current reconstruction server with 64 CPU cores, GRASP images are available in the PACS within 5 to 45 minutes after the exam (depending on the exact scan/reconstruction protocol). With this seamless integration of the GRASP prototype into our routine clinical workflow, a stable solution is now in place to evaluate the technique in a large number of patients and across our different MRI systems. Over the last two years, already several thousand GRASP reconstructions have been performed at our institution, and the setup has recently also been disseminated to multiple collaboration sites for an independent evaluation.

## Initial applications

As the development of GRASP was aimed at improving abdominal DCE-MRI, liver and kidney scans are logically among the main applications. Figure 3 shows exemplary images from a free-breathing GRASP liver exam of an adult patient, which are free from the typical MRI ghosting artifacts for continued respiration. In this reconstruction, 55 spokes were combined into each image, which yields a temporal resolution of 8.8 sec per image volume and fulfills the timing requirements for diagnostic abdominal DCE-MRI. However, a very powerful feature of GRASP is that the same dataset can be reconstructed with different temporal resolution as well. When grouping only 13 spokes into each image, the resulting temporal resolution is 2.1 sec and, thus, fast enough for quantitative tissue-perfusion analysis. Researchers in our group are currently exploring this

possibility for assessment of the liver function via dual-input dual-compartment modeling [13] and for assessment of the kidney function via estimation of the glomerular filtration rate (GFR). The key advantage here is that the perfusion information is obtained simultaneously without need for additional contrast injection or scan time. Thus, in the future, the GRASP concept might not only help to make abdominal examinations more robust but also provide new diagnostic measures.

Due to the high scan efficiency and simple workflow, GRASP is also very interesting for dynamic imaging of the prostate [14], which has become the GRASP application with the largest clinical scan volume at our institution. In prostate DCE-MRI, which is also with conventional techniques acquired during free breathing due to the required long readout (to properly capture the contrast washout), the main benefit of using GRASP consists in the higher achievable resolution (both spatially and temporally), which translates into an improved detectability and characterization of small tumors. Figure 4 shows images from our current GRASP protocol with 1.1 x 1.1 x 3.0 mm spatial and 2.2 sec temporal resolution, which represents a significant improvement in comparison to our former protocol and allows more precise assessment of the uptake/washout characteristics of suspicious lesions. In this application, data is acquired over a total duration of 5:38 min while the contrast agent is injected 20 sec after the start of the scan to ensure that sufficient pre-contrast data is available. In addition to the higher resolution, also the motion robustness of GRASP contributes to the achieved improvement in image clarity, as conventional prostate scans are often affected by ghosting artifacts caused by motion of the rectum or adjacent bowel loops.

Because GRASP handles such motion effects in a relatively benign manner, our clinical researchers have started using GRASP also for bowel imaging to investigate inflammatory

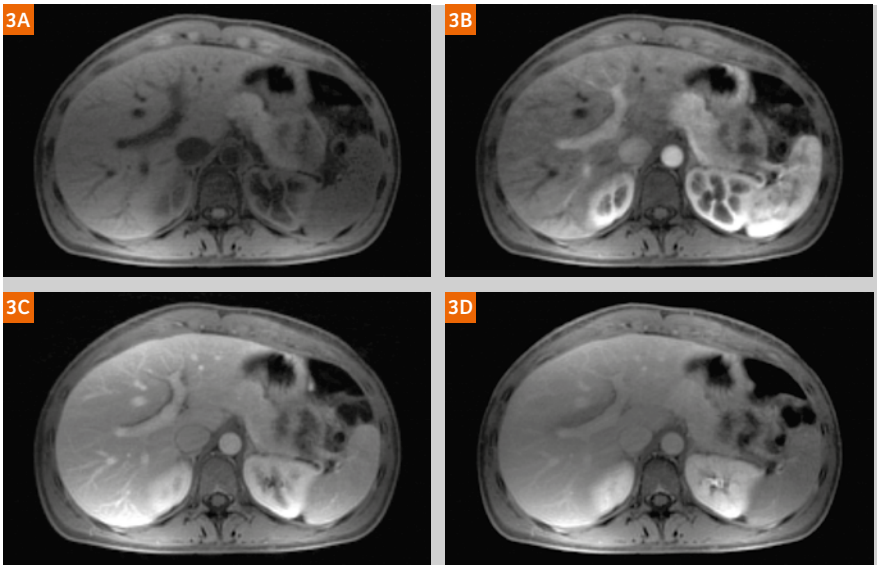


**Figure 3:** Free-breathing dynamic liver GRASP exam in an adult patient. Shown are images of the **(3A)** pre-contrast, **(3B)** arterial, **(3C)** venous, and **(3D)** delayed phase of enhancement. The reconstruction used 55 spokes per frame, corresponding to 8.8 sec per image (spatial resolution 1.5 x 1.5 x 3.0 mm, acquired at 1.5 Tesla).

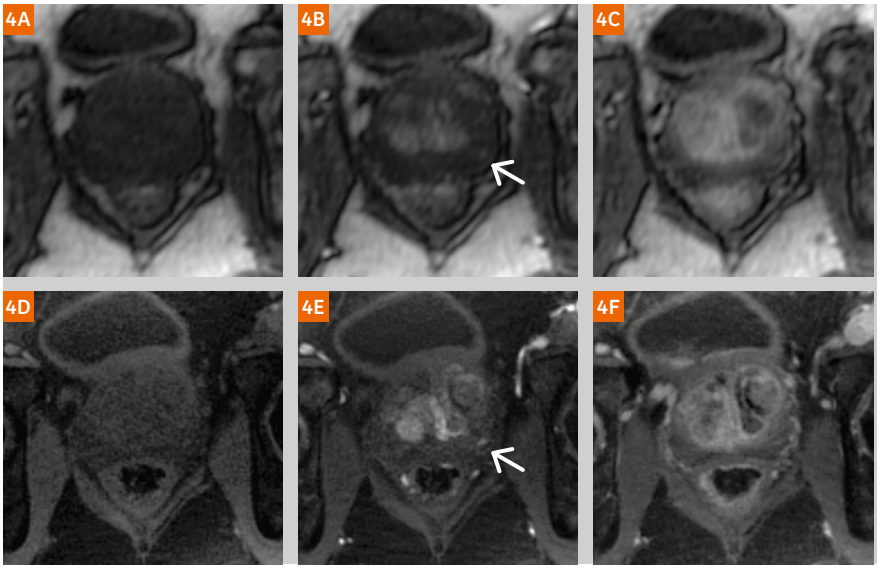


**Figure 4:** Dynamic prostate exam in a patient on active surveillance using **(4A, B, C)** conventional 3D FLASH with 5.5 sec temporal resolution and **(4D, E, F)** GRASP with 2.2 sec temporal resolution (both acquired at 3 Tesla). Images are shown from **(4A, D)** before the injection, **(4B, E)** the time of contrast arrival, and **(4C, F)** a late phase. Due to the higher spatial resolution (1.1 mm vs. 1.9 mm), a suspicious lesion in the peripheral zone with early enhancement and rapid wash-out (arrow) is more clearly visible on the GRASP scan. Note that the GRASP acquisition used fat suppression due to the off-resonance behavior of radial *k*-space sampling [4].

bowel diseases such as Crohn's disease [15]. Inflamed bowel sections are characterized by increased wall thickness and reduced motility, as well as increased vascularity. Therefore, these bowel sections can be easily identified on GRASP scans, as shown in Figure 5. In addition, signal-enhancement curves can be generated from region-of-interests of the dynamic GRASP images and used to calculate quantitative perfusion measures that have been found to correlate with inflammation [15]. These parameters can potentially be used to non-invasively predict disease progression as well as response to treatments. Again, an advantage is that the perfusion images are obtained together with morphologic information from the same dataset through GRASP reconstruction with variable temporal resolution.

Finally, applications of GRASP are of course not confined to abdominopelvic imaging. GRASP can be used as robust imaging technique for any other dynamic T1-weighted examination as well, and a large portion of our recent GRASP scans are actually done in the head and neck region, including dynamic imaging of the orbits, the neck, and the pituitary gland. In the latter application, it is again the improvement in spatial resolution that makes GRASP attractive. When compared to our previously employed 2D GRE protocol (see Fig. 6), GRASP provides much higher spatial resolution along the slice direction and, thus, makes it easier to accurately localize tiny lesions such as microadenomas or small cysts. The possibility to incorporate also perfusion information into the diagnosis adds to its value [16].

## Additional motion compensation

So, is GRASP now the ultimate solution for abdominopelvic DCE-MRI? Unfortunately, not quite yet. Our clinical evaluation showed that free-breathing abdominal GRASP exams work well in many patients with convincing results, but in a certain percentage of patients the image quality is

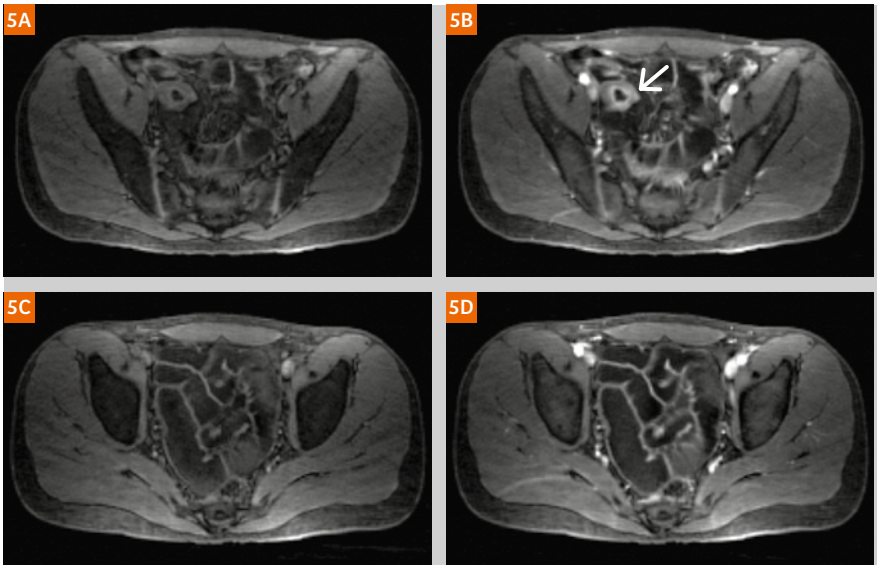


**Figure 5:** Bowel imaging using GRASP in a patient with Crohn's disease (acquired at 1.5 Tesla). Shown are time points **(5A, C)** before and **(5B, D)** shortly after the contrast injection. In the upper images **(5A, B),** a bowel section with increased wall thickness and mucosal hyperenhancement can be seen (arrow), which indicates active inflammation. For comparison, the lower row **(5C, D)** shows a different slice with normal-appearing bowel sections.

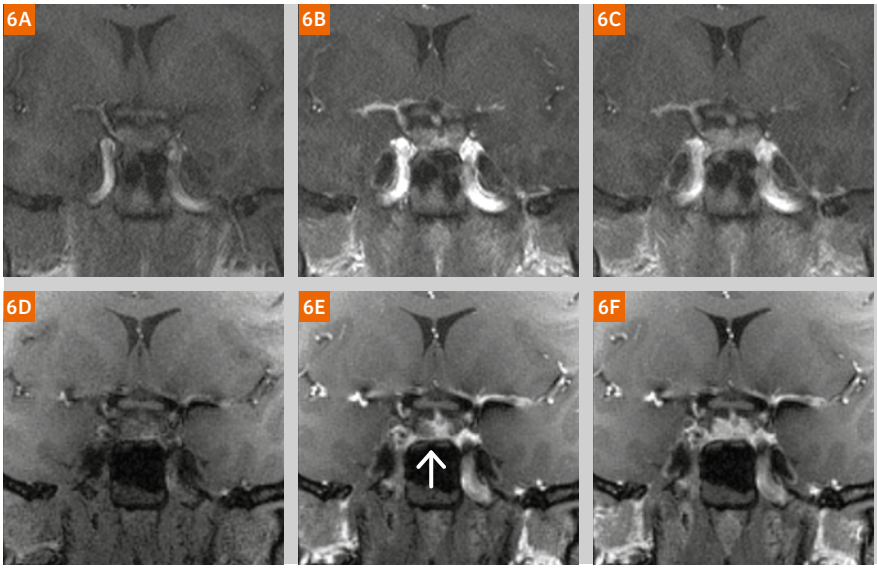


**Figure 6:** Dynamic imaging of the pituitary gland using **(6A, B, C)** a conventional 2D GRE sequence and **(6D, E, F)** GRASP (both acquired at 3 Tesla). Shown are images **(6A, D)** before the injection, **(6B, E)** shortly after contrast arrival, and **(6C, F)** at a later phase. A small area with delayed contrast uptake is visible in the inferior right gland (arrow), which likely reflects a micro-adenoma. Because of much thinner slices (1 mm vs. 3 mm) and higher overall image quality, such findings are easier to identify with GRASP.

still suboptimal. The problem here is that some patients perform deep respiration in the moment when the contrast agent is injected, most likely because they are surprised by the sudden onset of the injection and the resulting sensation. Some patients even start to cough, so that the liver and adjacent organs rapidly move up and down by up to 10 cm during the initial circulations of the contrast agent. While GRASP handles moderate motion relatively well, compromised image quality is obtained if the data for each time point is affected by strong inconsistencies due to varying motion states. For example, if during 50% of the spokes the liver was in an end-expiratory position and during the other 50% of the data in an end-inspiratory position, GRASP will not be able to find one reconstruction that is consistent with both of these motion states. As a result, the images show motion blurring and streak artifacts.

However, since GRASP is based on radial sampling, it is possible to apply additional tricks to resolve this situation. Because all of the spokes pass through the center of *k*-space, it is possible to extract a respiration curve from the *k*-space center that indicates how the patient was breathing during the examination [17]. This is possible because the percentage of (dark) lung tissue in the field-of-view changes during respiration, which leads to a modulation of the total signal power. The latter is reflected by the signal intensity at the *k*-space center, which therefore can be used to generate the respiration curve. Once it is known from the curve what the respiratory state for each acquired spoke was, the data can be sorted according to the respiratory state and the GRASP reconstruction can be extended to treat the respiratory state as an extra dimension, which allows freezing the respiration in the reconstructed images [18]. This extended approach, which we call XD-GRASP[2], is still under active development and accompanied by a further increase of the computational complexity. However, as shown in Figure 7, initial results look promising and we are convinced that the motion-compensated XD-GRASP approach is a leap towards the future of abdominopelvic DCE-MRI, soon delivering 100% reliability in every patient and at every imaging center, regardless of the patient's cooperation and regardless of the operator's training level.

## Conclusion

GRASP is a new concept to simplify DCE-MRI exams by acquiring all information using a single continuous scan instead of several individual scans, which eliminates the possibility of timing or synchronization mistakes. Because GRASP is based on radial sampling, acquisitions can be performed during free breathing, thus making abdominal DCE-MRI accessible for patients unable hold breath. Sufficiently high acquisition speed is achieved by synergistically combining the compressed-sensing and parallel-imaging principles. Due to use of the golden-angle scheme, the temporal resolution and desired image time points can selected retrospectively, which enables reconstructing both morphologic and perfusion information from the same exam. GRASP has already been tested in thousands of patient exams in our routine practice, making it one of the first compressed-sensing techniques that have been evaluated on a large scale for clinical feasibility. While results are convincing for patients with regular breathing activity, limitations still exist for those patients performing deep respiration/coughing during the injection. This remaining issue is now being addressed by integrating active motion compensation based on the radial self-navigation principle.

[2] WIP, the product is currently under development and is not for sale in the US and in other countries. Its future availability cannot be ensured.

### References

1 Elsayes KM, Narra VR, Yin Y, Mukundan G, Lammle M, Brown JJ. Focal hepatic lesions: diagnostic value of enhancement pattern approach with contrast-enhanced 3D gradient-echo MR imaging. Radiographics. 2005 Sep-Oct;25(5):1299-1320.
2 Griswold MA, Jakob PM, Heidemann RM, Nittka M, Jellus V, Wang J, Kiefer B, Haase A. Generalized autocalibrating partially parallel acquisitions (GRAPPA). Magn Reson Med. 2002 Jun;47(6):1202-1210.
3 Martin DR, Sharma P, Kitajima H. Challenges and Clinical Value of Automated and Patient-Specific Dynamically Timed Contrast-Enhanced Liver MRI Examination. Siemens MAGNETOM Flash 3/2009:40-45.
4 Block KT, Chandarana H, Milla S, Bruno M, Mulholland T, Fatterpekar G, Hagiwara M, Grimm R, Geppert C, Kiefer B, Sodickson DK. Towards Routine Clinical Use of Radial Stack-of-Stars 3D Gradient-Echo Sequences for Reducing Motion Sensitivity. J Korean Soc Magn Reson Med. 2014 Jun;18(2):87-106.
5 Chandarana H, Block TK, Rosenkrantz AB, Lim RP, Kim D, Mossa DJ, Babb JS, Kiefer B, Lee VS. Free-breathing radial 3D fat-suppressed T1-weighted gradient echo sequence: a viable alternative for contrast-enhanced liver imaging in patients unable to suspend respiration. Invest Radiol. 2011 Oct;46(10):648-53.
6 Feng L, Grimm R, Block KT, Chandarana H, Kim S, Xu J, Axel L, Sodickson DK, Otazo R. Golden-angle radial sparse parallel MRI: Combination of compressed sensing, parallel imaging,

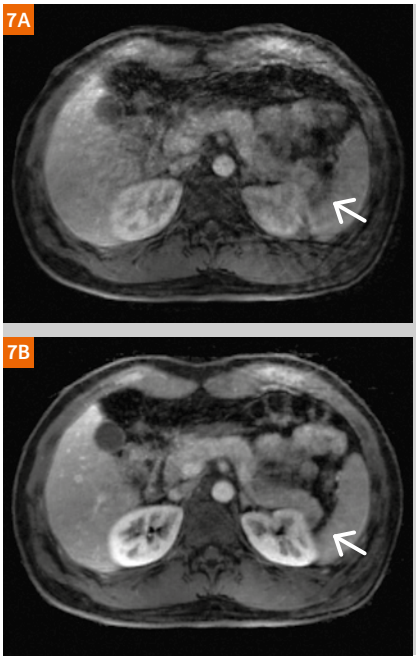


**Figure 7:** GRASP liver exam of a patient breathing deeply after the injection. Due to the inconsistent motion state of the acquired data, the normal GRASP reconstruction **(7A)** is affected by streak artifacts and motion blurring (arrow). These artifacts are clearly reduced when employing XD-GRASP with additional motion compensation **(7B)**.

and golden-angle radial sampling for fast and flexible dynamic volumetric MRI. Magn Reson Med. 2014 Sep;72(3):707-717.

7 Chandarana H, Feng L, Block TK, Rosenkrantz AB, Lim RP, Babb JS, Sodickson DK, Otazo R. Free-breathing contrast-enhanced multiphase MRI of the liver using a combination of compressed sensing, parallel imaging, and golden-angle radial sampling. Invest Radiol. 2013 Jan;48(1):10-16.

8 Winkelmann S, Schaeffter T, Koehler T, Eggers H, Doessel O. An optimal radial profile order based on the Golden Ratio for time-resolved MRI. IEEE Trans Med Imaging. 2007 Jan;26(1):68-76.

9 Lustig M, Donoho D, Pauly JM. Sparse MRI: The application of compressed sensing for rapid MR imaging. Magn Reson Med. 2007 Dec;58(6):1182-1195.

10 Pruessmann KP, Weiger M, Börnert P, Boesiger P. Advances in sensitivity encoding with arbitrary k-space trajectories. Magn Reson Med. 2001 Oct;46(4):638-651.

11 Block KT, Uecker M, Frahm J. Undersampled radial MRI with multiple coils. Iterative image reconstruction using a total variation constraint. Magn Reson Med. 2007 Jun;57(6):1086-1098.

## Contact

Dr. Kai Tobias Block

Center for Biomedical Imaging

NYU Langone Medical Center
660 First Avenue
New York, NY 10016
USA
tobias.block@nyumc.org

12 Information and free download available at http://ktblock.de/yarra

13 Chandarana H, Block TK, Ream J, Mikheev A, Sigal SH, Otazo R, Rusinek H. Estimating Liver Perfusion From Free-breathing Continuously Acquired Dynamic Gd-EOB-DTPA Enhanced Acquisition With Compressed Sensing Reconstruction. Invest Radiol. In press.

14 Rosenkrantz AB, Geppert C, Grimm R, Block TK, Glielmi C, Feng L, Otazo R, Ream JM, Romolo MM, Taneja SS, Sodickson DK, Chandarana H. Dynamic contrast-enhanced MRI of the prostate with high spatiotemporal resolution using compressed sensing,parallel imaging, and continuous golden-angle radial sampling: Preliminary experience. J Magn Reson Imaging. 2014 May 16. Epub ahead of print.

15 Ream JM, Doshi AM, Block KT, Kim S, Otazo R, Feng L, Chandarana H. High Spatiotemporal Dynamic Contrast-Enhanced MRI of the Small Bowel in Active Crohn's Terminal Ileitis using Compressed Sensing, Parallel Imaging, and Golden-Angle Radial Sampling. In Proc. Intl. Soc. Mag. Reson. Med. 22 (2014): 4292.

16 Espagnet CR, Bangiyev L, Block KT, Grimm R, Feng L, Ruggiero V, Babb J, Davis A, Sodickson DK, Fatterpekar G. High resolution DCE MRI of the Pituitary gland using Radial K space Aquisition with Compressed Sensing Reconstruction. In Proc. Intl. Soc. Mag. Reson. Med. 22 (2014): 4669.

17 Grimm R, Bauer S, Kiefer B, Hornegger J, Block KT. Optimal Channel Selection for Respiratory Self-Gating Signals. In Proc. Intl. Soc. Mag. Reson. Med. 21 (2013): 3749.

18 Feng L, Liu J, Block KT, Xu J, Axel L, Sodickson DK, Otazo R. Compressed Sensing Reconstruction with an Additional Respiratory-Phase Dimension for Free-Breathing Imaging. In Proc. Intl. Soc. Mag. Reson. Med. 21 (2013): 606.

# Learn more!

Listen to Professor Stuber's keynote on Compressed Sensing at

## www.siemens.com/magnetom-world

**go to > Clinical Corner > Clinical Talks**

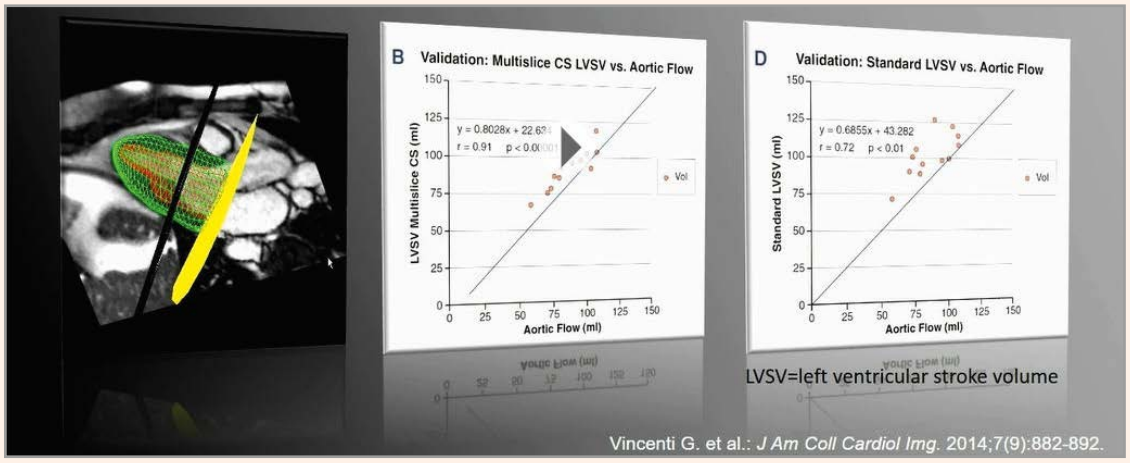


*Matthias Stuber, Ph.D.*

Centre Hospitalier Universitaire Vaudois (CHUV), Lausanne, Switzerland

# Free-breathing Late Enhancement Imaging: Phase Sensitive Inversion Recovery (PSIR) with Respiratory Motion Corrected (MOCO) Averaging

**Peter Kellman; Hui Xue; Michael S. Hansen**

National Heart, Lung, and Blood Institute, National Institutes of Health, DHHS, Bethesda, MD, USA

## Introduction

Late gadolinium enhancement (LGE) has become a gold standard in myocardial viability assessment [1, 2] providing excellent depiction of myocardial infarction (MI) and macroscopic scarring. The use of late enhancement in the diagnosis of ischemic heart disease and in guiding revascularization therapy has gained wide acceptance. More recently, late enhancement has been playing a broader role in characterizing fibrosis in non-ischemic cardiomyopathies [3,4], and in measurement of scar resulting from treatment of cardiac arrhythmias using radiofrequency ablation [5]. As the use of late enhancement imaging has matured and as the span of applications has widened, clinicians are examining late enhancement images for more subtle indication of fibrosis and the demands on image quality have grown [6].

Breath-held (BH), segmented FLASH has been the gold standard for LGE for many years [7] and is widely used with great success when patients are cooperative and can hold their breath. In instances where poor breath-holding results in ghost artifacts, single shot SSFP imaging has been used as an alternative. However, while single shot imaging mitigates ghosting artifacts, it generally has compromised spatial resolution and image quality compared to BH FLASH. Therefore, the single shot approaches are less sensitive to detection of subtle LGE and to detection of small lesions [8]. The development of PSIR LGE with respiratory motion corrected (MOCO) averaging [6, 9, 10] has led to a free-breathing (FB) approach which achieves the robustness of single shot approaches and the resolution and image quality of BH segmented FLASH. In addition to elimination of ghosting artifacts due to poor breath-holds (Fig. 1), the PSIR MOCO LGE is inherently less sensitive to arrhythmias.

In addition to being easier on the patients, free-breathing PSIR MOCO LGE eliminates pauses between BH slices and is therefore faster to acquire than a BH stack. Free-breathing, MOCO LGE greatly simplifies the clinical workflow, particularly since LGE is typically at the end of the study where patient compliance is frequently a problem. PSIR MOCO LGE has been demonstrated to improve the image quality in both pediatric[1] [11] and adult populations [12]. It has been shown to make a significant improvement in the most vulnerable population of sick patients [12].

1

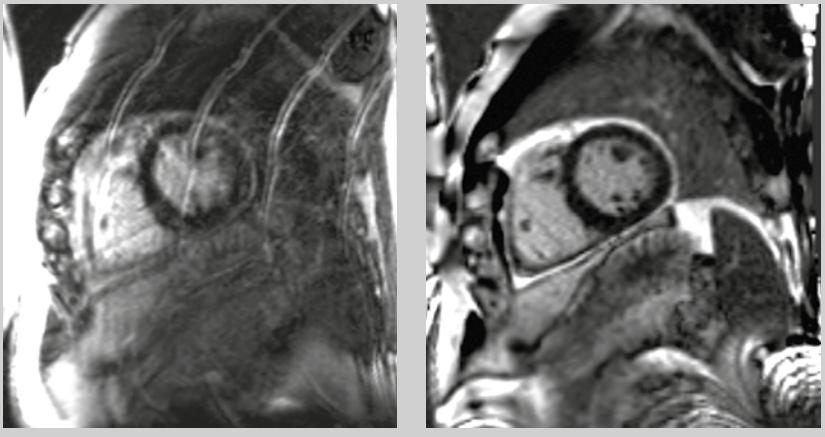


**Figure 1:** Free-breathing, MOCO PSIR LGE images eliminate ghosting artifacts and achieve high SNR by means of respiratory motion corrected averaging [6].

[1] MR scanning has not been established as safe for imaging fetuses and infants less than two years of age. The responsible physician must evaluate the benefits of the MR examination compared to those of other imaging procedures.

In a study of 390 consecutive patients [12], it was concluded that: "Myocardial infarction detection and quantification are similar between MOCO-LGE and BH-LGE when BH-LGE can be acquired well, but BH-LGE quality deteriorates with patient vulnerability. Acquisition time, image quality, diagnostic confidence, and the number of successfully scanned patients are superior with MOCO-LGE, which extends LGE-based risk stratification to include patients with vulnerability confirmed by outcomes." A number of sites have adopted PSIR MOCO LGE as their sole means of LGE imaging and combined they have been performing over 10,000 studies annually for the past several years.

Respiratory MOCO averaging can offer SNR improvements well beyond what is possible using BH FLASH by further increasing the number of averages. Therefore, with PSIR MOCO LGE, higher spatial resolution or thinner slices are achievable in clinical practice. Furthermore, PSIR MOCO LGE has been integrated with dark blood PSIR to provide improved contrast of subendocardial MI with the adjacent bright blood pool.

## Free-breathing approach

Motion correction may be used to correct respiratory motion [9, 10] in the case of free-breathing acquisition, or diaphragmatic drift in the case of breath-holding. The SNR for individual single shot PSIR-SSFP images is slightly worse than segmented PSIR-FLASH due to the increase in bandwidth, despite the increase in flip angle. However, the SNR of single shot PSIR-SSFP may be significantly improved by averaging multiple repeated measurements (Fig. 2). Typically, using 8 PSIR images acquired in 16 heartbeats provides an SNR comparable or better than the FLASH protocol for approximately the same duration and may be extended to a larger number of averages since the acquisition is not breath-held. Parallel imaging at higher acceleration factors may be used to reduce the imaging duration in diastole to achieve higher spatial resolution or reduce motion blur at higher heart rates. Use of non-rigid motion correction provides correction over the full FOV in a fully automated fashion. Selective averaging may be used to discard images that do not meet similarity criteria due to through plane motion [10]. This retrospective image based navigator strategy is robust and simple to use, thereby eliminating the complexity and unreliability of prospective navigators.

**Key points/implications:**

- Free-breathing imaging is easier for the patient
- Improves clinical workflow
- Free-breathing imaging reduces artifacts
- Improves diagnostic quality
- Is highly effective for the most vulnerable population

2

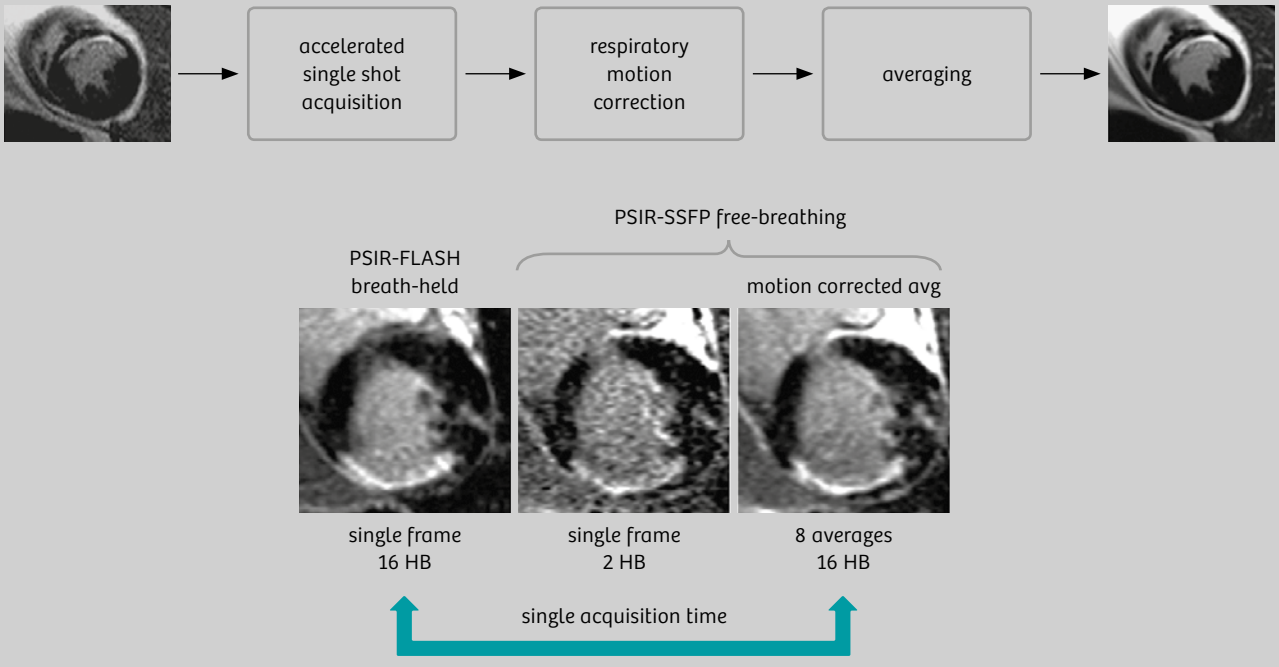


**Figure 2:** Respiratory motion corrected averaging strategy using accelerated single shot imaging to mitigate artifacts and motion corrected averaging to increase SNR [6].

## Imaging protocols

PSIR MOCO LGE has been integrated with a number of imaging protocols to include SSFP, FLASH, and multi-echo GRE for water fat separated LGE, and dark blood (DB) PSIR LGE (Fig. 3). Typical parameters for these protocols are listed in Table 1. Additionally, early gadolinium enhancement (EGE) protocols use reduced averaging for more rapid multi-slice coverage, and higher spatial resolution protocols (e.g. 256 x 224 or 320 x 244) use higher parallel imaging acceleration (PAT) factors and increased averaging.

3


**Figure 3:** Simplified diagram of sequence for PSIR LGE with interleaved acquisition of IR and PD images on alternate heartbeats (top) and dark blood (DB) PSIR LGE using IR-T2 RF preparation. Readout may be single-shot SSFP, FLASH, or multi-echo GRE for water fat separated PSIR LGE imaging.

| | Bright Blood (BB) | | Dark Blood (DB) | Fat Water (FW) |
|---|---|---|---|---|
| **Preparation** | Inversion Preparation | | Inversion Preparation & T2 preparation | Inversion Preparation |
| **Readout (single shot)** | SSFP<br>$FA_{IR}$ = 50°<br>$FA_{PD}$ = 8° | FLASH<br>$FA_{IR}$ = 10°<br>$FA_{PD}$ = 5° | SSFP<br>$FA_{IR}$ = 50°<br>$FA_{PD}$ = 8° | 3-echo GRE<br>($FA_{IR}$ = 25°, $FA_{PD}$ = 5°)<br>monopolar readout |
| **Typical FOV / resolution** | 360 x 270 mm²<br>1.4 x 1.9 x 8 mm³ | | | 360 x 270 mm²<br>1.4 x 2.2 x 8 mm³ |
| **Matrix size** | 256 x 144 (parallel imaging factor 2) | | | 256 x 123 (parallel imaging factor 3) |
| **Number of acquired measurements** | 8 | | 16 | 9 |
| **T2 prep TE** | n/a | | 10–40 ms | n/a |
| **TE / TR** | 1.2/2.8 ms | 1.25/3.1 ms | 1.2/2.8 ms | (1.5,3.8, 6.1)/7.2 ms |
| **ECG triggering** | Inversions every 2 RR (HR < 90 bpm)<br>Inversions every 3 RR (HR > 90 bpm) | | | |

**Table 1:** Typical imaging parameters for various PSIR LGE MOCO protocols.

## PSIR motion corrected averaging

Non-rigid image registration is used to correct respiratory motion between repeated measurements acquired during normal free-breathing PSIR LGE imaging [6, 9, 10]. The motion correction (MOCO) is done independently for the IR and proton density (PD) images and the MOCO averaged complex images are co-registered prior to the PSIR demodulation step (Fig. 4, current implementation). The non-rigid image registration corrects in-plane motion and through-plane motion is dealt with by discarding 50% of the acquired measurements which are most dissimilar. The selection of the reference frame used for image registration as well as which frames to be discarded is based on the similarity of frames as estimated from a global mean square difference metric [10]. In this way, the retrospective image-based strategy averages the most frequent respiratory phase which is typically at end-expiration. The co-registered MOCO PD image is used for both PSIR demodulation, which preserves the sign of the IR signal by removing the background phase, as well as for correcting the surface coil intensity roll-off (Fig. 5). To improve the reliability of IR/PD co-registration which is critical for both PSIR demodulation and surface coil intensity correction, a volume preserving non-rigid co-registration is used to deal with the challenge of different contrasts between IR and PD images.

In dark blood imaging protocols SNR is typically lower due to T2 weighting and more averages are needed compared to the bright blood PSIR MOCO protocol. Likewise, for higher spatial resolution with higher PAT factors and smaller voxels, the loss in SNR in raw images may be compensated for by increased averaging.

## Implementation

The PSIR MOCO implementation has evolved over the last several years and has achieved high quality and reliability used at a large number of sites in their clinical workflow. Initial off-line implementations [9, 10] were quickly moved to the scanner as works-in-progress (WIP) packages as part

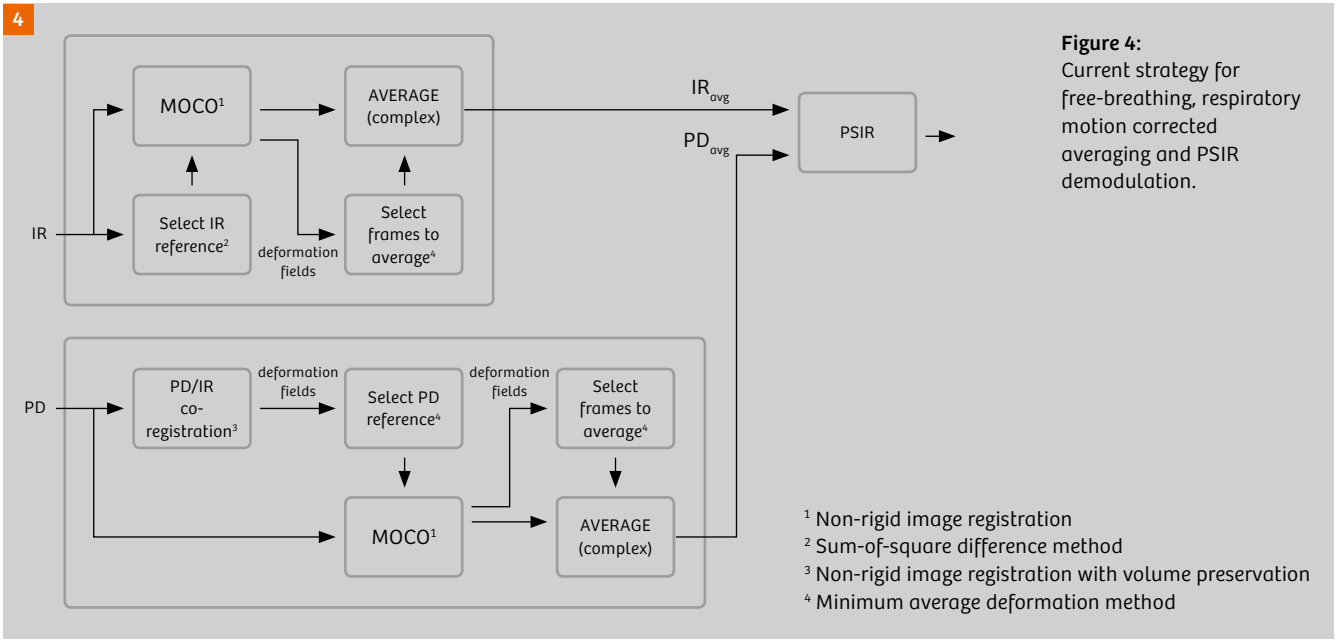


**Figure 4:**
Current strategy for free-breathing, respiratory motion corrected averaging and PSIR demodulation.

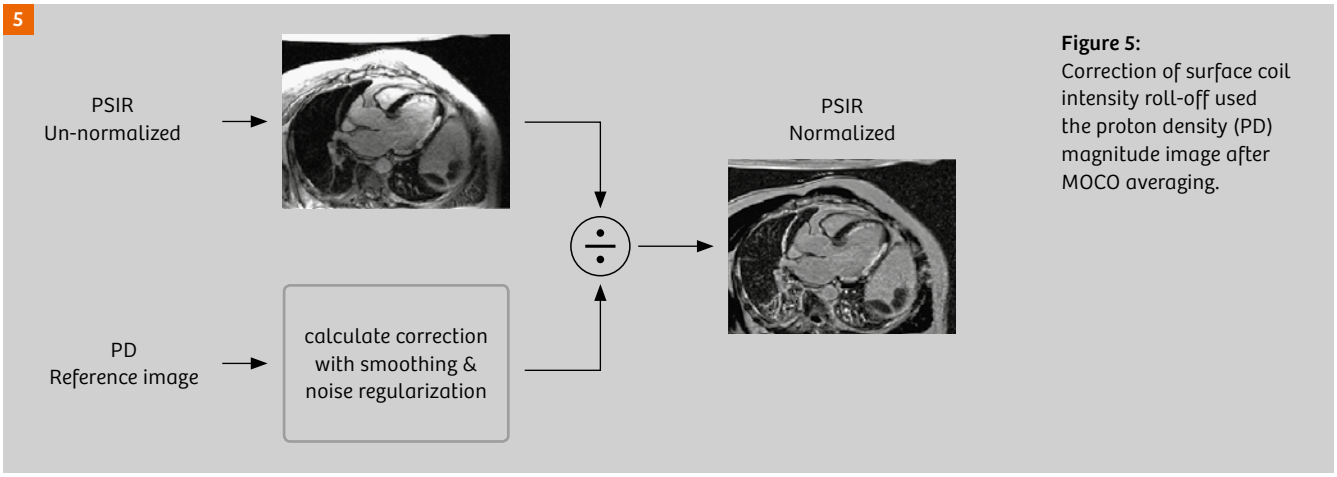


**Figure 5:**
Correction of surface coil intensity roll-off used the proton density (PD) magnitude image after MOCO averaging.

of co-development between NIH and Siemens under a cooperative research and development agreement (CRADA). Initial WIPs began in 2007 with WIP 373 (*syngo* MR B13A) for MAGNETOM Avanto and Espree, and were re-released with various improvements over the ensuing years.

Initial implementations applied respiratory MOCO and averaging directly to the individual single shot SSFP images, and significant through plane motion was dealt with by discarding frames as described above. Subsequent development applied MOCO averaging independently to the IR and PD, and performed the PSIR between IR and PD after motion corrected averaging. This mitigated artifacts arising due to respiratory motion between IR and PD. Early versions would output a number of intermediate series to include the raw images, MOCO images, as well the averages. As the development matured, the final versions output only the MOCO average.

A recent development has been the implementation of the PSIR MOCO reconstruction using the Gadgetron image reconstruction framework [13]. The Gadgetron framework provides increased speed and 'on-the-fly' reconstruction for multi-slice acquisitions. On-the-fly reconstruction immediately starts the computation when the image acquisition of the first slice is completed. For a scan covering multiple slices, this scheme allows image display during the acquisition of a stack of slices. Gadgetron software may be installed on the *syngo* MR E11 platforms (1.5T MAGNETOM Aera, 3T MAGNETOM Skyra and Prisma) to run on the scanner's image reconstruction computer (MARS) or may be run on an external computer connected over the network (currently a C2P with NIH research collaboration partners). Using on-the-fly reconstruction, the time to complete the full stack of slices (9 slices/8 measurements) is approximately 6 or 8 seconds after completion of the acquisition, when performed on a 24 core external Linux PC or 16 core MARS, respectively. For on-the-fly reconstruction, all measurements for a given slice are acquired consecutively (inner loop).

## PSIR MOCO LGE

Free-breathing PSIR MOCO LGE protocols are now widely used at a number of clinical research sites. At many of these sites, the free-breathing protocol is used exclusively since it saves time and provides excellent quality. Examples of late enhancement for a wide range of patterns (Fig. 6) in both ischemic and non-ischemic heart disease illustrate that PSIR MOCO provides excellent image quality and high spatial resolution to detect small focal enhancement as well as more subtle enhancement.

The typical acquisition of a SAX stack of 9-slices (Fig. 7) is acquired in 9 slices × 8 measurements × 2 RR = 144 heart beats = 2:24 min at 60 bpm. The reconstruction is performed 'on-the-fly' and is completed within 10 seconds of the end of scan. Long axis views may be prescribed individually or as multi-slice. When prescribing long axis views off of free-breathing SAX images, the long axis may be at a different respiratory position and possibly not optimal. Some sites find it simpler to prescribe a parallel stack of 3 long axis slices for each view (Fig. 8) to ensure acquisition of the best position.

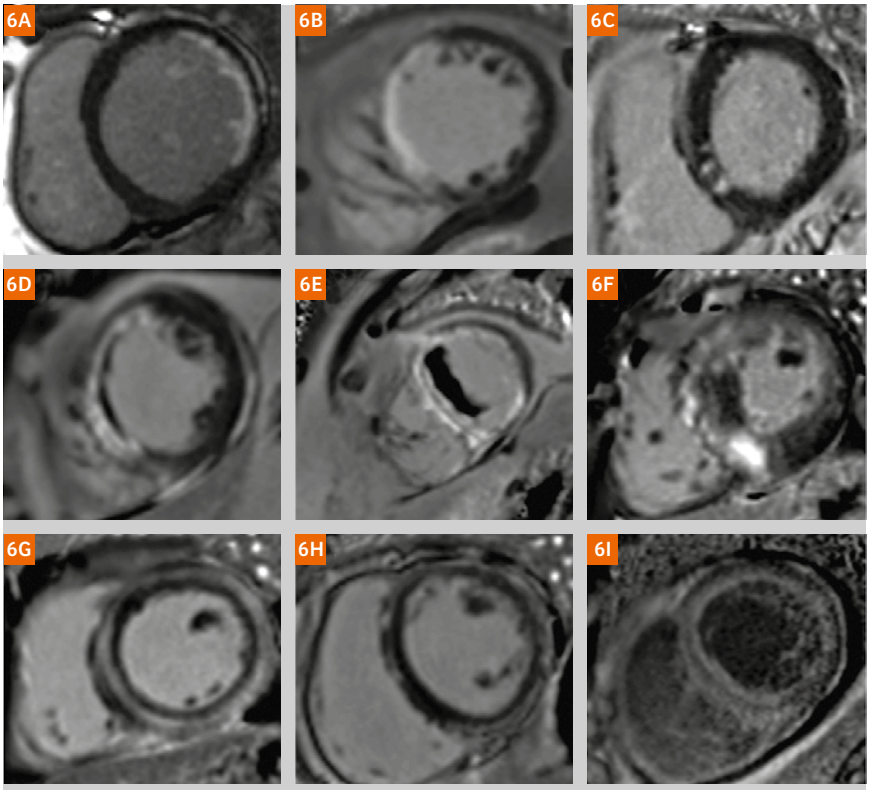


**Figure 6:** Examples of free-breathing PSIR MOCO LGE images illustrating the a variety of late enhancement patterns: **(6A)** sub-endocardial chronic MI, **(6B)** transmural chronic MI, **(6C)** small focal scar, **(6D)** acute MI with dark core due to microvascular obstruction (MVO), **(6E)** MI with thrombus, **(6F)** heterogeneous focal enhancement in a patient with HCM, **(6G)** mid-wall enhancement in patient with myocarditis, **(6H)** sub-epicardial enhancement in patient with myocarditis, and **(6I)** subendocardial fibrosis in patient with amyloidosis.

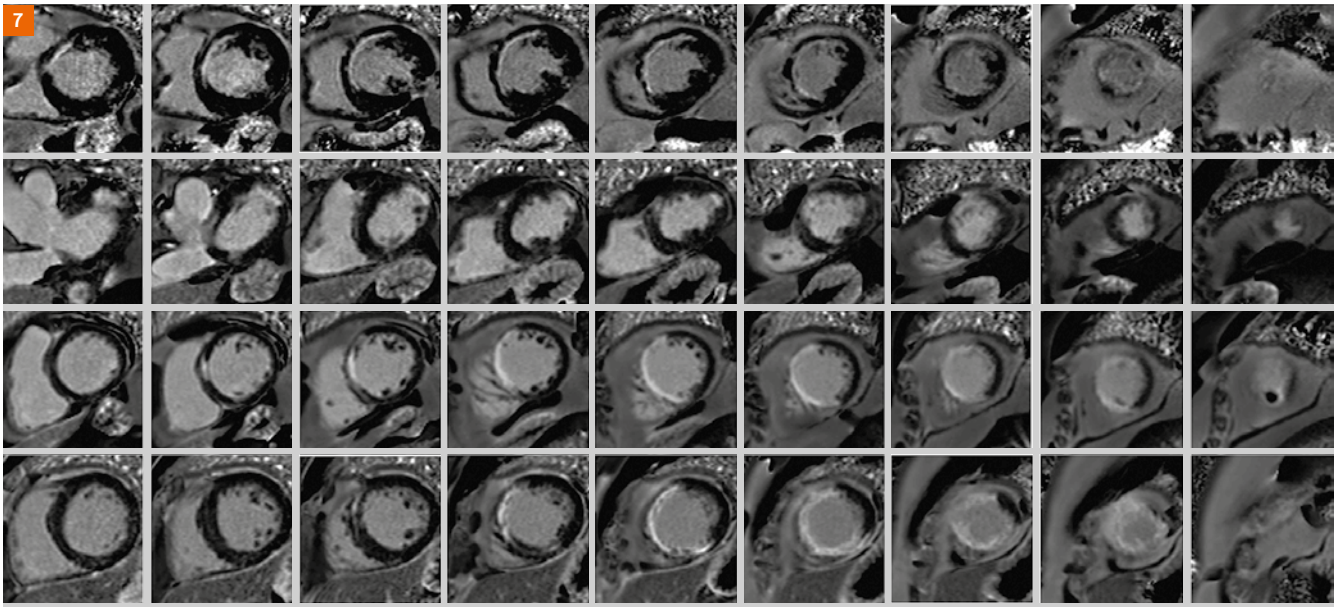


**Figure 7:** Examples of free-breathing acquisition of stacks of 9 short axis slices using PSIR MOCO LGE acquired and reconstructed on-the-fly in approximately 2.5 min, depending on heart rate.

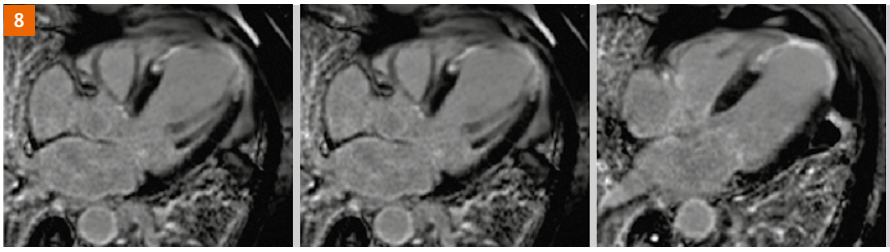

**Figure 8:** Example of free-breathing acquisition of a stack of 3 parallel long axis slices to ensure that the 4-chamber view is correctly obtained when prescribed off images that are potentially at a different respiratory position.

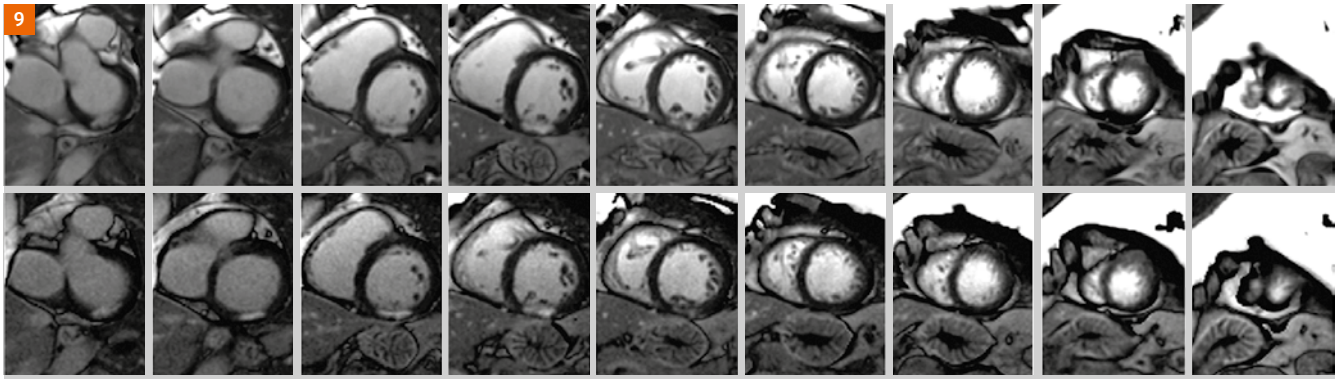

**Figure 9:** Comparison of 9 slice short axis stack acquired at 3T using the free-breathing PSIR MOCO LGE with SSFP (top) and FLASH (bottom) readouts, respectively.

The PSIR MOCO protocol most frequently used is the SSFP based protocol. A FLASH based protocol has also been tested, and is beneficial in situations with large off-resonance variations that are difficult to shim. There is a reduction in SNR that may be compensated by increased averaging. A comparison of SSFP and FLASH protocols at 3T is shown in Fig. 9 using the same averaging (protocols in Table 1).

## Early enhancement imaging

Early gadolinium enhancement (EGE) during the phase between 1–5 minutes following gadolinium administration is often more sensitive to detection of edema, thrombus, or microvascular obstruction (MVO). MVO may be less apparent for LGE when the gadolinium may reach the MI core. Furthermore, in the case of acute MI, the early enhancement may show the area at risk since the edematous tissue will experience a more rapid early enhancement than the central core. Similarly the edematous region in acute myocarditis is more conspicuous in early phase.

The free-breathing PSIR MOCO LGE protocol may be used for EGE without tiring the patient. The EGE may use the same LGE protocol, or may use a reduced number of averages, e.g. 4, in order that a full SAX stack can be acquired in just over minute, in cases where better time resolution is desired.

## Dark Blood PSIR LGE

Late-enhancement imaging typically achieves excellent contrast between infarcted and normal myocardium. However, the contrast between the MI and the blood pool is frequently suboptimal. A large fraction of infarctions caused by coronary artery disease are sub-endocardial and thus adjacent to the blood pool. The contrast between the blood and MI in the inversion recovery (IR) image depends on variables such as contrast agent dosage, time from gadolinium administration, clearance rate, and imaging parameters. Blood velocity may also have a role in the contrast, even though non-slice-selective IR is used. Therefore, as a result of mechanisms that are not fully characterized or controlled, it is not infrequent that sub-endocardial MIs are difficult to detect or clearly delineate.

A dark blood (DB) LGE may be achieved by combining a T2 preparation [14–16] with IR. In these schemes, the myocardial signal is reduced relative to the blood signal thereby reducing the inversion times to null the myocardium. In this way, it is possible to null both the myocardium and the blood at the same time. The order of the T2 and IR preparations may be applied as T2-IR [16] or IR-T2 [14]. Both of these previously reported schemes used a FLASH readout. We combined an IR-T2 with a single shot SSFP readout and respiratory motion corrected averaging to achieve the acceptable SNR while maintaining the desired spatial and temporal resolution. In this manner, imaging is conducted free-breathing which has benefits for image quality, patient comfort, and clinical workflow. Furthermore, by using a PSIR reconstruction [17] the blood signal may be made darker than the myocardium (i.e. negative signal values) thereby providing contrast between the blood and both the MI and remote myocardium [15].

Dark blood LGE schemes provide contrast between the MI and the blood pool at the expense of SNR. However, the SNR cost of the proposed DB may be recovered by increased averaging. The DB PSIR MOCO LGE protocol in Table 1 achieves comparable contrast-to-noise ratio (CNR) between the MI and myocardium as the conventional bright blood protocol.

Free-breathing, dark blood PSIR LGE imaging has been demonstrated to improve the visualization of subendocardial MI and fibrosis in cases with low contrast with adjacent blood pool (Fig. 10). The proposed method also improves visualization of thin walled fibrous structures such as atrial walls and valves, as well as papillary muscles.

## Fat water separated late enhancement

Lipomatous metaplasia is prevalent in chronic myocardial infarction (MI) [18] and other nonischemic cardiomyopathies. Using conventional late enhancement imaging, it is difficult to discriminate between fibrosis and intramyocardial fat since both have low T1 and appear bright. Furthermore, the presence of fat may create image

10

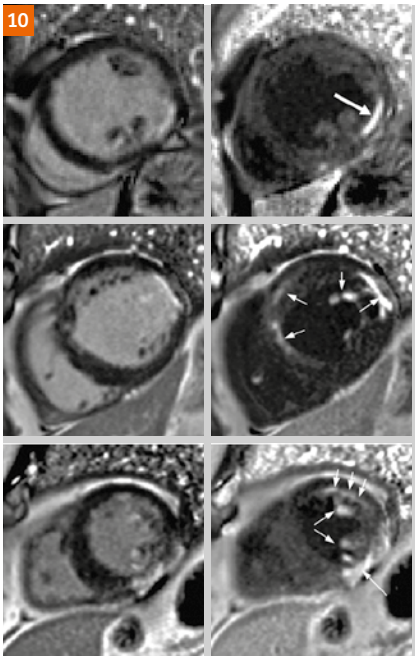

**Figure 10:** Examples of bright blood (left) and dark blood (DB) (right) PSIR MOCO LGE illustrating improved contrast between subendocardial MI and blood pool. The areas of scar indicated by LGE are more conspicuous on the DB PSIR images (see arrows) and in some cases might have been missed entirely in the bright blood PSIR images.

11

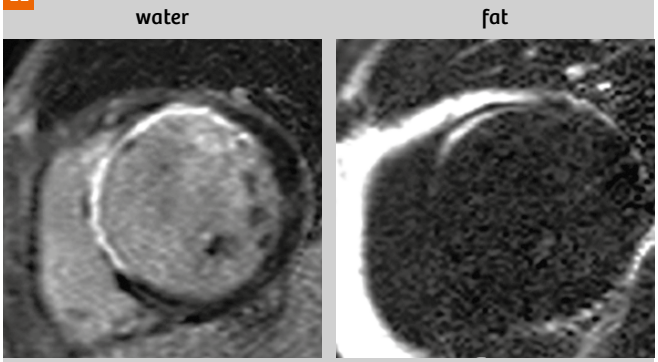


**Figure 11:** Patient with chronic MI in anteroseptal region with lipomatous metaplasia seen in fat-water separated PSIR MOCO LGE [19].

12

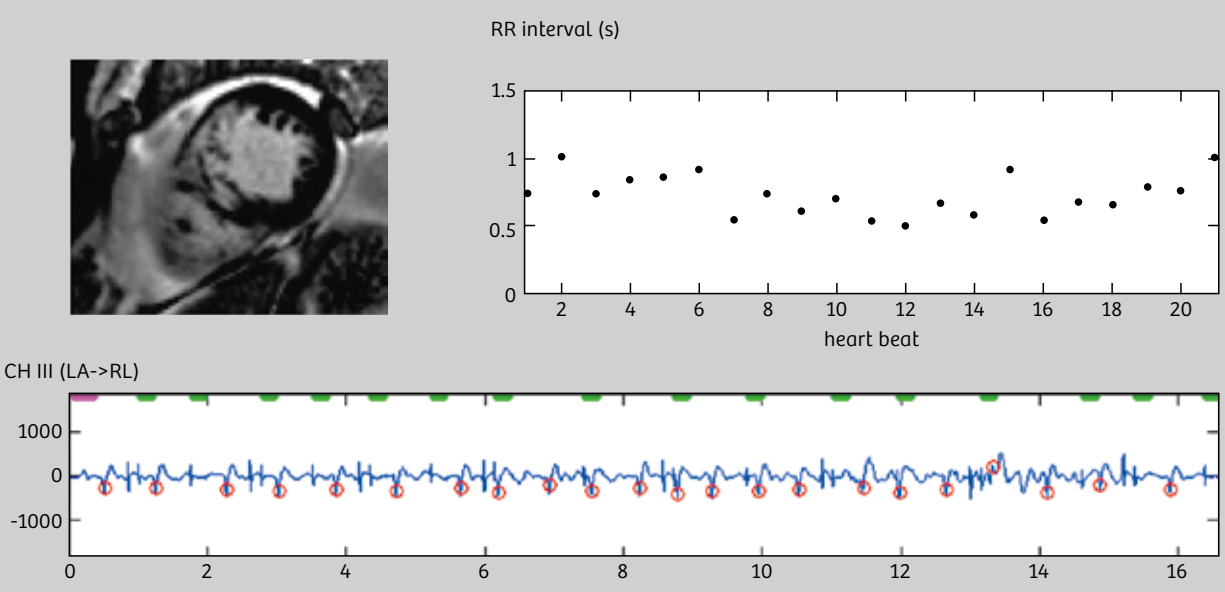


**Figure 12:** Free-breathing, PSIR MOCO LGE in patient with chronic MI in atrial fibrillation (shown at SCMR 2014 Annual Scientific Meeting, Real-time imaging: in case of atrial fibrillation, Kellman P).

artifacts due to the chemical shift of fat or the bright epicardial fat signal may obscure the sub-epicardium. Using fat-water separated late-enhancement imaging it is possible to distinguish the fibrosis from fat with improved sensitivity and to avoid erroneous tissue classification [19]. Detecting the presence of fibrofatty infiltration or other intramyocardial fat may have diagnostic value. The presence of intramyocardial fat may form a substrate for arrhythmias due to the lower electrical conductivity of fat. It has been shown that fibrofatty infiltration of the myocardium is associated with sudden death, and therefore noninvasive detection could have prognostic value. Fat water separated imaging may be performed free-breathing [20] with multi-echo PSIR MOCO LGE (Table 1). An example of lipomatous metaplasia in chronic MI is shown in Figure 11. It is also used to improve visualization of pericardial disease and in general mass characterization.

## Insensitive to arrhythmias

The free-breathing PSIR MOCO LGE imaging based on single shot imaging is inherently insensitive to arrhythmias since it is free from ghosting artifacts experienced with breath-held segmented acquisitions. In patients with arrhythmias during scanning, there may be some variation in the cardiac phase of repeated measurements depending on the precise nature of the variation. It is possible to retrospectively discard heart beats outside of specified criteria, however in practice the MOCO average has been found to be relatively insensitive to a large variation in RR intervals and is even robust in subjects with atrial fibrillation (Fig. 12). Furthermore, some patients experience arrhythmias that are brought on or worsened by breath-holding, and are in sinus rhythm during normal free-breathing.

## Discussion

The free-breathing approach to LGE using PSIR MOCO performs reliably with excellent image quality. The image is often better than breath-held LGE in the most vulnerable population that cannot breath-hold [12] and for pediatric subjects[2] [11]. The paradigm shift to free-breathing CMR has benefits to the clinical workflow in terms of speed, ease of use, and patient comfort. A number of other free-breathing protocols that incorporate retrospective MOCO have been recently developed and allow for a complete free-breathing CMR study to include real-time cine function [21, 22], T2-SSFP [23], T2* mapping [24], and myocardial perfusion mapping [25]. These afford a significant reduction in overall exam time when combined. The PSIR MOCO LGE has been adopted at a number of sites as the new standard and is widely used.

## Acknowledgements

We would like to acknowledge our colleagues at Siemens, in particular Xiaoming Bi and Randall Kroeker, for their role in development of the PSIR MOCO LGE WIP, and to our numerous clinical collaborators for their insights and clinical examples: Andrew E. Arai, W. Patricia Bandettini, Erik B. Schelbert, James C. Moon, Marianna Fontana, Martin Ugander, Patricia Feuchter, Cavan McGurk, Sofie Olsson, Jenny Rasck, Sarah Anderson, and Christine Mancini.

Supported by the National Heart, Lung and Blood Institute, National Institutes of Health by the Division of Intramural Research.

[2] MR scanning has not been established as safe for imaging fetuses and infants less than two years of age. The responsible physician must evaluate the benefits of the MR examination compared to those of other imaging procedures.

### References

1 Fieno DS, Kim RJ, Chen E, Lomasney JW, Klocke FJ, Judd RM. Contrast-Enhanced Magnetic Resonance Imaging of Myocardium at Risk Distinction Between Reversible and. 2000;36:1985–91.
2 Kim RJ, Fieno DS, Parrish TB, Harris K, Chen E-L, Simonetti O, et al. Relationship of MRI Delayed Contrast Enhancement to Irreversible Injury, Infarct Age, and Contractile Function. Circulation. 1999;100:1992–2002.
3 Bohl S, Wassmuth R, Abdel-Aty H, Rudolph A, Messroghli D, Dietz R, et al. Delayed enhancement cardiac magnetic resonance imaging reveals typical patterns of myocardial injury in patients with various forms of non-ischemic heart disease. Int. J. Cardiovasc. Imaging. 2008;24:597–607.
4 Hunold P, Schlosser T, Vogt FM, Eggebrecht H, Schmermund A, Bruder O, et al. Myocardial Late Enhancement in Contrast-Enhanced Cardiac MRI: Distinction Between Infarction and Non-Infarction-Related Disease. AJR. Am. J. Roentgenol. 2005;184:1420–6.
5 Vergara GR, Marrouche NF. Tailored management of atrial fibrillation using a LGE-MRI based model: from the clinic to the electrophysiology laboratory. J. Cardiovasc. Electrophysiol. 2011;22:481–7.
6 Kellman P, Arai AE. Cardiac imaging techniques for physicians: Late enhancement. J. Magn. Reson. Imaging. 2012;36:529–42.
7 Kim RJ, Shah DJ, Judd RM. How We Perform Delayed Enhancement Imaging. J. Cardiovasc. Magn. Reson. 2003;5:505–14.
8 Lee D, Wu E, Chung Y, Simonetti O, Elliot M, Holly T, et al. Comparison Between Single Shot TrueFISP and Segmented TurboFLASH for the Detection of Myocardial Infarction. J. Cardiovasc. Magn. Reson. 2003;5:79–80.
9 Kellman P, Larson AC, Hsu L-Y, Chung Y-C, Simonetti OP, McVeigh ER, et al. Motion-corrected free-breathing delayed enhancement imaging of myocardial infarction. Magn. Reson. Med. 2005;53:194–200.
10 Ledesma-Carbayo MJ, Kellman P, Hsu L-Y, Arai AE, McVeigh ER. Motion corrected free-breathing delayed-enhancement imaging of myocardial infarction using nonrigid registration. J. Magn. Reson. Imaging. 2007;26:184–90.
11 Olivieri L, Cross R, O'Brien KJ, Xue H, Kellman P, Hansen MS. Free-breathing motion-corrected late-gadolinium-enhancement imaging improves image quality in children. Pediatr. Radiol. Pediatric Radiology; 2016;46:983–90.
12 Piehler KM, Wong TC, Puntil KS, Zareba KM, Lin K, Harris DM, et al. Free-Breathing, Motion-Corrected Late Gadolinium Enhancement Is Robust and Extends Risk Stratification to Vulnerable Patients. Circ. Cardiovasc. Imaging. 2013;6:423–32.
13 Hansen MS, Sørensen TS. Gadgetron: an open source framework for medical image reconstruction. Magn. Reson. Med. 2013;69:1768–76.
14 Basha T, Roujol S, Kissinger K V, Goddu B, Manning WJ, Nezafat R. Black blood late gadolinium enhancement using combined T2

magnetization preparation and inversion recovery. J. Cardiovasc. Magn. Reson. BioMed Central Ltd; 2015;17:O14.
15 Kellman P, Xue H, Olivieri LJ, Cross RR, Grant EK, Fontana M, Ugander M, Moon JC, Hansen MS. Dark blood Late Enhancement Imaging. J. Cardiovasc. Magn. Reson. 2016; In press.
16 Liu C-Y, Wieben O, Brittain JH, Reeder SB. Improved delayed enhanced myocardial imaging with T2-Prep inversion recovery magnetization preparation. J. Magn. Reson. Imaging. 2008;28:1280–6.
17 Kellman P, Arai AE, Mcveigh ER, Aletras AH. Phase-Sensitive Inversion Recovery for Detecting Myocardial Infarction Using Gadolinium-Delayed Hyperenhancement. Magn. Reson. Med. 2002;383:372–83.
18 Mordi I, Radjenovic A, Stanton T, Gardner RS, McPhaden A, Carrick D, et al. Prevalence and Prognostic Significance of Lipomatous Metaplasia in Patients With Prior Myocardial Infarction. JACC. Cardiovasc. Imaging. American College of Cardiology Foundation; 2014;1–2.
19 Kellman P, Hernando D, Arai AE. Myocardial Fat Imaging. Curr. Cardiovasc. Imaging Rep. 2010;3:83–91.
20 Kellman P, Hernando D, Shah S, Chefdhotel C, Liang Z-P, Arai A. Free-breathing, single shot fat-water separated cardiac imaging with motion corrected averaging. ISMRM 2010 Sci. Meet. 2010;18:3662.
21 Kellman P, Chefd'hotel C, Lorenz CH, Mancini C, Arai AE, McVeigh ER. Fully automatic, retrospective enhancement of real-time acquired cardiac cine MR images using image-based navigators and respiratory motion-corrected averaging. Magn. Reson. Med. 2008;59:771–8.
22 Xue H, Kellman P, LaRocca G, Arai AE, Hansen MS. High spatial and temporal resolution retrospective cine cardiovascular magnetic resonance from shortened free breathing real-time acquisitions. J. Cardiovasc. Magn. Reson. 2013;15:102.
23 Kellman P, Aletras AH, Mancini C, McVeigh ER, Arai AE. T2-prepared SSFP improves diagnostic confidence in edema imaging in acute myocardial infarction compared to turbo spin echo. Magn. Reson. Med. 2007;57:891–7.
24 Kellman P, Xue H, Spottiswoode BS, Sandino CM, Hansen MS, Abdel-Gadir A, et al. Free-breathing T2* mapping using respiratory motion corrected averaging. J. Cardiovasc. Magn. Reson. 2015;17:3.
25 Xue H, Hansen MS, Nielles-vallespin S, Arai AE, Kellman P. Inline quantitative myocardial perfusion flow mapping. JCMR/ISMRM Workshop. 2016;18:4–6.

**Contact**

Peter Kellman

National Heart, Lung, and Blood Institute

National Institutes of Health, DHHS

10 Center Drive MSC-1061
Bethesda, MD 20892
USA
kellman@nih.gov

# Recent Advances in In-bore Optical Prospective Motion Correction

**Aditya Singh[1,2]; Will Alameida[1]; Maxim Zaitsev[3]; Jeffrey Yu[1,2]**

[1] KinetiCor Inc., Honolulu, HI, USA
[2] Queen's Health Systems and University of Hawaii, Honolulu, HI, USA
[3] University Medical Center Freiburg, Department of Radiology, Medical Physics, Freiburg, Germany

Researchers have attempted to compensate for patient motion in the scanner for two decades. Several research studies have demonstrated the advantages of using an in-bore optical tracking system in conjunction with customized software interface to perform real-time motion correction [1–9].

Clinical adoption of prospective motion correction (PMC) will require seamless integration into the MR clinical workflow and acceptable patient comfort levels with fiduciary markers, as well as consistent and significant improvements in MR image quality. This article highlights efforts made by KinetiCor Inc. (Honolulu, HI, USA) and its world-wide scientific collaboration network to elevate in-bore optical tracking based PMC technology into clinical applications specific to neuroimaging.

## Introduction

Motion artifacts caused by patient motion remain one of the last unsolved challenges to improving quality and reliability of MR imaging. As MR scanners reach higher levels of resolution, the need for motion correction becomes even more apparent. Unfortunately, those patient populations in the greatest need of a clear scan are often unable to obtain diagnostic quality images due to uncontrolled motion caused by pain, trauma, neurological disorders, or age. The costs of repeating scans, rescheduling appointments, and sedating patients are high. A recent study by Andre et al. [10] estimates the annual operational cost impact per scanner at $98,697.

| | Motion Artifacts | Diagnostic Quality |
|---|---|---|
| MPRAGE | None | Diagnostic |
| FLAIR | None | Diagnostic |

**Table 1:** Radiologist ratings.

## How it works

KinetiCor motion correction technology[1] includes an in-bore retrofit motion tracking system (Fig. 1A) and software to update sequence parameters in real-time with actual head position. This allows the scanner to determine where the head precisely is at any given moment.

The motion tracking works by tracking a small fiducial marker that can be affixed to forehead, nose (Fig. 1B), or upper jaw. The translations and rotations of head are transmitted to the customized software, libXPACE, that resides on the real-time controller of the MR scanner.

[1] WIP, the product is currently under development and is not for sale in the US and in other countries. Its future availability cannot be ensured.


**Figure 1: (1A)** KinetiCor quad camera retrofit system mounted inside a MAGNETOM Skyra 3T MR scanner (Siemens Healthcare, Erlangen, Germany) and **(1B)** dual-marker nose bridge mount with markers.

## Benefits of KinetiCor system

Some of the major challenges to in-bore optical tracking include marker visibility as head coils may vary from scanner to scanner. KinetiCor has solved this problem by designing a 4-camera system that is optimized for various head coil geometries. The system can simultaneously track 5 markers at the rate of 60 frames/s.

KinetiCor's prospective motion correction system does not consume any scanner bandwidth and therefore does not increase the scan time. This allows for clearer images and actually improves efficiency because time doesn't need to be wasted repeating sequences that were compromised by motion. The tracking information can be used to correct both in-plane and through-plane motion and it can be incorporated into pulse sequences easily.

In addition, KinetiCor and its academic partners at Freiburg are developing the ability to remove motion correction post-scanning to view uncorrected images [11]. The KinetiCor system and associated research sequences are currently for investigational use only.

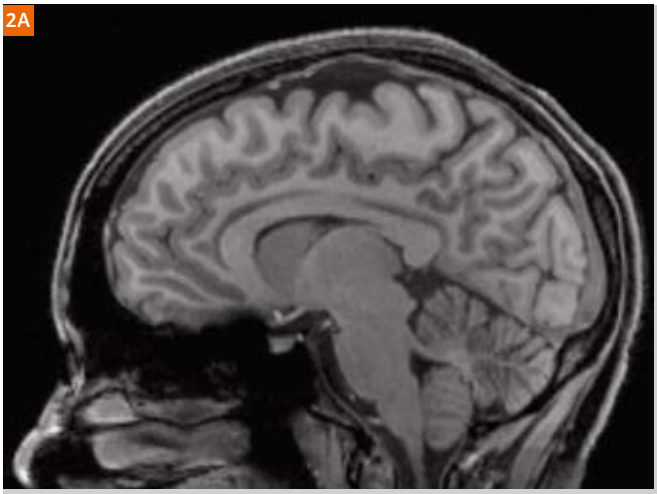


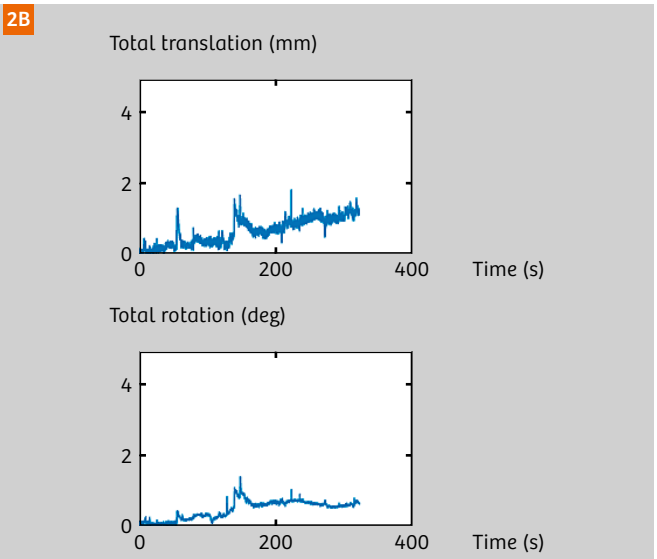


**Figure 2:** MPRAGE data from one of the study volunteers showing a slice from the MPRAGE **(2A)** and the motion traces **(2B)**.

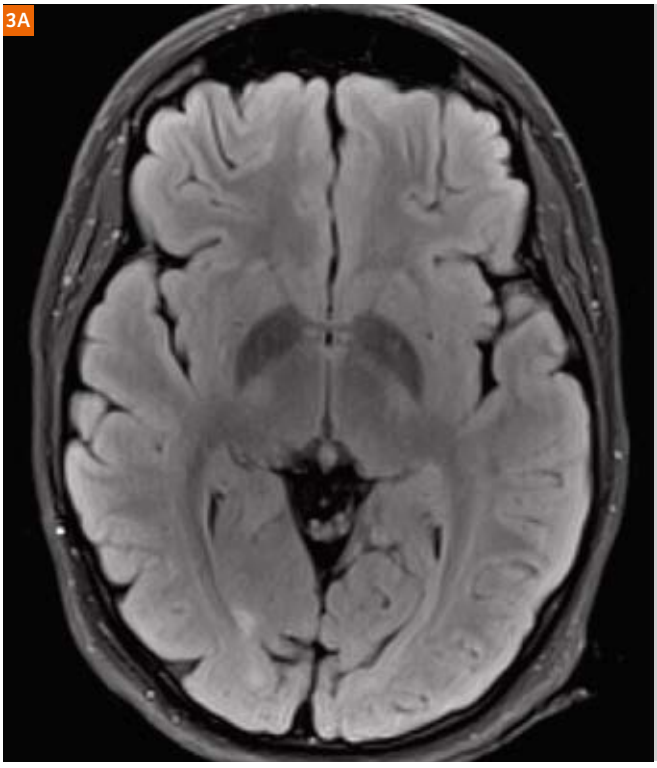


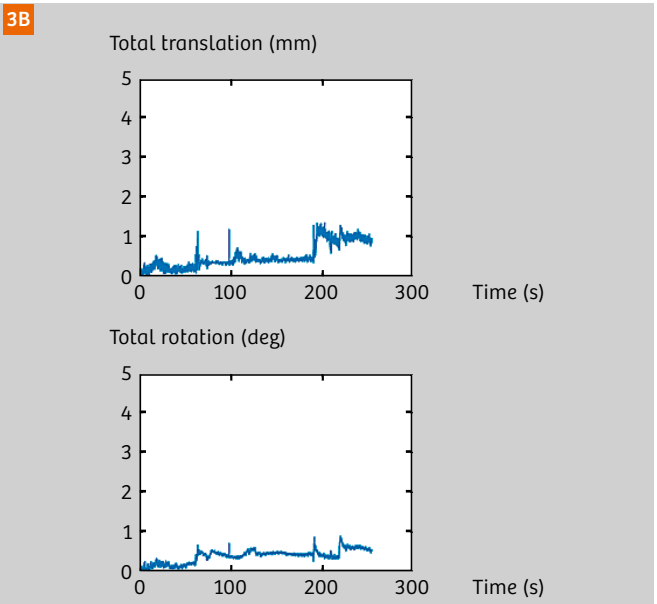


**Figure 3:** FLAIR data from one of the study volunteers showing a slice from the FLAIR images **(3A)**. The motion traces **(3B)** indicate that the participant shifted head position during the scan. The maximum rotation is approximately 1 degree.

## Clinical study overview

To understand the impact of PMC technology in a clinical workflow, KinetiCor is currently running a multi-center clinical study. Two of the study centers are conducting the study on MAGNETOM Skyra scanners and one site is using a 3T MAGNETOM Prisma (Siemens Healthcare, Erlangen, Germany). The study is IRB (institutional review board) approved and informed consents were obtained from all the participants. The goals of the study are to:

1) Characterize the prevalence of motion in a clinical setting
2) Evaluate the use of KinetiCor PMC enabled research sequences (MPRAGE, FLAIR) that have been added to the clinical protocol.
3) Obtain feedback from MR technologists and patients on the time required to affix markers, as well as overall comfort levels for patients.

Two markers were mounted on the bridge of the nose through a 3D printed marker mount fabricated in-house. The marker mount with markers is shown in Figure 1B.

## Preliminary evaluation outcomes

The images obtained in the study were evaluated by a board certified Radiologist who was blinded to the motion traces. Acquired motion data was processed to calculate the total translation (norm of translation) and total rotation.

Figures 2 and 3 show the results from one study participant. Figure 2 shows the motion traces and an image from motion corrected MPRAGE and Figure 3 shows the motion traces and an image from the FLAIR sequence. The comments from the Radiologist for the participant for both images are shown in Table 1. The images from both sequences were rated to be of diagnostic quality. Of the initial 15 datasets reviewed by the radiologist, none of the MPRAGE or FLAIR images were rated as non diagnostic.

MR technicians reported that markers were easily affixed in under one minute, including the time required to prepare the area with an alcohol wipe, for 29 of the 30 subjects studied (in the remaining case it took between one and two minutes). Of interest, it took less time to affix the tracking marker than it took to affix earplugs on the subjects.

Patient comfort levels with wearing and removing the marker were also studied. Initial study results revealed that 29 subjects indicated favorable comfort levels with the marker, with one subject not providing any input.

## Conclusions and outlook

At present the technical issues related to the previous prototype implementations of the PMC technology are largely resolved: the current solution occupies very little bore space and is compatible with routine operations at the scanner. The handling of the marker and patient comfort has also improved substantially. In particular, the present solution addresses the hygiene aspects by introducing single-use markers and mounts as required for the future clinical use. The initial evaluation of the imaging outcomes reveals a favorable performance of the PMC system.

### References

1 Maclaren J, Herbst M, Speck O, Zaitsev M. Prospective motion correction in brain imaging: a review. Magn Reson Med. 2012 May; 69(3):621–636. doi:10.1002/mrm.24314.
2 Speck O, Hennig J, Zaitsev M. Prospective real-time slice-by-slice motion correction for fMRI in freely moving subjects. Magn Reson Mater Phy 2006 May; 19(2):55–61. doi:10.1007/ s10334-006-0027-1.
3 Zaitsev M, Dold C, Sakas G, Hennig J, Speck O. Magnetic resonance imaging of freely moving objects: prospective real-time motion correction using an external optical motion tracking system. Neuroimage 2006 July; 31(3):1038–1050. doi:10.1016/j.neuroimage.2006.01.039.
4 Qin L, van Gelderen P, Derbyshire JA, Jin F, Lee J, de Zwart JA, Tao Y, Duyn JH. Prospective head-movement correction for high-resolution MRI using an in-bore optical tracking system. Magn Reson Med. 2009 Oct ;62(4):924–934. doi:10.1002/mrm.22076.
5 Andrews-Shigaki BC, Armstrong BS, Zaitsev M, Ernst T. Prospective motion correction for magnetic resonance spectroscopy using single camera Retro-Grate reflector optical tracking. J Magn Reson Imaging 2011 Jan 27; 33(2):498–504.
6 Schulz J, Siegert T, Reimer E, Labadie C, Maclaren J, Herbst M, Zaitsev M, Turner R. An embedded optical tracking system for motion-corrected magnetic resonance imaging at 7T. Magn Reson Mater Phy 2012 Dec; 25(6):443–453. doi:10.1007/ s10334-012-0320-0.
7 Lange T, Maclaren J, Herbst M, Lovell-Smith C, Izadpanah K, Zaitsev M. Knee cartilage MRI with in situ mechanical loading using prospective motion correction. Magn Reson Med. 2014 Feb; 71(2):516-523. doi:10.1002/mrm.24679.
8 Gummus K, Keating B, White N, Andrews-Shigaki B, Armstrong B, Maclaren J, Zaitsev M, Dale A, Ernst T. Comparison of optical and MR-based tracking. Magn Reson Med. 2014 Sept; 74(3):894-902.
9 Forman C, Aksoy M, Hornegger J, Bammer R. Self-encoded marker for optical prospective head motion correction in MRI. Med Image Anal. 2011 Oct;15(5):708-19. doi: 10.1016/j.media.2011.05.018.
10 Andre JB, Mossa-Basha, M, Bresnahan BW, Hoff MN, Smith CP, Anzai Y, Cohen WA. Toward Quantifying the Prevalence, Severity and Cost Estimates Associated With Patient Motion During Clinical MR Examinations. J Am Coll Radiol, 2015; 12(7):689-695.
11 Zahneisen B, Keating B, Singh A, Herbst M, Ernst T. Reverse Retrospective motion correction. Magn Reson Med. 2015 July 3; 75(6):2341-2349.

### Contact

Aditya Singh
Kineticor

3465 Waialae Avenue
Suite 300A
Honolulu, HI 96816
USA
Phone: +1 (808) 380-1444
aditya.singh@kineticor.com

# Case Study: Simultaneous Multi-Slice Accelerated Turbo Spin-Echo Magnetic Resonance Imaging of the Spine

**Stephen F. Kralik, M.D.[1]; Dingxin Wang, Ph.D.[2]; Bruce Spottiswoode, Ph.D.[3]; Mary McCrate, M.D.[1]; Chen Lin, Ph.D.[1]**

[1] Indiana University Department of Radiology and Imaging Sciences, Indianapolis, IN, USA
[2] Siemens Medical Solutions USA, Inc., Minneapolis, MN, USA
[3] Siemens Medical Solutions USA, Inc., Chicago, IL, USA

## Introduction

Magnetic Resonance Imaging (MRI) of the spine may be performed for a wide range of clinical symptoms and indications including evaluation of back pain, radiculopathy, spondylosis, infection, and neoplasms. Standard MRI spine protocols include multiplanar T1-weighted (T1w), T2-weighted (T2w), and short tau inversion recovery (STIR) or a T2w fat-saturated sequence most commonly in the sagittal and axial planes. Post-contrast imaging is indicated for evaluation of infection, neoplasm, and in the post-operative setting. Because imaging of the spine in the axial plane requires a large number of slices to adequately detect pathology, the simultaneous multi-slice (SMS) imaging technique using multiband (MB) pulses may be valuable for imaging the spine as it reduces imaging time while providing similar detection of pathology and similar image quality. In this case study we describe the use of SMS turbo spin echo (SMS TSE)[1] for evaluation of the lumbar spine among patients who have been given intravenous contrast for various clinical indications including neoplasms and post-operative scenarios.

## Sequence details

MRI of the lumbar spine was performed at a 1.5T MR scanner (MAGNETOM Symphony, A Tim System, Siemens Healthcare, Erlangen, Germany). Post-contrast axial T1 TSE sequences (conventional and SMS) with fat saturation (T1w contrast-enhanced (CE) TSE FS) were performed following administration of 0.1 mmol/kg intravenous gadolinium dimeglumine (Multihance; Bracco Diagnostics, Princeton, NJ, USA) contrast. Parameters for the conventional TSE sequence were TR 637-684 ms, TE 12-13 ms, 4 mm slice thickness, and 192 x 256 matrix. The SMS T1w CE TSE fat saturation sequence consisted of TR 632 ms, TE 14 ms, 4 mm slice thickness, and 192 x 256 matrix. Average acquisition times for conventional axial T1w CE FS TSE and SMS T1w CE TSE FS were 5:33 min (range 5:24 to 5:48 min) and 4:00 min respectively.

[1] The product is still under development and not commercially available yet. Its future availability cannot be ensured.

### Case 1

A 60-year-old female with a previous history of an intradural schwannoma resection in 2013 who reported continued low back pain and left lower extremity radiculopathy. Representative images from the conventional axial T1w CE TSE FS **(1A, C)** and SMS axial T1w CE TSE FS **(1B, D)** demonstrate a laminectomy site at L2-3 with small amount of enhancing scar tissue at the laminectomy site but no evidence of recurrent schwannoma in the thecal sac.

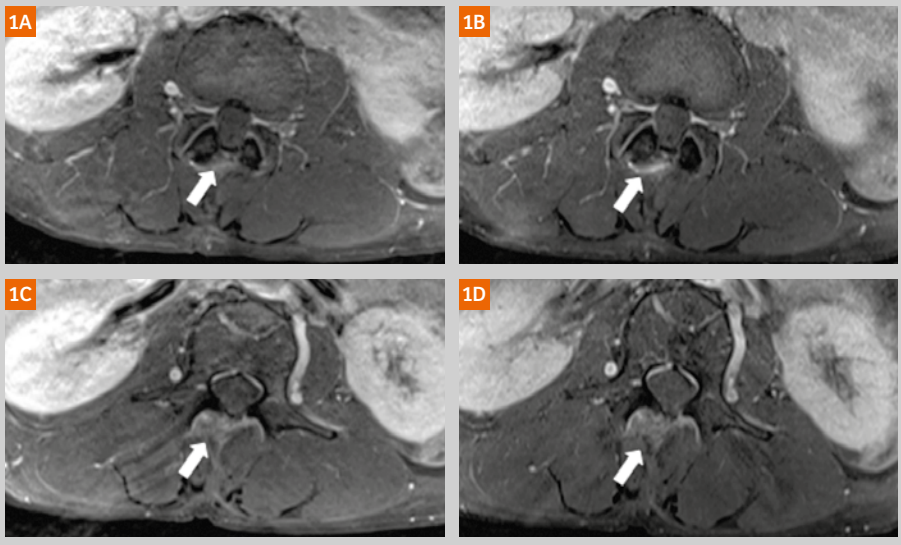

## Case 2

An 80-year-old male presented with a history of metastatic cholangio-carcinoma and left leg weakness. Both, the conventional axial T1w CE TSE FS **(2A)** and SMS axial T1w CE TSE FS **(2B)** demonstrated no evidence of metastatic disease. Representative images of the lumbar spine demonstrate similar differentiation of the bones, muscles, spinal canal, and remainder of the extraspinal soft tissues.

## Case 3

A 58-year-old patient with metastatic breast cancer and low back pain. Representative images from both the conventional axial T1w CE TSE FS **(3A, C, E)** and SMS axial T1w CE TSE FS **(3B, D, F)** demonstrate multifocal enhancing lesions in the bones consistent with osseous metastases. There is similar conspicuity of the bone lesions with the SMS TSE compared to the conventional TSE.

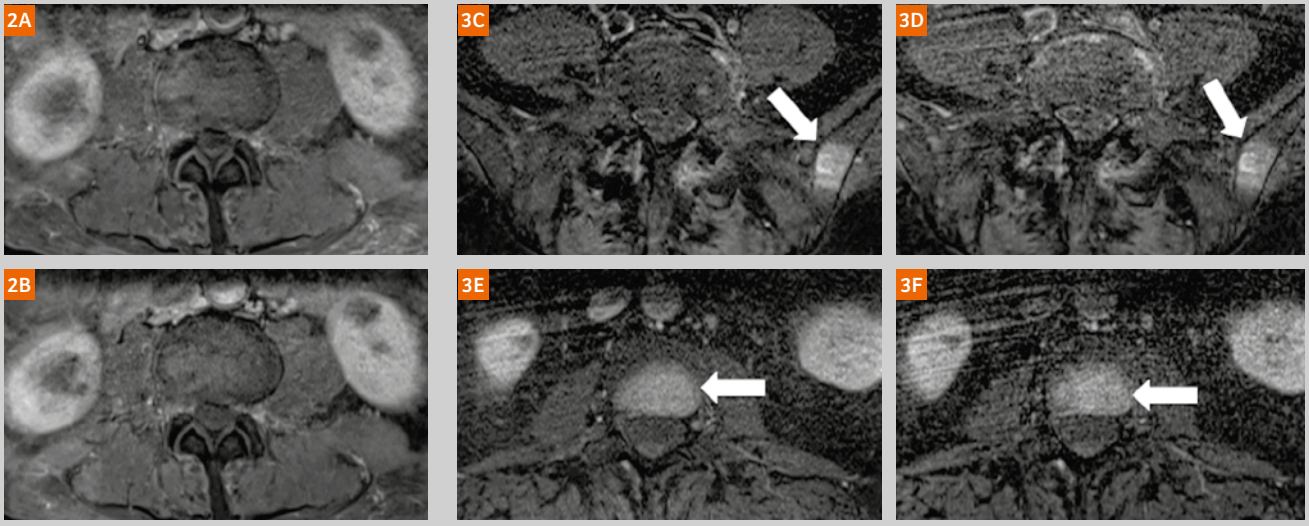


## Conclusion

We performed SMS TSE of the lumbar spine in this small clinical case series and determined that SMS TSE can be reliably performed in the clinical setting. Compared to the conventional T1w CE TSE, the T1w CE SMS TSE demonstrates similar detection of pathology while reducing imaging time compared to conventional TSE which is considered a clinical advantage of the SMS TSE. No qualitative differences in image quality, such as anatomic detail or imaging artifacts, were encountered with SMS TSE which would preclude its use in the clinical setting. Further quantitative investigation of image quality and pathology detection in the clinical setting using SMS TSE will be undertaken to evaluate if this technique can replace conventional TSE imaging of the spine in the near future.

### References

1 Wang D, Kollasch P, Auerbach EJ et al. T1-weighted Imaging of Lumbar Spine using Multiband Slice Accelerated Spin Echo Proceedings of the International Society for Magnetic Resonance in Medicine (21) 2013, 244.

2 Wang D, Kollasch P, Li X et al., "Multiband Slice Accelerated TSE: Clinical Applications in Brain imaging", Proceedings of the International Society for Magnetic Resonance in Medicine (22) 2014, 4317.

3 Wang D, Padua A, Ellermann J et al., "Multiband Slice Accelerated TSE for High Resolution Knee Imaging", Proceedings of the International Society for Magnetic Resonance in Medicine (22) 2014, 1216.

### Contact

Stephen F. Kralik, M.D.
Assistant Professor of Radiology

Indiana University
Department of Radiology and Imaging Sciences
714 N Senate Ave #100
Indianapolis, IN 46202, USA
Phone: +1 317-274-5555
skralik@iupui.edu

# Case Report: Evaluation of Simultaneous Multi-Slice Accelerated TSE for Knee Joint MR Imaging

**Xiaona Li[1]; Zhigang Peng[1]; Panli Zuo[2]; Dingxin Wang[3]; Jianling Cui[1]**

[1] Department of Radiology, Hebei 3rd Hospital, Province Biomechanical Key Laboratory of Orthopedics, Shijiazhuang, China
[2] Siemens Healthcare, MR Collaborations NE Asia, Beijing, China
[3] Siemens Medical Solutions USA, Inc., Minneapolis, MN, USA

## Introduction

The turbo spin echo (TSE) sequence is one of the most utilized sequences in clinical routine MRI, providing high image quality, strong lesion conspicuity and multiple tissue contrasts (T1w, T2w, FLAIR and proton density-weighted (PD)). In musculoskeletal (MSK) imaging, TSE is widely used as it offers excellent depiction of cartilage, ligaments, menisci, and periarticular soft tissues. However, high spatial resolution with a large number of slices is rarely used clinically because of the prolonged acquisition time for complete coverage when using a conventional 2D-TSE sequence.

Simultaneous multi-slice (SMS) is a promising parallel imaging method to increase the acquisition speed without a significant decrease to the signal-to-noise ratio (SNR). SMS has been proved to work well with echo-planar imaging (EPI) readout for both diffusion-weighted and BOLD functional magnetic resonance imaging (fMRI). The SMS method excites multiple spatially distributed slices simultaneously using a multi-band (MB) radiofrequency (RF) pulse and separates the simultaneously acquired slices by parallel imaging reconstruction technique utilizing the multiple receiver coils sensitivities [1-4]. With integration of the 'controlled aliasing in parallel imaging result in higher acceleration' (CAIPIRINHA) method the g-factor related SNR penalty is significantly reduced [3, 7; also see articles by the same authors in this issue]. SMS allows an increase in the imaging coverage with higher spatial resolution and shorter acquisition time [2, 3, 5-7].

Several recent studies have addressed the possibility of applying the SMS method to TSE acquisition schemes [8-10].

In this study, we applied the SMS 2D-TSE sequences[1] with gradient-based CAIPIRINHA in MSK examination to assess its value for MSK related diseases.

## Method

All MR scans were performed on a 3T MAGNETOM Verio system (Siemens Healthcare, Erlangen, Germany) with an 8-channel knee coil or a 4-channel flex coil. Sagittal T1-weighted TSE, sagittal, coronal and transverse PD-weighted TSE with fat suppression imaging were performed for the whole knee joint to compare the image quality of conventional TSE and SMS TSE sequences.

Imaging parameters include field-of-view (FOV) of 160 × 160 mm$^2$, matrix of 320 × 256, slice thickness of 3 mm with a gap of 10%, 36 slices, excitation/refocusing flip angle of 90/150°. Slice acceleration factor is 2 and FOV shift factor is 2 for all SMS TSE sequences. Matching imaging parameters including TR/TE and turbo factor were used for conventional and SMS TSE. For covering the 36 slices, SMS TSE used only half number of concatenations as conventional TSE. Sagittal T1w imaging was performed using TR 499 ms, TE of 13 ms and turbo factor of 3. Sagittal T1w imaging with fat saturation was performed using TR 573 ms, TE 13 ms and turbo factor of 3. All T1w imaging acquisitions used 4 concatenations for conventional TSE and 2 concatenations for SMS TSE. Sagittal PD-weighted imaging with fat saturation was performed using TR 3200 ms, TE 40 ms and turbo factor of 8. Coronal

[1] The product is still under development and not commercially available yet. Its future availability cannot be ensured.

**Table 1:** Other imaging ameters

| Parameter | sag-T1 | sag-T1+fs | sag-PD+fs | cor-PD+fs | tra-PD+fs |
|---|---|---|---|---|---|
| **TR/TE (ms)** | 499/13 | 573/13 | 3200/40 | 3200/40 | 3200/41 |
| **ETL** | 3 | 3 | 8 | 9 | 10 |
| **Concatenation** | 4 (Conv.)<br>2 (SMS) | 4 (Conv.)<br>2 (SMS) | 2 (Conv.)<br>1 (SMS) | 2 (Conv.)<br>1 (SMS) | 2 (Conv.)<br>1 (SMS) |

**Table 2:** Acquisition time for conventional TSE and SMS TSE (in minutes).

| Sequences | sag-T1 | sag-T1+fs | sag-PD+fs | cor-PD+fs | tra-PD+fs |
|---|---|---|---|---|---|
| **conventional TSE** | 5:11 | 5:57 | 5:41 | 5:32 | 4:24 |
| **SMS TSE** | 2:36 | 2:58 | 2:48 | 2:47 | 2:38 |

## Case 1

40-year-old female with a painless slow-growing swelling for 10 years in the right distal femur. CT sagittal image demonstrated an irregular bone protuberance with a wide base in the posterior of right distal femur. Calcification shadow and continuity of the lesion with the cortical bone were seen in the lesion (Fig. 1A). MRI with both SMS TSE and conventional TSE demonstrated a local thickened cartilaginous cover in the rim of the bone protuberance (Figs. 1B-G).

The cortical and medullary continuity between the osteochondroma and host bone can be observed. Calcified areas of the cover presented low signal intensity in T1 and PD-weighted images with fat saturation. Water in the non-calcified portion showed a low signal to the surrounding bone on T1w images and a high signal on PD-weighted images with fat saturation.


**Figure 1:** A patient (40-year-old, female) with osteochondroma in the bone of the distal femoral. **(1A)** is the CT sagittal image. **(1B-D)** are SMS TSE and **E**, **F**, and **G** are conventional TSE images for sagittal T1-weighted imaging **(1B, E)**, sagittal PD-weighted imaging with fat saturation **(1C, F)** and axial PD-weighted imaging with fat saturation **(1D, G)**.

## Case 2

68-year-old male with pain in the right leg for half a year without an adequate history of corresponding trauma. CT coronal image demonstrated a round-shaped lesion with a sclerosis rim (Fig. 2A). The size of the lesion was 3 × 4 × 7 $cm^3$. A calcification shadow was seen in the lesion with a sharp rim. MRI with both SMS TSE and conventional TSE demonstrated the lesion of inhomogeneous isointense to surrounding muscles on T1w images (Figs. 2B (SMS) and E (conventional)). Foliated hyperintensity signals were also seen in the lower lesion. On PD-weighted images with fat saturation (Figs. 2C (SMS) and F (conventional)), the lesion predominantly presented high signal intensity, within punctiform hypo- and isointensity. Post-Gadoteridol T1w images with fat saturation showed partly slightly enhancement intensity (Figs. 2D (SMS) and G (conventional)). The diagnosis was fibrous dysplasia in the bone of proximal tibia.


**Figure 2:** A patient (68-year-old, male) with fibrous dysplasia of proximal tibia. **(2A)** is the coronal CT image. **(2B-D)** are SMS TSE and **(2E-G)** are conventional TSE images for sagittal T1w imaging **(2B, E)**, sagittal T1w imaging with fat saturation after contrast agent injection **(2C, F)**, and PDw imaging with fat saturation **(2D, G)**.

## Case 3

31-year-old female with pain in the left knee since 2 months. Both SMS TSE and conventional TSE MR sagittal images demonstrate a geographic lesion in the distal femur and proximal tibia with slight hypointensity of the skeletal muscle on T1w images (Figs. 3B (SMS) and D (conventional)) and hyperintensity in PDw fat saturation images (Figs. 3A (SMS) and C (conventional)). The diagnosis was bone infarction.

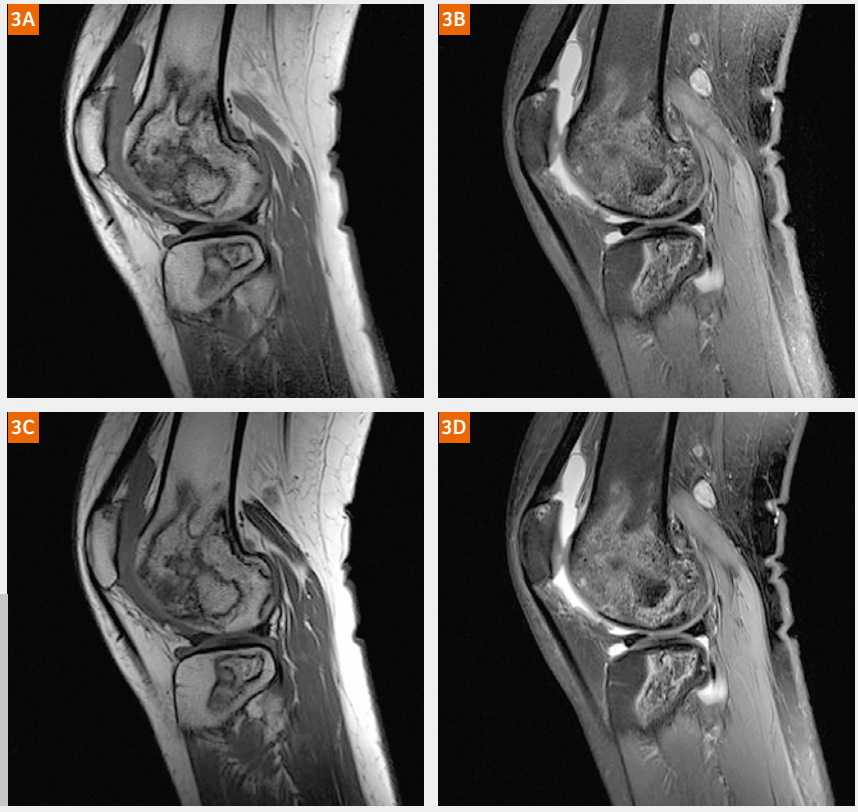


**Figure 3:** A patient (31-year-old, female) with fibrous bone infarction. **(3A, B)** are SMS TSE, **(3C, D)** are conventional TSE images for sagittal T1w imaging **(3A, C)**, and sagittal PDw imaging with fat saturation **(3B, D)**.

## Case 4

71-year-old male with pain in the right knee since 10 years after sprain. Both SMS TSE and conventional TSE MR sagittal images demonstrate an anterior cruciate ligament tear and multiple bone proliferation which supports the diagnosis of osteoarthritis. There was a slight hypointensity to skeletal muscle on T1w images (Figs. 4A (SMS) and C (conventional)) and hyperintensity with slightly low intense clumps on PDw images (Figs. 4B (SMS) and D (conventional)).

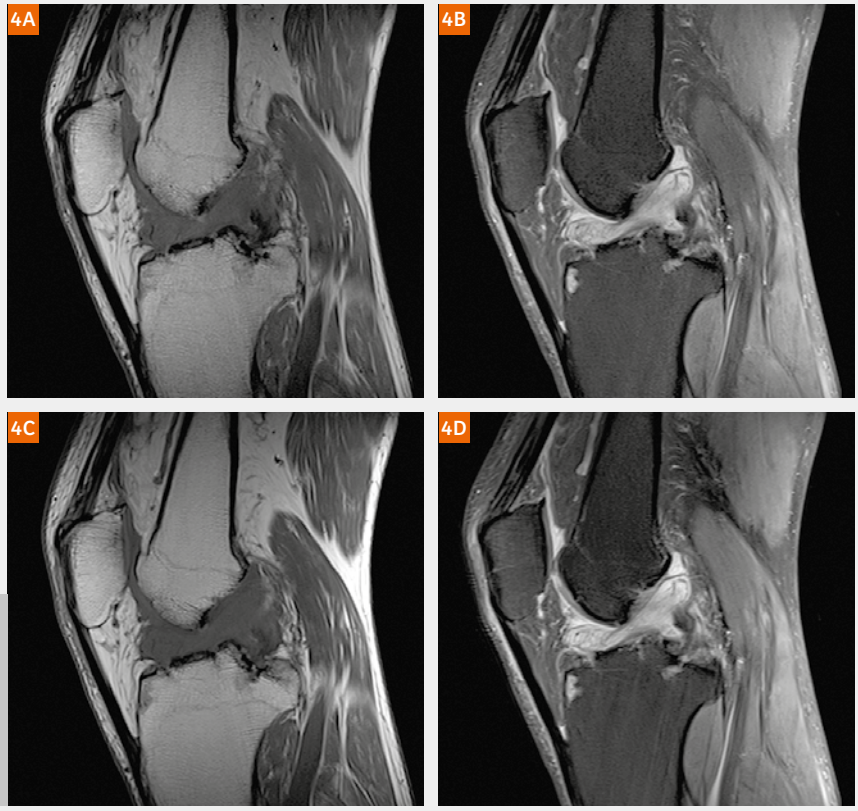


**Figure 4:** A patient (71-year-old, male) with osteoarthritis. **(4A, B)** are SMS TSE, and **(4C, D)** are conventional TSE images for sagittal T1w imaging **(4A, C)**, and sagittal PDw imaging with fat saturation **(4B, D)**.

PD-weighted imaging with fat saturation was performed using TR 3200 ms, TE 40 ms and a turbo factor of 9. Axial PD-weighted imaging with fat saturation was performed using TR 3200 ms, TE 41 ms, and turbo factor of 10. All PD-weighted imaging acquisitions used 2 concatenations for conventional TSE and 1 concatenation for SMS TSE. Other imaging parameters are shown in Table 1 and 2.

## Conclusion

SMS TSE reduced the scanning time for TSE imaging significantly without compromise to diagnostic image quality, bringing strong value to routine musculoskeletal examinations. This especially benefits patients with larger tumors where full coverage may be difficult to achieve using conventional TSE sequence and also for patients with small injuries to ligaments and cartilage who will require higher spatial resolution imaging for an accurate diagnosis.

### References

1 Xu J, Moeller S, Auerbach EJ et al (2013) Evaluation of slice accelerations using multiband echo planar imaging at 3 T. Neuroimage 83:991-1001.

2 Moeller S, Yacoub E, Olman CA et al (2010) Multiband multislice GE-EPI at 7 tesla, with 16-fold acceleration using partial parallel imaging with application to high spatial and temporal whole-brain fMRI. Magn Reson Med 63:1144-1153.

3 Setsompop K, Gagoski BA, Polimeni JR, Witzel T, Wedeen VJ, Wald LL (2012) Blipped-controlled aliasing in parallel imaging for simultaneous multislice echo planar imaging with reduced g-factor penalty. Magn Reson Med 67:1210-1224.

4 Sotiropoulos SN, Moeller S, Jbabdi S et al (2013) Effects of image reconstruction on fiber orientation mapping from multichannel diffusion MRI: reducing the noise floor using SENSE. Magn Reson Med 70:1682-1689.

5 Feinberg DA, Moeller S, Smith SM et al (2010) Multiplexed echo planar imaging for sub-second whole brain FMRI and fast diffusion imaging. PLoS One 5:e15710.

6 Smith SM, Miller KL, Moeller S et al (2012) Temporally-independent functional modes of spontaneous brain activity. Proc Natl Acad Sci U S A 109:3131-3136.

7 Breuer, FA, Blaimer M, Heidemann RM et al., (2005) Controlled aliasing in parallel imaging results in higher acceleration (CAIPIRINHA) for multi-slice imaging. Magnetic Resonance in Medicine 53(3): 684–691.

8 Norris DG, Boyacioglu R, Schulz J, Barth M, Koopmans PJ (2014) Application of PINS radiofrequency pulses to reduce power deposition in RARE/turbo spin echo imaging of the human head. Magn Reson Med 71:44-49.

9 Wang D, Kollasch P, Li X et al., "Multiband Slice Accelerated TSE: Clinical Applications in Brain imaging", Proceedings of the International Society for Magnetic Resonance in Medicine (22) 2014, 4317.

10 Wang D, Padua A, Ellermann J et al., "Multiband Slice Accelerated TSE for High Resolution Knee Imaging", Proceedings of the International Society for Magnetic Resonance in Medicine (22) 2014, 1216.

### Contact

Jianling Cui
Department of Radiology

The Third Hospital of Hebei Medical University
Hebei Province Biomechanical Key Laborary of Orthopedics
Ziqiang Road 139
Shijiazhuang, Hebei 050051
China

# *syngo* MR XA Software Line – Your New Work Environment for More Comfortable Scanning and Intuitive Image Processing

**Alexander Aulesjord; Gregor Thörmer, Ph.D.**

Siemens Healthineers, Erlangen, Germany

To counter falling reimbursement and increasing cost pressure many imaging facilities seek ways to both increase productivity and patient throughput. One example of these efforts can be seen directly in the continuously increasing number of patients scheduled for MRI per hour over the course of the last years.

Higher patient throughput not only increases the technologists' workload but also their expectations towards the tools available to them. The user interface (UI) to the MR scanner is arguably the most important tool that technologists have at their disposal. Most interactions with the MR scanner over the course of the examination will happen via the UI. As such, the UI can have substantial influence over how productive an MR scanner is operated. Great care should be taken such that when designing a new UI, it will be easy to navigate, task cards for scanning and processing should not overlap, and the workflow should follow the natural course of the MR examination.

It is also crucial to carefully preserve the overall functionality and the known appearance of any new software, be it in MR technology or consumer electronics, in order to make the transition to a new UI for experienced users easy.

Our new 3T MRI system, MAGNETOM Vida, introduces a completely redesigned MR UI running on a new hardware platform. Evolving from the successful *syngo* MR E11 platform, the new *syngo* MR XA software platform is a user-centric control center for patient registration, scanning, post-processing, and result distribution.

## Optional dual monitor setup

Studies have shown that even standard office applications substantially benefit from a dual monitor setup, resulting in 45% easier task tracking, 32% higher performance, and 24% more comfortable use than single monitor setups [1].

To ease the work of the MR technologist in a similar manner, *syngo* MR XA software platform offers a dual monitor scanning workplace with two large 24-inch monitors with a reorganized user interface.

For a more natural scanning and viewing process, different tasks have been clearly separated: The left screen is reserved for patient registration, scanning, and protocol management, while the right screen, especially with the new MR View&GO application which encompasses reconstructions, post-processing, image quality check, and distribution of results to the PACS and other DICOM nodes (Fig. 1). This dual monitor setup, with separated scan and viewing monitors, makes for a more natural working environment in which the technologist has a complete overview of the examination and results. Constant context switches and distractions are reduced, enabling stronger focus on the patient and true multitasking for increased quality and productivity.

*syngo* MR XA platform builds on the established *syngo* MR E11 platform, inheriting many known features and UI elements, which makes orientation for users of the existing platform easy.

1


**Figure 1:** *syngo* MR XA software line offers optional dual monitor setup with two 24-inch screens. Clear task separation with image acquisition on the left-hand side and processing with MR View&GO on the right-hand side.

As shown in Figure 2, central UI elements and features on the left screen have been preserved but newly arranged on the larger monitor. Furthermore, the new layout now provides fixed positions for UI elements like the physio display and the inline display. Other useful components like the Dot Cockpit for protocol management have not been changed in their appearance. They do, however, offer the ability to be opened on the right monitor while scanning, therefore not interfering with other processes.

> ***"The new interface is clearly structured. It is easy to get used to it."*[1]**
>
> **Andreas Lingg, MTRA**
> Tübingen University Hospital, Tübingen, Germany

[1] The statements by Siemens' customers presented here are based on results that were achieved in the customer 's unique setting. Since there is no 'typical' hospital and many variables exist (e.g., hospital size, case mix, level of IT adoption), there can be no guarantee that other customers will achieve the same results.

## MR View&GO

MR View&GO is a dedicated MR viewer that allows viewing, routine post-processing, filming and result distribution in one comprehensive workflow with consecutive steps (Fig. 3A). As soon as a patient has been registered a corresponding MR View&GO automatically opens for the respective patient. Every scan that has been acquired and reconstructed automatically appears on the right screen in MR View&GO.

## Pre-processing with Recon&GO

Powerful image pre-processing capabilities, e.g. automatic InlineSubtraction of dynamic series, InlineMPR calculation of 3D datasets or InlineComposing of multi-station exams, which are all standard, run automatically in the background. This helps to reduce the workload for the MR technologist.


**Figure 2:** The new workplace on the *syngo* MR XA platform **(2B)** evolves from *syngo* MR E11. Planning segments (orange), queue (yellow), scan parameters (purple) have kept their appearance but were newly arranged. The new layout provides fixed positions for hovering UI elements such as the physio display and the inline display (blue).

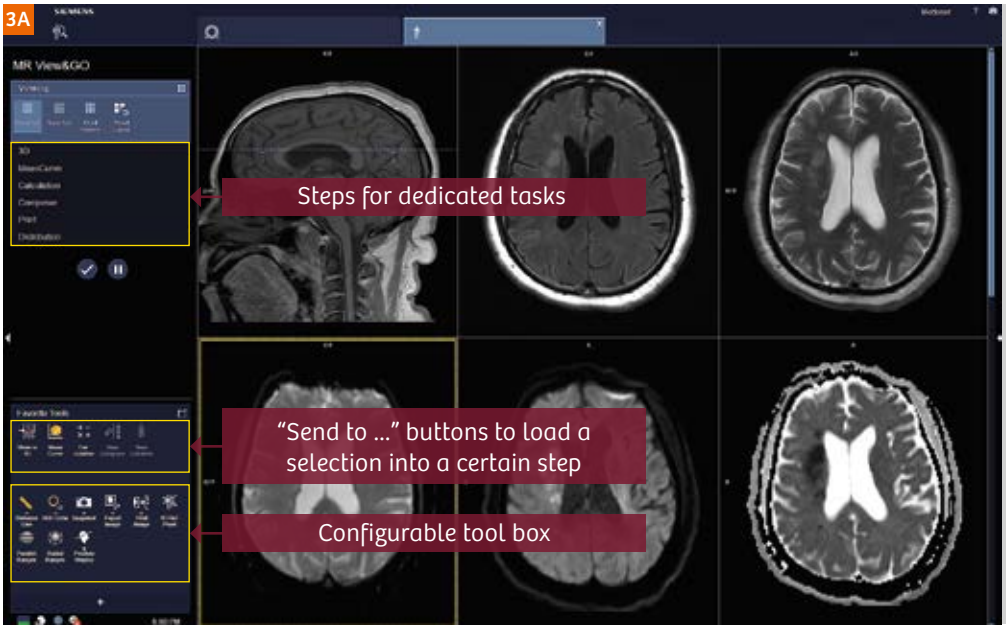


**Figure 3A:** MR View&GO is a dedicated viewer for MR studies, offering consecutive steps for image viewing, processing and distribution. The user can configure an individual tool box of frequently used features such as image markers, distance measurements or ROI analysis in the lower left corner. Further analysis tools can be found in so- called "corner menus" in the edges of individual image segments.

## Step-by-step from quality control to distribution

Following the natural workflow, MR View&GO guides you from basic viewing and quality control towards result distribution to the PACS and other DICOM nodes (Fig. 3B). Intermediate post-processing steps which might be indicated depending on the case can be easily launched by selecting an image series and transferring it to the respective step with one mouse click.

This, for example, enables the reformatting of images in 3D as Multiplanar Reconstructions (MPR), Maximum Intensity Projection (MIP), or with a Volume Rendering Technique (VRT). Furthermore, arithmetic image analysis or the interactive extrapolation of very high b-values (up to 5000 s/mm²) can be easily performed while the scan is running. The resulting images, for example multiplanar reconstructions of a 3D dataset, can be easily inserted to the planning segments to precisely plan subsequent scans.

To evaluate dynamically acquired contrast-enhanced image series, MR View&GO also offers a dedicated MeanCurve analysis step as a standard feature. This, for example, helps in the evaluation of a test-bolus scan, prostate DCE series (Fig. 4) or contrast-enhanced breast MRI.

In addition to InlineComposing, MR View&GO provides manual composing for complex cases to support, e.g., whole-spine, whole-body, or angiography exams.

## Advanced image processing

For more advanced image processing requirements, e.g. to perform neuro perfusion and mismatch analysis (Fig. 5), dedicated applications are optionally available. These applications cover the entire radiological spectrum from neurology (MR Neurology, Neuro3D Tractography and fMRI), cardio-vascular evaluations (Cardiac Perfusion, Cardiac Flow, 4D Ventricular Function, Vascular Analysis), to oncology (Breast, Prostate, OncoCare, 3D Lesion Segmentation)[1]. Many of these only require minimal user interaction: for example, flow quantification is fully automated after a vessel has been selected for analysis. This allows preparing MR datasets ready-to-read, saving one of the most precious resources: the radiologists' time. Depending on the institutional setup and needs, it is also possible to operate a satellite console with a shared database for basic (MR View&GO) and advanced processing purposes (Fig. 6). This configuration has the particular advantage that licenses for advanced applications are shared between the acquisition workplace and the satellite console.[2]

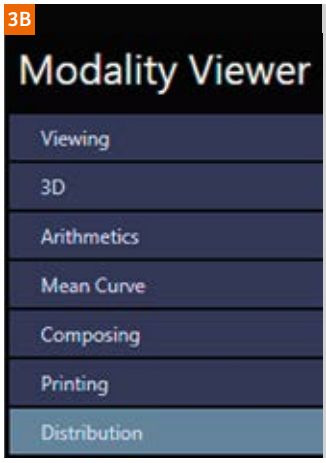


**Figure 3B:** MR View&GO offers consecutive steps to guide you from basic quality control through potential further processing steps towards result distribution. To launch a specific step, e.g. the 3D card, you only have to select a series of images and press the "Show in 3D" button on the left-hand side (see Figure 3A).

[1] This reflects only a selection of advanced applications, further options are available.
[2] Only one user can process data at a time with one license.

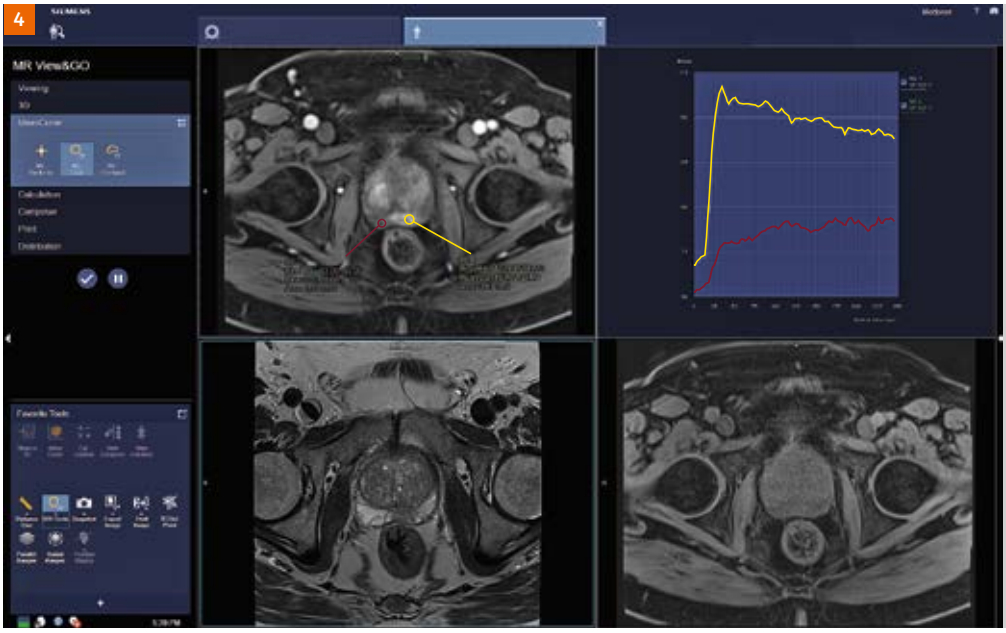


**Figure 4:** The standard MeanCurve analysis step for evaluation of the dynamic behavior of contrast enhancement in tissues. As shown in this example of a patient with prostate cancer, ROIs have been placed in the peripheral zone, illustrating fast wash-in and distinct wash-out for the yellow selection while the purple ROI is showing moderate enhancement and a plateau.


**Figure 5:** The standard MR Neurology workflow can be enhanced with the capability to perform mismatch evaluation. As shown, the penumbra (yellow outline) is substantially larger that the core infarction (turquoise area) in this patient, prompting immediate treatment.

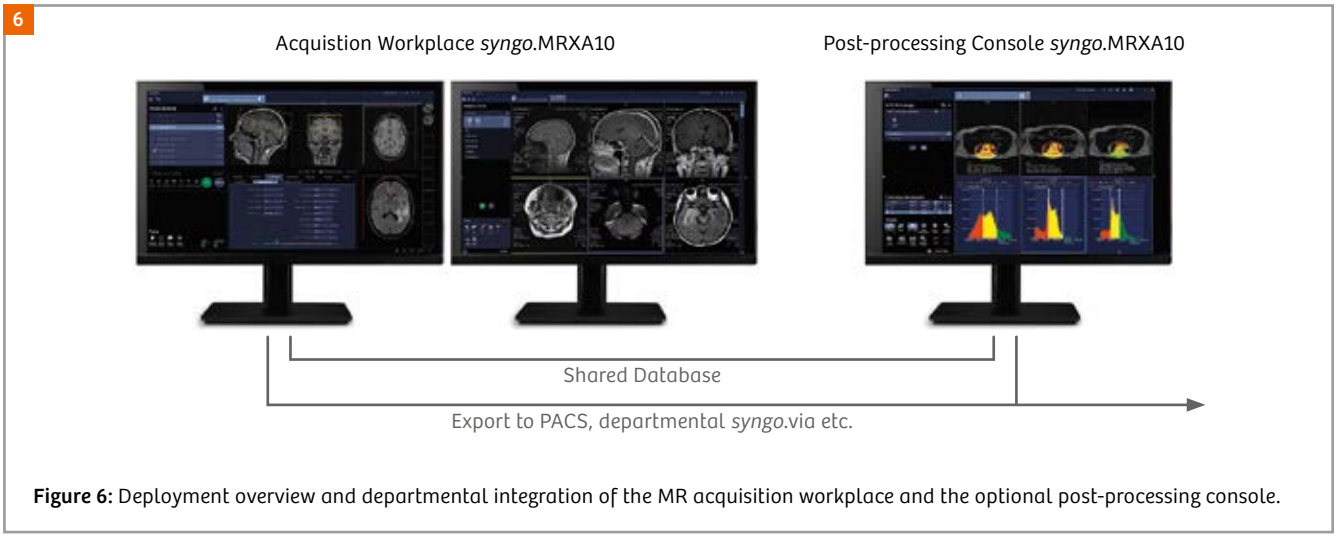


**Figure 6:** Deployment overview and departmental integration of the MR acquisition workplace and the optional post-processing console.

Finally, the appearance and usability of all applications has been harmonized with our departmental post-processing platform *syngo*.via, helping to improve workflow efficiency.

## Summary

The new user interface on the *syngo* MR XA platform is designed to improve the technologist's user experience with clearly separated tasks following the natural flow of their work. This not only helps to make routine exams more comfortable to perform and focus more on the patient than on the machine, but also supports in cases where rapid results are decisive. For example in imaging of acute stroke the combination of highly optimized exams using GOBrain, which only needs 5 minutes acquisition time, together with subsequent mismatch analysis (Fig. 5) right at the scanner can save precious time and may help to gain therapy-relevant information faster.

### Reference

1 Anderson, JA; et al. CIC Report 200311.

### Contact

Gregor Thörmer, Ph.D.

Global Segment Manager
MR Imaging in Oncology

Siemens Healthcare GmbH
HC DI MR CRM AW
Phone: +49 (9131) 84-7726
gregor.thoermer@siemens-healthineers.com

# Meet Siemens Healthineers

**Our brand name Siemens Healthineers embodies our pioneering spirit and engineering expertise in the healthcare industry. The people working for Siemens Healthineers are highly passionate about providing medical technology that improves your clinical, operational and financial performance, leading also to positive patient experience. In this section we introduce colleagues from all over the world to you – people who put their hearts into what they do.**

Andrew Dewdney



Erlangen, Germany

*Having studied Physics at Oxford University, Andrew Dewdney went on to Imperial College in London, researching the optical properties of III-V semiconductors for his Ph.D., before joining Oxford Magnet Technology to design magnets for MRI in the mid '90s. Being able to use his physics background to advance healthcare is a combination that fascinates him to this day. So much so, that when offered the opportunity in 1998 to be a delegate in Erlangen for two years, he quickly said yes, despite not being able to speak German! Two years has evolved into becoming a permanent resident, marrying a German wife and becoming a father of two dual-nationality children (and being fluent in German). He has worked in Erlangen since then, as part of the R&D team developing magnets and passive shimming for all of MR's products to be launched after that.*

***How did you first come in contact with MRI?***
It was a shock – some German physicists from Siemens came over to Oxford and explained what was wrong with our new magnets and I had to measure it! It was a steep learning curve, but my fascination grew with the challenges it presented … and MAGNETOM Symphony went on to be a very successful system.

***What is most fascinating about MRI?***
MRI is such a sensitive physical phenomena, it never ceases to amaze me that it is possible to install thousands of MRIs around the world, all capable of producing such detailed images and every time I get the chance to see the results of some new imaging technique, I am astonished at just how much we can measure in the human body, by simply flipping nuclear spins.

***What is your role in the development of MAGNETOM Vida?***
MAGNETOM Vida is the next development in a long line of MR systems I have worked on. In particular I contributed to the magnet design and homogeneity specifications and also a totally new field stabilisation concept, advancing it from the first invention through early development and final testing until reaching the goals we had set, addressing a long-standing problem for high-performance MRI.

***What is most motivating about your job?***
I am involved in many aspects of the life of an MR system: developing a new product is one part, but I am also responsible for continuing support, long after the initial launch excitement is over and therefore quality is important to me: many of my friends and family have needed MRI scans over the years – who knows which system will be needed next? And it's satisfying to know that I contribute to people's health and well-being all over the world.

In contrast to this, I have the occasional chance to support university research customer projects with innovative hardware such as multi-channel non-linear gradient or shim arrays – the excitement of academic research and working with multi-national teams on unique systems fosters innovation and brings fresh ideas for future products.

***What would you do, if you could do for one month whatever you wanted?***
In the MR world, I would appreciate a month's secondment to one of the university research groups, with time to learn something new within the broad spectrum of MR. With the family, I would love to take a large RV with mountain bikes on board through the northern Rockies – and for my other hobby, attend a large annual Scottish Country Dance Festival near Boston MA on the way home!

*Martin Vitzthum graduated in Mechanical Engineering from Friedrich-Alexander University (FAU), Erlangen, Germany in 2012 and joined Siemens MR in the same year. A Customer Use Test team member, he is responsible for the coordination of several market entrance phases, including the software versions syngo MR E11 and E11C. Additionally, Martin was appointed the MR Compliance Ambassador in February 2016.*




Erlangen, Germany

***How did you first come in contact with MRI?***
At a young age: just 17. My first job with Siemens was to assemble parts for X-ray systems. Being part of the Siemens family I always wanted to learn more about our products, especially for diagnostic imaging. So far, I have had an injury-free life and have never required an MRI examination. This meant that I only really got to know our MRI systems while working as an intern in the Business Line Magnetic Resonance. I still remember the first time I saw the system and heard the whistling of the cold heads: I was totally fascinated!

***What is most fascinating about MRI?***
Being able to visualize moving organs. Seeing is believing. Photography is a passion of mine and thus, I know about the difficulties of creating images with an ideal sharpness, brightness and contrast, especially for moving items. In MR we have technologies able to do just that. And, we are continuously working to improve these technologies and tackle new fields, such as free-breathing cardiac imaging. Looking back over the innovations of the last 30 years really makes me excited as to what lies ahead.

***What was your first reaction to hearing about MAGNETOM Vida?***
When I first heard of the plans for developing a new 3T flagship system, I was pretty excited. I still remember the MAGNETOM Aera and MAGNETOM Skyra introduction in 2009 and I felt really proud to be working within Siemens MR even, at that time, as a lowly student. Now I can see what the MAGNETOM Vida is able to do, I have another reason for pride. It's another breakthrough. The name itself sounds nice to me. It embodies life and vitality.

***What is your role in the development of MAGNETOM Vida?***
Before introducing a new system to the market, we evaluate its functionalities – hardware, software, application, and workflow – at a customer site by means of a clinical trial. For the new MAGNETOM Vida I was in charge of coordinating this clinical trial.

***How does such a clinical trial work?***
The German Medical Devices Act requires that clinical trials initially be conducted in a non-clinical environment, protected from the gaze of all but those most closely involved in such a top-secret project. After all, we are dealing with a system not yet on the market that is kept undercover right up to its official launch, known only to a few, and even then only by a code name. A clinical trial lasts between three and four months before the system receives the CE label.

Siemens is responsible for the setup, organization, and execution of the clinical trial, which is split into two phases – the preparatory phase and the execution phase (starting with the first scan at the customer site). We work closely with our clinical partner in this process.

Approximately six months before the installation of the new system at the institution of our clinical partner, we both set up teams to closely collaborate on the upcoming trial. The teams initially meet to establish a common understanding of the goal of the clinical trial and the necessary steps ahead. At several meetings during the following weeks and months, a range of documents are finalized. Siemens acts as the coordinator of all these activities, but the input here from our clinical partner is essential. A clinical investigation plan is drawn up: It describes the examinations to be performed as well as all important boundaries such as including and excluding criteria for patient and volunteer exams. During this preparatory phase, Siemens remains in close contact with the German Federal Institute for Drugs and Medical Devices and with the corresponding ethics commission where the clinical trial has to be registered. A positive decision by both authorities allows us to start the execution phase.

***And how is the clinical trial for MAGNETOM Vida set up?***

We work alongside our clinical partner the Diagnostic and Interventional Radiology Department of the University Hospital Tübingen (UKT). It sounds obvious perhaps, but our relationship with our clinical partner is exactly as the name implies: a partnership. Professor Konstantin Nikolaou and his team were very excited to be the first users worldwide to receive the new MAGNETOM Vida in a prototype status and to perform the first scans at their institute.

In May 2016 we began developing a joint understanding of our shared goals and of each party's needs for this phase. Professor Mike Notohamiprodjo has been the principal investigator of this clinical trial and we wanted him and his team to be very close to the system from the very beginning. Therefore, prior to the start of the clinical trial, we invited technicians from radiology and neuroradiology to Erlangen for a first training on the new system. At that time, the system had a code name and was kept under cover to hide it from visitors and guided tours in our manufacturing location. Secrecy was paramount. During these first tests on the enigmatic system we had fruitful discussions on several topics, responding to initial user feedback to make further improvements to functionalities.

Thanks to a very effective, mutually trusting collaboration between all parties on site – our clinical partner (UKT) and the national authorities – we were able to finalize all negotiations and registrations in time, thereby enabling a first scan to be performed in December 2016. Since then, the team at UKT has been performing scans in line with the clinical investigation plan. But this success story would not have been possible without the commitment and enthusiasm of the team at UKT, for which we at Siemens are extremely grateful.

***What most motivates you about your job?***

Cooperating with our MAGNETOM users and getting feedback is of great importance for our business. Such close cooperation via Clinical Trials or Customer Use Tests help both parties to improve – the user to improve with our help, for example, image quality and workflow, and Siemens Healthineers to learn about our user's evaluation, acceptance, and wishes for our products. Knowing we have helped our users through such collaboration and being able to learn about the needs for future projects is something that makes me feel very motivated in my job. Being part of this great Siemens Healthineers team really makes me proud.

***What would you do if you could do for one month whatever you wanted?***

Understanding our customers' aims and ambitions is of great importance for future developments. Therefore, I'd take the opportunity to spend time at our MAGNETOM user's institutions. Outside of work, I'd go travelling and explore my passion for photography even more deeply. I would love to go to the colder and more extreme regions of the world, such as the Arctic or Alaska. I am excited at the thought of confronting an untamed but beautiful natural world, and the opportunity to make the best photographic record of such visits that I can.

**The entire editorial staff at University Hospital Tübingen and at Siemens Healthineers extends their appreciation to all the radiologists, technologists, physicists, experts, and scholars who donate their time and energy – without payment – in order to share their expertise with the readers of MAGNETOM Flash.**

MAGNETOM Flash – Imprint



Publisher:
**Siemens Healthcare GmbH**
Magnetic Resonance,
Karl-Schall-Str. 6, D-91052 Erlangen, Germany

**Editor-in-chief:**
Antje Hellwich
(antje.hellwich@siemens-healthineers.com)

**Guest Editor:**
Professor Konstantin Nikolaou
University Hospital Tübingen
Diagnostic and Interventional Radiology
Hoppe-Seyler-Str. 3
72076 Tübingen
Germany

**Editorial Board:**
Reto Merges; Wellesley Were; Sunil Kumar S.L., Ph.D.; Gary R. McNeal, MS (BME)

**Review Board:**
Lisa Chuah, Ph.D.; Daniel Fischer; Berthold Kiefer, Ph.D.; Heiko Meyer, Ph.D.; Efren Ojeda; Gregor Thörmer, Ph.D.

**Production:**
Norbert Moser,
Siemens Healthcare GmbH

**Layout:**
Agentur Baumgärtner,
Friedrichstr. 4, D-90762 Fürth, Germany

**Printer:**
G. Peschke Druckerei GmbH,
Taxetstr. 4, D-85599 Parsdorf b. Munich, Germany

Note in accordance with § 33 Para.1 of the German Federal Data Protection Law: Despatch is made using an address file which is maintained with the aid of an automated data processing system.

MAGNETOM Flash is sent free of charge to Siemens MR customers, qualified physicians, technologists, physicists and radiology departments throughout the world. It includes reports in the English language on magnetic resonance: diagnostic and therapeutic methods and their application as well as results and experience gained with corresponding systems and solutions. It introduces from case to case new principles and procedures and discusses their clinical potential. The statements and views of the authors in the individual contributions do not necessarily reflect the opinion of the publisher.

The information presented in these articles and case reports is for illustration only and is not intended to be relied upon by the reader for instruction as to the practice of medicine. Any health care practitioner reading this information is reminded that they must use their own learning, training and expertise in dealing with their individual patients. This material does not substitute for that duty and is not intended by Siemens Healthcare to be used for any purpose in that regard. The drugs and doses mentioned herein are consistent with the approval labeling for uses and/or indications of the drug. The treating physician bears the sole responsibility for the diagnosis and treatment of patients, including drugs and doses prescribed in connection with such use. The Operating Instructions must always be strictly followed when operating the MR system. The sources for the technical data are the corresponding data sheets. Results may vary.

Partial reproduction in printed form of individual contributions is permitted, provided the customary bibliographical data such as author's name and title of the contribution as well as year, issue number and pages of MAGNETOM Flash are named, but the editors request that two copies be sent to them. The written consent of the authors and publisher is required for the complete reprinting of an article.

We welcome your questions and comments about the editorial content of MAGNETOM Flash. Please contact us at magnetomworld.med@siemens.com.

Manuscripts as well as suggestions, proposals and information are always welcome; they are carefully examined and submitted to the editorial board for attention. MAGNETOM Flash is not responsible for loss, damage, or any other injury to unsolicited manuscripts or other materials. We reserve the right to edit for clarity, accuracy, and space. Include your name, address, and phone number and send to the editors, address above.

MAGNETOM Flash is also available online:

**www.siemens.com/magnetom-world**

On account of certain regional limitations of sales rights and service availability, we cannot guarantee that all products included in this brochure are available through the Siemens sales organization worldwide. Availability and packaging may vary by country and is subject to change without prior notice. Some/All of the features and products described herein may not be available in the United States.

The information in this document contains general technical descriptions of specifications and options as well as standard and optional features which do not always have to be present in individual cases, and which may not be commercially available in all countries. Due to regulatory reasons their future availability cannot be guaranteed. Please contact your local Siemens organization for further details.

Siemens reserves the right to modify the design, packaging, specifications, and options described herein without prior notice. Please contact your local Siemens sales representative for the most current information.

Note: Any technical data contained in this document may vary within defined tolerances. Original images always lose a certain amount of detail when reproduced.

**Siemens Healthineers Headquarters**
Siemens Healthcare GmbH
Henkestr. 127
91052 Erlangen
Germany
Phone: +49 9131 84-0
siemens.com/healthineers

*Published by Siemens Healthcare GmbH · Order No. A91MR-1000-130M-7600 · Printed in Germany · 5894 02181.5 ·* 